Stochastic modelling of cellular populations: Effects of latency and feedback

Daniel Sánchez Taltavull

Stochastic modelling of cellular populations: Effects of latency and feedback

Daniel Sánchez Taltavull
Advisor: Tomás Alarcón
Tutor: Alex Haro

tesi inscrita al programa de doctorat en Matemàtiques
per optar al títol de doctor
Universitat de Barcelona
Facultat de Matemàtiques
Departament de Matemàtica Aplicada i Analisi

October 9, 2014

Acknowledgements

Aquesta ha estat un llarg camí ple de pujades i no hauria estat possible sense tota la gent que he tingut al voltant, ja sigui donant-me consells o simplement fent una birra amb mi quan ho necessitava.

Tinc que donar les gràcies al meu director de tesi, Tomás Alarcón, per tota la paciència, tot l'esforç i la gran feina feta en dirigir-me la tesi i alhora dirigir tot el grup, i en ajudar-me cada cop que li he demanat o ha vist que el necessitava. Quan vaig prendre la decisió de venir al CRM, sense saber gairebé res d'ell, tenia por de no haver comes un error, però ara se que venir aquí amb ell ha estat una de les millors decisions de la meva vida, i si ho hagués de tornar a fer tornaria a triar igual.

També he d'agraïr al meu pare i la meva mare tot el que han fet per mi i per fer-me costat amb totes o casi totes les meves decisions i ajudar-me a ser qui sóc ara. També donar-li les gràcies al meu germà gran Àlex per ser, a part d'un germà, un amic i ser allà sempre que l'he necessitat i també per fer-me costat en aquesta aventura. Gràcies també a s'àvia Juanita, s'àvia Tònia, a en Toni, na Sili i en Victor (que arribarà on vulgui al mon de la poesia) per tot el que feu per mi, per ser allà i per estimar-me i ajudar-me en lo que es pot. Sense vosaltres això no seria el mateix.

I al Centre de Recerca Matemàtica pel finançament i totes les facilitats que m'han proporcionat perquè pogués fer la tesi. Gràcies per confiar en mi.

I com no, als membres del meu grup. A Pily por ser como un atardecer de otoño, por haberme animado cada día que estuvo ahí y por lo bién que nos lo pasamos cada vez que quedabamos para cotillear. A l'Esther per no tirar-nos una galleda d'aigua (o lejia) el dia que vam anar a cantar al seu portal. A Roberto por ser una de las pocas personas dispuestas a bajar las escaleras para venir a verme y hacerme compañía, y por pasar de los casinos. A Ivon porque, las pocas veces que sale del bunker en que se esconde, consigue sacarme una sonrisa. Y a las dos nuevas incorporaciones: Juan, que aún no le conozco mucho, pero que por ahora nos lo estamos pasando bién y Elisa, que encaja mejor 4 parrafos más abajo.

Agraesc molt sincerament, efusivament i de tot cor a nes meu gran amic Andreu que hagi cregut durant tants anys que $\pi = 3$, y estoy muy agradecido al chico de Movistar que me ayudó a elegir un buen movil. Aram gracias por dejarme siempre un sofá donde dormir y cuidarnos siempre. A n'Alex li agraesc que no hagi decidit començar a tocar es violí fins as final de sa meua tesi, ja que m'hauria provocat danys cerebrals irreversibles. Gemma, merci per ser sa millor amiga que es pot tenir, i merci per lo bona que està sa teua germana petita, lo qual me recorda que estic molt agraït a na Maria Galeta per lo bona que està. A en Mati per no pigar-me mai. A n'Ester per totes ses ties que mus ha presentat a jo i n'Andreu. A en Sus per ses lans party que vam montar. A en Nel per haver estat as costat meu des de fa 23 anys. a n'Afryca per fer-me colacaos es mati i per donar-me una cullerada d'oli d'oliva quan vaig tornar borratxo de Son Bou. a na Maite per clavar-me una forquilla i mossegar-me. A na Falsa Vegana per menjar carn. Christian, siento mucho haberte abandonado en ese pueblo... y siento que nos llevásemos tu movil, cartera, dinero y llaves. a Tere por no pedir una orden de alejamiento. A en Jordi Bosch per totes ses juergues mítiques. A na Sara Velez per tot lo que no sap sobre es porter de Allà de sempre. A n'Andrea per ser sa meua consciència i no deixar-me fer res dolent. A

en Francis si. A en Xoric per estar amb jo durant tot es Diablo 3. a en Jake i en Kid per salvar la tierra media destruint el anillo único.

Molta gent que m'ha acompanyat en aquest camí han estat els amics que he fet a Barcelona, aquest va per ells: Mariano, ets es millor company de pis que es pot tenir, lo únic que te diré és: clucs. Lluis, encaixaries a nes parraf de dalt pero millor posar-te aquí que és on mus hem fet amics, merci per totes ses borratxeres. Cristina que decir de ti, te echaré taaaanto de menos, pero se que me vendrás a ver muy pronto! Y Marta te prometo que en el próximo viaje buscaremos una canción que puedas cantar tú también, pero por favor, pasanos ya las fotos de Berlin. Cesar, sigo sin entender como te puede gustar Bran Stark, pero sabes que te apoyo. Eva Martinez, saps que ets la única persona que https://www.youtube.com/watch?v=q5V01fIjN-s. Anouk m'encanta lo guay que ets! Miriam Doooooniga, si d'alguna cosa estic segur es de que mai més tornaré a trobar ningú com tu. Gerard gràcies, de ve, moltes gràcies per aguantar a tothom en aquella casa de locus i mantenir sa calma en tot moment. Laura Silvestre em vaig riure molt quan em va contestar el whatsapp de Menorca. Aracelis te he perdido la pista del todo pero seguro que te va tan bien como siempre. Laura Marfill m'encanta la d'aventures que vius sempre, estic segur que en algun viatge raru que faci et trobaré. Yasser porque un día de estos nos vamos a tomar una cerveza. Andres me encanta cuando me preparas la cena.

Otro grupo de amigo que he hecho son los E.coli & friends. David m'encanta que sempre estiguis de festa fins al final, trobo a faltar que trenquis portes i espero que no t'obris el cap per California... Maria graaaaaacies per les galetes que em vas fer, en vull més. Edgar merci pel deck de hunter, m'ho vaig passar molt bé amb ell. Joan merci pel tota la ginebra que ens hem begut. Roser em preguntava... ens hem vist algun cop de dia? Alba tots els records que tinc de tu són molt borrosos ;). Gabriel graaaacias por ese guacamole. Y Maggie gracias por ser la mejor! Me encanta que aunque te hayas ido tan lejos sigamos siendo igual de amigos (o más) y perdon por lo que voy a poner ahora... Y Rebecca, me encanta que tengas un león tatuado y me apetece darte un mordisco.

Mi tesis no habría sido la misma de no haber ido a la II Summer School del GEFENOL en Benasque (sitio donde deberían organizarse todas las summer schools del Gefenol, no se porque se montan en otros sitios últimamente...), donde conocí a mi grupo favorito de científicos. Uri desde el moment que vas dir "se me ha ido de las manos" hem viscut innumerables aventures que no canviaria per res del mon. Edgar, ¿cuándo fué la última vez que salimos un sabado? creo que el Martes. Edoardo *El Sabio*, eres el protagonista del mejor momento que ha vivido nuestro grupo, siempre recordaré como Juan, Edgar y yo te mirabamos y vas ahí... y luego te das la vuelta y vuelves andando sin mirar atrás... madre mia... Y ahí con la boca abierta dos minutos y tu: "voy a por otro cubata". Svetozar el vallekano GAAS! GAAAAAAS! A Tipo De Incognito porque eres la persona con quien más he bebido durante la tesis... A mi higado le caes tan bien como yo a tu novia... Ula Sagarra no puc posar aquí el motiu pel qual et tinc en un pedestal així que et guardo pel parraf de les JIPI. A Virginia por tener unos ojos tan bonitos. A Paula Villa Maravilla por ser un sol, y por dejarnos quedarnos en casa de sus abuelos aka El Gran Hotel Paula Villa, y por no enfadarse cuando inundamos la casa de vecino, pasase lo que pasase: Mereció la pena. A Ruben Perez Carrasco por esa mirada que me echó en la discoteca esa... Magia! Unicornios! Que gran noche. Ana Kalt por la mejor tortilla de patatas que he probado en mi vida. A Toñi por estar siempre dispuesta a irse de fiesta. A Àngel Maximilià per l'Àngel. A Nicole por esas conversaciones sobre Hannah Montana. A Rafa por todas esas fiestas, he sido incapaz de encontrar el antro ese al que nos llevaste. A Alessio que aún no

me ha pagado lo de la apuesta... Alessio Paga el cubata segundo aviso. A Nacho por no matarme todas las veces que le desperté la segunda semana en Benasque... A Eustaquio por esas cenas en el japonés de Passatge de Marimon. A Trapote per ser una taza. Y a Elisa Beltran por enseñarme a valorar la verdadera belleza de las playas. Lo cual me recuerda... Gracias Massimiliano por enseñarme como NO funciona un GPS y gracias Fran por los zapatos. Y a nuestros amigos de Dawn Meats por suministrarnos siempre alimentos de la mejor calidad. Y por último, aunque no estuvieron en este congreso, aquí encajan bien: Joaquin aka Marcelino Adbekunkus eres mi heroe, seré el primero en venir a verte y Raquel gracias por pagarme ese vodka con limón, pero sabes que yo no bebo.

Durant la carrera de Matemàtiques he conegut a molta gent i molts d'ells no poden faltar en els agraïments d'aquesta tesi. David Martí moltes gràcies per tot lo que vas fer quan em van ingressar a l'hospital i per tot el suport que em vas donar, encara em ric quan penso que abans de que m'operessin et vaig dir: "tranquil no és res" i tu "però si d'això et pots morir!!". Narcis ets un crack, merci per totes les converses censurades per whatsapp... tic tac tic tac. Arturo, gràcies per totes les mates que m'has ensenyat aquest últim any, sense tu mai hauria dominat l'aproximació semi-classica, i aviam quan et tornes a venir a fer unes birres. Jordi, encara que fas veure que ets dolent se que ets un gran amic, cal ser-ho per no anar a una esquiada que ja has pagat quan un colega ho necessita. Dani, gràcies per totes les classes de gnuplot i tex, i per haver estat "al pie del cañon" constantment. Meri que bé m'ho vaig passar amb tu i que gran va ser aquella setmana al congres dels espais de moduli. Ari merci pels snapchats brutals que ens envies. Juan Von Mälder sempre m'animes a superar-me a mi mateix. Marta Canadell moltes gràcies pel vodka de Russia. Ramon, vas ser el primer amic que vaig fer a mates i m'encanten totes les aventures que hem viscut. Anna ets la millor, la meva matemàtica preferida. Iñaki Puigdollers m'ho he passat molt bé en totes aquelles nits de jocs. Marcel ets el matemàtic més fiestero que he tingut l'honor de coneixer, aviam quan tornes i ens bevem un altre bar. Marta Palau fas que m'agradin els chupitos de tequila. Roca merci per tot aquell vodka que ens hem fotut. Roc em fa molta gracia la frase per lligar que em vas ensenyar, algun dia la faré servir.

También quiero agradecerle a Alex Haro todo lo que ha hecho por mi estos años, sobretodo gracias por todos los papeles que has firmado y por hacer que me decidiese por la matemática aplicada. I també gràcies als professors que més m'han influenciat, Juan Luis, vas fer que em decidis a començar aquest camí de les matemàtiques. I gràcies Carles Simó, que ets qui m'ha convertit en un matemàtic tant bo com sóc.

I tinc que dedicar un paràgraf als JIPIs (que no hippys, be n'hi ha algun que si, però això és una altre historia), l'Anna Alemanai per totes aquelles birres a la Terreta Valenciana i totes aquelles falses acusacions sobre que organitzo congressos per conèixer ties. A la Maria Van Der Waals (aka Mireia Martí) per ser tant bona dic... per estar tant bona, no espera! ja ho havia dit bé al principi: per ser tant bona. I a l'Anna May per ser tant maca i tant happy i tant de tot, et vull adoptar com germana petita. I a l'Ula per lo genials que són les festes a casa seva i per la quantitat indecent d'alcohol que me begut amb ell. I al Martí per lo bé que li queda la barba, la llista exhaustiva de les qualitats que ha de tenir una noia i per les mossegades que la seva xicota, la Vero, va donar al Mario o al Pol, no recordo a qui dels dos va ser. A Daniel Reta por esa serenidad que nos transmite siempre. I al Joan Camuñas per aquelles xerrades sobre matemàtiques, ell ja sap a quina matemàtica em refereixo ;). I al Rebled per les nits de karaoke i sauna i les xerrades sobre com ser un gran amant. I a la Teresita de Jesus, al Chileno i a la filosofa

for fruitful discussions.

Un altre congres que ha estat molt important per mi, per la gent que vaig conèixer va ser el FisEs. Allà vaig conèixer al Pol, que espero que aquest any la convidi... I a la Sara la Jabata, que apart de demostrar se una persona molt flexible... bé... medallon, chuleta, fresa, frambuesa, encara espero una trucada teva. Celia me encantaron todas esas conversaciones sobre monstruos. I al David Palau, que estava per allà parlant de gossos i mariners. I Mario, que és un fiestero com deu mana, i quan no em censura els agraïments encara és més guay. I a la Lorena, que encara em ric quan penso en la trucada del divendres a les tantes. También estaban por ahí 4 chicas muy simpaticas que me ayudaron mucho cuando estaba algo perdido, Patricia la de los ojos verdes, Vanessa Cobi, y las otras dos que nunca supe como se llamaban... Romualda y Eustaquia por ejemplo. Luiño cada vez que dicen la palabra depravado pienso en ti. Y Jordi de Granada a ti te diré ;) ;).

I evidentment a totes les persones que he trobat al CRM. Michelle I miss you so much!! Fran Martinez, merci per tota la calma que em transmeties sempre. Marina, moltes gràcies per ajudar-me a construir la urna amb l'unicorn. Carles a tu t'estic molt agraït per allò de la tassa aquella que NO era robada. Rosalba ets una persona molt especial... però no vull dir rara, que també, ets molt rara, però aquí amb ningú m'ho passo tant bé com amb tu. Bernat, sempre que penso en tu recordo el dia de l'incendi a l'orfanat. Isabel I ja tinc ganes de saber on acabarem el pròxim cop que sortim de festa. A Luis le agradezco todas las conversaciones sobre las causas justas que apoya. Jordi gràcies per fer que tot funcioni. Dani Balagué et poso en aquí també! gràcies per ajudar-me en un dels moments que més ho he necessitat, espero veure't més ara que estarem més aprop. A Álvaro que siempre me apoya cuando me cambio de despacho. A Tim que me hizo ganar un dinero extra con apuestas deportivas. A Andrei que montó uno de los congresos en que mejor me lo he pasado. Al Joaquim, que sempre m'ha recolzat en tot lo que he volgut fer. Guillem gràcies per ensenyar-me l'starlink. Mihail el poco tiempo que estuviste aquí tuve una gran suerte. Y gracias Mikel Brun por enseñarme valores, el día que le conocí vi un ejemplo de rectitud.

Y dió la casualidad que a la primera summer school que fuí en la tesis fué el Biomat en Granada, y la última (tres años más tarde) el Biomat en Granada. Donde estaba Nico, que este si que es un fiestero como Dios manda. Y Paloma que es malvada (y lo digo como algo bueno). Y Maite que tenía una sonrisa contagiosa. Y Pablo, el otro Pablo, y el otro Pablo. Y el chico ese que no se como se llamaba con la camiseta de berlin que sale sin cabeza en las fotos. Y tambien estaba Isabel II, que no salió... A ver si ahora que te tengo más cerca te veo algun día de fiesta, gracias por ayudarme a organizar el seminario! También estoy muy agradecido a Rica Schnei que le tiraba cacahuetes a Nico mientras intentaba ligar. Y también a Ainize por ser tan fiestera.

A Soraya Garcia, Daniel Inglorion, Alvaro Riera Bable, Marc Parti, al vendedor de gemas de Geffen (por la cantidad de negocios que aceptó), al sacerdote de Elune por ser el elfo más feo de la historia. Al agente imperial Cipher 9, a la contrabandista Pancracia. Al Bounty Hunter Firex por todos esos partidos de Huttball y por su estrategia en Ironman. Al legítimo rey de los siete reinos y protector del reino Joffrey Baratheon. Al High Priest y palabra de Dios en Rune-Midgars, Walter Sullivan. Y al verdadero señor de Rune-Midgars, el Wizard Wallace. Special thanks to Cave Johnson and his secretary, the sweet Caroline, authors of the project GLaDOS that inspired my scientific career.

Contents

Chapter 0

Resum en català

En aquesta tesi doctoral es tracten alguns problemes sobre fluctuacions en poblacions amb una estructura complexa, en particular aquelles caracteritzades per l'existència d'un estat latent. El nostre objectiu és entendre millor algunes qüestions que sorgeixen en la dinàmica de les poblacions de cèl·lules amb estructura jeràrquica, com ara les que es troben en els organismes multicel·lulars caracteritzats per la diferenciació cel·lular, i la dinàmica del VIH-1 en pacients infectats que es troben amb teràpia antiretroviral. Els dos sistemes estan caracteritzats per la presència d'una població en estat latent, és a dir, cèl·lules mare en el primer cas, i cèl·lules infectades en estat latent en el segon.

0.1 Motivació i rerefons biològic

Els problemes biològics han estat estudiat pels científics amb 4 models diferents: *In vivo*, *In vitro*, Data Driven i mechanistic models. Encara que aquests últims són els que donen un millor enteniment sobre la dinàmica del proces que s'estudia, han estat els que menys èxit han tingut en biologia.

Els mechanistic models s'han utilitzat tradicionalment per matemàtics i físics per estudiar problemes biològics fent servir aproximacions continues i deterministes. No obstant, en alguns casos, aquests models poden no ser molt correctes. Si les poblacions són petites no podem assumir que un model de camp mitjà sigui una bona aproximació de la realitat. Això és important en molts problemes biològics, on sovint, un es troba poblacions petites.

S'ha provat que el soroll intrínsec, és a dir, fluctuacions en el sistema degut a un tamany petit, pot tenir una forta influència en el comportament d'un sistema dinàmic [14, 85, 42]. Presentem una introducció als processos estocàstics a l'Apèndix A, concretament tracta sobre modelització estocàstica i l'algoritme de Gillespie de simulació estocàstica, que serà la nostra principal eina.

0.1.1 Latència en poblacions de cèl·lules

Pels propòsits d'aquesta tesi, la latència es defineix com un estat de la cèl·lula en que la majoria de les seves funcions, prominent proliferació, estan desactivades. Aquest mecanisme sovint sorgeix en entorns hostils per sobreviure. Un exemple d'aquest comportament s'ha analitzat en [3], on s'ha provat que la latència pot actuar com un mecanisme que permet a una població maligne eludir l'acció d'un medicament, fent que les cèl·lules d'aquesta població tinguin la capacitat d'entrar en un estat de repòs, en el qual són immunes a

l'efecte de la droga. Al entrar en aquest estat, una petita població latent és capaç de sobreviure, i, finalment, tornar a créixer un cop que el medicament ha deixat d'aplicar-se. Un cas particular en que aquest model és rellevant, és la resistència a la quimioteràpia o radioteràpia en els tumors amb regions amb hipòxia (falta d'oxigen). Les cèl·lules hipòxiques es sotmeten a una gran reducció de la seva taxa de proliferació, que les fa menys sensibles a aquests tractaments que les cèl·lules de cicle ràpid, proporcionant així un reservori de cèl·lules immunes, que, quan es para la teràpia, fan que aquesta població torni a créixer. A més d'escapament a la teràpia, els fenòmens de latència han provat tenir un paper en el càncer per eludir els controls homeostàtics del teixit normal. Roesch et al. [108] han caracteritzat un cicle lent (latent) d'una subpoblació dins de la població del melanoma, que te una proliferació de cèl·lules molt més ràpida necessària per al creixement tumoral.

Un altre exemple on la latència ha provat ser crucial, és per entendre certs aspectes del VIH i la seva resposta a la teràpia. El VIH es controla amb molta eficàcia amb teràpia antiretroviral. No obstant, aquestes teràpies no suprimeixen completament el virus. Encara que eviten que els virus infectin cèl·lules T, estudis a llarg termini de la carrega viral en pacients tractats revela que un nivell baix del virus (per sota dels límits de detecció estàndard) persisteix molt de temps [110, 123]. Aquests resultats suggereixen que la infecció persisteix en els pacients tractats en forma de compartiment insensible a la droga. Moltes hipòtesis han estat formulades sobre la naturalesa d'aquest compartiment, però la més consolidada és la que ho explica amb una població de cèl·lules infectades en estat latent. Aquest compartiment cel·lular consisteix en unes cèl·lules (probablement de memòria) que proliferen lentament i guarden el virus però no el repliquen. Com aquestes cèl·lules no repliquen el virus no són afectades per la teràpia antiretroviral. A mes, després de l'estimulació amb antígens específics, passen a un estat actiu i reprenen la producció de virus. Aquest cicle manté aquest baix nivell de virèmia. La presència d'aquesta infecció latent ha estat reconeguda com la principal barrera per a la completa eradicació de la infecció, i la recerca de mitjans per combatre-la s'ha convertit en una molt activa línia de recerca [121, 113, 65, 66].

El fenomen de la latència també és part de la regulació fisiològica normal dels teixits. En particular, les cèl·lules mare, que són els components essencials dels teixits dels organismes multicel·lulars, passen la major part del seu cicle de vida en un estat latent, és a dir, sense proliferar. Només després de rebre els senyals apropiats, les cèl·lules mare s'activen i la proliferen. Aquestes senyals són secretades en resposta a una disminució en el nombre de cèl·lules madures (totalment diferenciades) que estan al final de la corresponent cadena de diferenciació: quan el nombre de cèl·lules madures disminueix, la proliferació cel·lular s'activa per tal de reposar les cèl·lules madures. Encara que aquest mecanisme és part de la regulació normal del teixit, pot ser subvertit per patologies com el càncer que segresten les propietats de les cèl·lules mare.

L'objectiu general d'aquesta tesi és utilitzar models estocàstics, juntament amb tècniques asimptòtiques i mètodes numèrics per a comprendre millor els mecanismes bàsics que intervenen en la dinàmica de les poblacions del cèl·lules latència retroalimentada amb la finalitat de proposar estratègies de control que ajudin a formular millor, els enfocaments terapèutics per situacions patològiques que resulten de la des-regulació de les cascades de diferenciació i del VIH-1 en estat latent.

0.1.2 Dinàmica estocàstica de les cascades de diferenciació regulades retroactivament

En el Capítol 2 analitzem els factors que afecten a la robustesa de les poblacions de cèl·lules amb estructura jeràrquica. Els teixits en organismes multicel·lulars com els mamífers, mantenen l'homeostàsi per mitjà de cascades de diferenciació de cèl·lules en sèrie [4]. Aquestes cascades estan compostes per compartiments jeràrquicament organitzats de diferents tipus de cèl·lules. La pedra angular d'aquest sistema són les cèl·lules mare (SCS) que sostenen el teixit produint més cèl·lules mare, una propietat coneguda com auto-renovació, i les cèl·lules diferenciades d'un llinatge específic. La cascada de diferenciació procedeix a través d'una sèrie d'etapes intermitges o compartiments de cèl·lules amplificadores transitòries (TAC) i acaba amb el compartiment de cèl·lules madures o totalment diferenciades (MCS).

Hi ha hagut molta discussió sobre la qüestió de com les SC mantenen tota la cadena a partir de l'auto-renovació i la diferenciació [91, 92, 71, 114, 72]. Una estratègia mitjançant la qual les SCS poden realitzat aquestes dues tasques és la divisió cel·lular asimètrica, d'aquesta manera, en la divisió d'una SC, una cèl·lula conserva la identitat de la seva mare mentre que la seva germana es diferencia [71, 72].

Encara que la divisió asimètrica és una solució simple i elegant, hi ha hagut molta controvèrsia al voltant del que es percep com un defecte fonamental d'aquest model, és a dir, la divisió asimètrica no permet que el compartiment de les cèl·lules mare creixi [91, 92]. En situacions com lesions, on la taxa de renovació cel·lular ha d'augmentar en gran mesura, amb la finalitat de regenerar el teixit afectat, el compartiment de les SC ha de créixer. Això suggereix que la divisió asimètrica podria no ser la solució completa.

Hi ha evidències experimentals que les SC, en alguns teixits, com el sistema nerviós central [50] i l'epidermis [74], es poden dividir de forma simètrica. La divisió simètrica de SC consisteix en que les dues filles són iguals, o bé SC o bé cèl·lules diferenciades. D'aquesta manera, el nombre de cèl·lules està regulat per les freqüències de divisions simètriques que produeixen SC o cèl·lules diferenciades. Com aquest tipus de divisió permet l'expansió del compartiment de les SC, apareixen models alternatius [91] on la majoria de les SCs pot dividir-se d'ambdues formes, simètricament o asimètricament, l'equilibri entre aquests dos tipus de proliferació està controlat per senyals ambientals per produir el nombre apropiat de SC i cèl·lules diferenciades. Però s'ha reconegut que, si bé la divisió simètrica confereix la capacitat de creixement millorat i una major capacitat de regeneració, també augmenta la probabilitat de càncer. Aquesta idea està recolzada pels resultats d'acord amb els quals la maquinària cel·lular involucrada en la divisió asimètrica ha estat conservada, perquè te un paper en la supressió de tumors, els gens que promouen la divisió simètrica també funcionen com oncogens [91].

El nostre objectiu és analitzar la dinàmica estocàstica de les cascades de la diferenciació cel·lular on trobem les dues formes de proliferació de les SC. Estudiarem les estratègies òptimes entre divisió simètrica (que millora la capacitat d'adaptació) i la divisió asimètrica (que dota d'estabilitat).

0.1.3 Dinàmica estocàstica i extinció del VIH-1 en pacients sota teràpia anti-retroviral potent

El VIH es controla de manera efectiva amb l'administració de teràpies antiretrovirals (ART). Però a pesar del gran èxit de la teràpia antiretroviral de gran activació (HAART),

aconseguir curar-la, en el sentit d'eliminar completament el virus, no s'ha aconseguit [105]. Anàlisis quantitatius de l'evolució temporal de la càrrega viral en plasma després del tractament HAART suggereix l'existència de diverses fases en el decaïment induït pel tractament de la càrrega viral [102, 69, 111]. Primer s'observa una fase en la que la càrrega viral decau exponencialment, en aquesta fase la càrrega viral es redueix d'un a dos ordres de magnitud en unes dos setmanes. Aquesta etapa reflecteix que el temps mitjà de vida de virus en plasma i de les cèl·lules infectades produint virus, els limfòcits T CD4+, és molt curt [57, 124, 83]. Després d'aquesta primera fase, una segona etapa més lenta reflecteix la contribució a la càrrega viral de cèl·lules infectades amb un major temps mitjà de vida, com els macròfags i les cèl·lules T CD4+ infectades que presenten una menor taxa de replicació viral [99, 58, 126]. Després d'aquesta segona fase, la càrrega viral en plasma normalment ha caigut per sota del llindar de detecció dels assaigs clínics estàndards ($\sim$ 50 còpies d'ARN / ml). No obstant, després d'aquesta segona fase, la HAART no aconsegueix eradicar completament la infecció. Es produeix una tercera etapa (de l'ordre d'anys [69]) en que els nivells residuals (1-5 còpies d'ARN / ml) persisteixen en plasma, aixi com en altres llocs del cos com el semen.

La pregunta de quin és la font d'aquesta carrega viral residual ha generat molt debat i s'han creat diverses hipòtesis de treball. Una d'aquestes hipòtesi es basa en la possibilitat de que la teràpia HAART no arriba a tot el cos i hi ha uns reservoris on la teràpia no afecta [102], els anomenats "drug sanctuaries", on la infecció persisteix [67].

Un model alternatiu, que està molt recolzat pels estudis recents, suggereix que, tot i que la teràpia HAART és totalment supressora, hi ha un reservori cel·lular que permet a la infecció romandre en forma latent [102], i la càrrega viral residual és el resultat de l'activació de les cèl·lules latents [102]. Aquestes cèl·lules latents s'estableixen dins de la població de les cèl·lules T de memòria CD4+ infectades [25, 24] i, per tant, romanen en l'estat de repòs en la presència de la HAART durant períodes prolongats de temps. Com a conseqüència, les cèl·lules infectades de forma latent son capaces d'escapar a l'efecte de la droga i al sistema immune a causa del fet que presenten nivells molt baixos de ARN de VIH-1 [111]. Peró ja que les cèl·lules amb infecció latent alliberen virus quan son estimulades amb l'antigen apropiat, si es retira la HAART la carrega viral torna a créixer i la infecció VIH-1 reapareix, això és consistent amb que la latència serveix com a mode d'escapament dels medicaments [3].

Un cop que la infecció ha entrat en aquest estat latent, un pot observar episodis transitoris en que la carrega viral puja per sobre dels límits estàndards de detecció (50 còpies d'ARNm/ml) durant un breu període de temps [33, 104, 54, 95]. Aquests episodis es coneixem com *blips*. L'origen i la rellevància mèdica d'aquests blips encara no està clara i nombroses hipòtesis s'han formulat [111].

Degut a la incapacitat de la HAART per acabar amb les cèl·lules en estat latent, s'han proposat teràpies combinades que suprimeixen el reservori latent [105]. Un camí prometedor en aquesta direcció consisteix en la combinació de HAART amb agents que activen específicament les cèl·lules latents, el que les fa susceptibles als atacs de la HAART. El fonament d'aquesta teràpia combinada és que si s'augmenta el ritme d'activació de les cèl·lules amb infecció latent, el número d'aquestes ha de decaura ràpidament i, degut a fluctuacions estocàstiques, aquestes cèl·lules poden ser completament eliminades i, amb elles, tota la infecció.

0.2 Marc matemàtic

En termes generals, els problemes adreçats en aquesta tesi es refereixen a la dinàmica estocàstica de poblacions amb diferents tipus de cèl·lules. El marc més adequat per fer front a aquests problemes és el de dinàmica de poblacions. Degut a que el número de cèl·lules en estat latent és molt baix, hem de modelar les nostres poblacions en termes de processos estocàstics, en particular, dels processos de Markov [44]. El procés de Markov per la dinàmica de poblacions en formularà en termes de la corresponent Equació Mestre (Master Equation). Aquestes equacions son molt difícils de resoldre exactament i en qualsevol cas pràctic, s'ha de recórrer a mètodes aproximats per tractar amb elles.

En alguns casos treballem amb poblacions molt petites, en altres situacions buscarem rare events. Per aquesta raó farem servir l'aproximació semi-classica, que és una aproximació del tipus WKB [73] per calcular les probabilitats dels rare events.

Hem inclòs una explicació detallada sobre l'aproximació semi-clàssica en l'Apèndix B. Aquesta aproximació transforma el nostre problema de treballar amb una equació mestre en un problema de mecànica clàssica amb un Hamiltonià amb diversos graus de llibertat, tants com tipus diferents de cèl·lules. Calcular les varietats invariants del sistema, que, normalment és el primer pas en l'estudi d'un sistema dinàmic, no és fàcil i una aproximació lineal no és suficient i requereix tècniques com el mètode de la parametrització [17, 18] per obtenir expansions a ordres alts. Més dificultats associades a aquests sistemes apareixen degut a la naturalesa slow-fast dels problemes. A més, l'estudi del moviment aprop de punts hiperbòlics pot ser necessari. Per integrat les equacions del moviment fem servir mètodes de Taylor [64] combinats amb tècniques de diferenciació automàtica [64], el que ens permet prendre passos molt llargs i aconseguir més precisió del que que altres mètodes explícits, com el Runge-Kutta, ens poden donar. El mètode de Taylor no és un integrador simplèctic, és a dir, no preserve l'estructura Hamiltoniana de les equacions, no obstant, això és irrellevant, ja que un pot demanar un error local per sota del roundof de la màquina. A l'apèndix C expliquem els mètodes que hem fet servir per estudiar aquests sistemes Hamiltonians.

Encara que hem fet alguns progressos en l'estudi asimptòtic d'aquests problemes, depenem molt dels mètodes de simulació. La nostre principal eina per estudiar les equacions mestre és l'Algoritme de Gillespie de Simulació Estocàstica (SSA), que és un mètode de Monte Carlo basat en una reinterpretació de l'equació mestre. A l'Apèndix A aquesta metodologia està explicada en detall. el Gillespie SSA requereix un gran temps de computació, en particular quan (i) el sistema considerat és molt gran i (ii) quan la separació d'escales temporals apareix. En aquest últim cas, podem fer servir la separació d'escales temporals per formular una variant més eficient del SSA proposat per Cao et al. [20], aquest mètode està explicat en detall a l'Apèndix D.

0.3 Objectius

L'objectiu principal d'aquesta tesi doctoral és l'estudi de l'efecte de les fluctuacions en poblacions acoplades en sistemes biològics, on cèl·lules en estat latent juguen un paper important. Intentant trobar el significat biològic de la dinàmica dels sistemes. Els punts específics que volem abordar i la organització de la tesi estan explicats a continuació.

En el Capítol 2, estudiem el comportament de les poblacions de cèl·lules amb estructura jeràrquica des de el punt de vista de les propietats d'estabilitat, En particular

1. Divisió simètrica contra asimètrica en el compartiment de les cèl·lules mare. Estudiem la robustesa de les poblacions amb estructura jeràrquica, depenent de si les cèl·lules mare es divideixen simètricament, asimètricament o de les dues maneres. Estudiem com la divisió simètrica afecta a l'estabilitat de la població, ja que això te una gran importància en la progressió del càncer.

2. La competició entre dues poblacions amb diferents tipus de divisió de les cèl·lules mare. Això és crucial per trobar estratègies òptimes que maximitzin la robustesa (supervivència a llarg termini, resistència a invasions i habilitat per invadir) de poblacions amb estructura jeràrquica.

3. La influència de paràmetres com son la duplicació i el ritme de mort de les cèl·lules mare, el temps de vida mitjà de les cèl·lules completament diferenciades, la longitud de les cadenes de diferenciació i les fluctuacions al compartiment de les cèl·lules mare en la robustesa i arquitectura òptima de les cascades de diferenciació.

En el Capítol 3 presentem un model homogeni de combinació de HAART amb teràpies d'activació de les cèl·lules latents del VIH-1 a la sang. Estem interessats en

1. L'Efecte del ritme d'activació de les cèl·lules latents en el temps mitjà de vida de la infecció. En particular analitzem si les teràpies basades en incrementar aquest ritme són capaces de suprimir la infecció en un temps raonable.

2. La importància de l'eficiència de les teràpies antiretrovirals, incloent els casos límit en que l'eficàcia és del 100%, en la quantitat de carrega viral.

3. La formulació d'una teoria asimptòtica basada en l'aproximació semi-clàssica amb aproximacions quasi estacionaries per descriure la dinàmica del procés. La precisió d'aquest mètode asimptòtic és comparat amb simulacions multi-scale proposades pel Cao et al. [20].

En el Capítol 4, estenem el model proposat pel Rong i el Perelson [110] a un model no homogeni de la dinàmica del VIH-1 en el corrent sanguini, considerant que les cèl·lules i els virus no estan distribuïts de manera uniforme en la sang. Els punts específics que volem estudiar són:

1. El mecanisme que fa que apareguin els episodis de virèmia per sobre els límits de detecció, coneguts com viral blips. En particular volem investigar si són producte de fluctuacions estocàstiques degudes a la inhomogenietat o un altre mecanisme ha de ser considerat.

2. Si l'aparició dels viral blips esta afectada pels procediments duts a terme en el laboratori, com el temps d'espera entre les extraccions i les observacions.

3. Si la probabilitat, l'amplitud i la freqüència dels viral blips es veu afectada pels diferents possibles tipus de producció viral, és a dir, continua vs burst.

En el capítol 5 presentem i discutim els resultats obtinguts, i comparem, quan és possible, amb altres models o amb resultats experimentals, i discutim el treball que deixem pel futur.

Els detalls relatius a qüestions metodològiques, així com una introducció a la modelització estocàstica fent servir equacions mestres es donen en els apèndixs. Per a aquells que no estan familiaritzats amb els models basats en equacions mestres, l'autor recomana llegir primer l'apèndix A que proporciona la base matemàtica per entendre el capítol 2. Els Apèndixs B, C i D juntament amb l'Apèndix A donen la base matemàtica necessària per seguir el capítol 3 i el capítol 4.

Chapter 1

Introduction

This PhD Thesis deals with some issues concerning the fluctuations in complex structured populations in particular those characterised by the existence of a latent state. Our aim is to better understand some questions arising in the dynamics of hierarchically organised populations of cells, such as the ones encountered in long-lived multicellular organisms characterised by ongoing cell differentiation, and the dynamics of HIV-1 in infected patients under anti-retroviral therapy. Both systems are characterised by the presence of a latent population, namely, stem cells and latently infected cells, respectively. This chapter is devoted to present the necessary biological background and motivation, summarising previous work done on the subject. We also give an overview of the mathematical models used in this PhD Thesis. Finally, we summarise our aims and objectives.

1.1 Motivation and biological background

Biological problems have been studied by scientists via four different type of models: *In vivo*, *In vitro*, Data Driven and Mechanistic Models. Although, Mechanistic Models are the ones which gives a better understanding of the dynamics of the process that are studying, has also been the less successful in biology.

Mechanistic Models have been traditionally used by mathematicians and physicists to study biological problems using continuous and deterministic approaches. However, in some cases, this models can be not very accurate. If the population is small, we can not can not assume that the mean-field model will be a good approximation of the reality. This is relevant in many biological problems, where often one finds small populations.

It has been shown that intrinsic noise, i.e. fluctuations to the system due to its small size, can have very strong influence on the behaviour of dynamical systems [14, 85, 42]. An introduction to the stochastic processes that we use have been included in the Appendix A about stochastic modelling and the Gillespie stochastic simulation algorithm, which will be the main tool to deal with our problems.

1.1.1 Latency in cell population dynamics

For the purposes of this thesis, latency or quiescence is defined as a cell state such that most cell functions, prominently proliferation, are slowed down. This down-regulation of cellular functions often emerges as a trade-off in exchange for longevity and survival in hostile environments. An example of this behaviour has been analysed in [3], where it

has been shown that latency can act as a an escape mechanism that allows a malignant population to elude the action of a drug, provided that cells of such population have the ability to go into a quiescent state in which cells are immune to the drug. By going into quiescence, a small latent population is able to survive, and eventually re-grow once the drug has been cleared off. A particular instance in which this model is relevant is resistance to chemo- or radio-therapy in tumours with hypoxic (ill-oxygenated) regions. Hypoxic cells undergo radical reduction of their proliferation rate, making them less sensitive to these therapies than fast-cycling cells, thus providing a reservoir of immune cells which, upon stopping the therapy, provide a reservoir for which (partial) re-grow occurs. Besides escape from therapy, quiescence-like phenomena have been shown to play a role in cancer to elude not only therapy but the homeostatic controls of normal tissue. Roesch et al. [108] have characterised a slow-cycling (latent) sub-population within the much faster proliferating population of melanoma cell which is necessary for continuous tumour growth.

Another example of a pathology where latency has proved crucial to understand certain aspects of HIV-1 infection and its response to therapy. HIV infection can be effectively controlled by potent anti-retroviral therapies. However, such therapies do not accomplish total eradication of the disease. Although they effectively eliminate virus-producing infected T cells, early study of the long-term viral load in treated patients revealed that low-level (below the detection limit of standard clinical analysis), residual viremia persisted for very long time (months or even years) [110, 123]. These results suggested that the infection persisted in the treated patients in the form of a compartment that was insensitive to the drugs. Several hypothesis were formulated regarding the nature of this compartment, but the one that appears to have consolidated itself as the most likely explanation is that of a latently infected population of T cells. This cellular compartment consists of slow-proliferating cells (probably memory cells) which store the virus but do not replicate it. Since this cells do not replicate the virus they remain unaffected by the anti-retroviral drugs. Furthermore, upon stimulation with specific antigens, they become active and resume virus production and proliferation, which, in turn, replenishes the latent compartment. This feed-back cycle sustains the persistent low-level viremia. The presence of this latent infection has been recognised as major barrier for complete eradication of HIV-1 infection and the search for ways to tackle it has become a very active of research [121, 113, 65, 66].

Quiescent behaviour is also part of normal physiological regulation of tissues. In particular, stem cells, which are the essential building blocks of tissues in multi-cellular organisms, spend most of their life span in a latent, non-proliferative state. Only upon reception of the appropriate signalling cues, stem cells activate and proliferation ensues. These signalling cues are secreted in response to a decrease in the number of mature (terminally-differentiated) cells that are at the summit of the corresponding differentiation cascade: when mature cell numbers decline stem cell proliferation activates in order to replenish the partially depleted mature cell compartment. Although, this mechanism is part of normal tissue regulation, it can be subverted by pathologies such as cancer which highjack the properties of stem cells.

The overarching aim of this thesis is to use stochastic modelling along with asymptotic and numerical techniques to better understand the basic mechanisms involved in the dynamics of cell populations with feed-back regulated latency in order to propose control strategies that help in formulating better, more rationally grounded therapeutic approaches for pathological situations arising from disregulation of differentiation cascades

and HIV-1 latent infection.

1.1.2 Stochastic dynamics of differentiation cascades with regulatory feed-back

In Chapter 2 we analyse the factors that affect the robustness of cell populations with hierarchical structure. Tissues in higher organisms such as mammals maintain homeostasis by means of cascades of serial cell differentiation [4]. These cascades are composed by hierarchically-organised compartments of different cell types. The cornerstone of this system is stem cells (SCs) which sustain the tissue by producing both more stem cells, a property known as self-renewal, and lineage-specific differentiated cells. The serial differentiation cascade proceeds through a number of intermediate stages or compartments of transient amplifying cells (TACs) until it terminates with the compartment of fully-differentiated mature cells (MCs).

There has been much discussion around the issue of how SCs accomplish the feat of undergoing both self-renewal and differentiation [91, 92, 71, 114, 72]. One strategy by which SCs can perform these two tasks is asymmetric cell division, whereby, upon SC division, one daughter cell retains the cellular identity of its mother whereas its sister differentiates. Asymmetric cell division seems to proceed through segregation of the material that determines cell fate so that, when the SC divides, one of the daughters keep the stem cell-fate determinants. Lineage-specific determinants are thus passed onto its sister cell [71, 72].

Although asymmetric SC division is a simple and elegant solution to the stem cell puzzle, there has been much controversy around what is perceived to be a fundamental flaw of this model, namely, asymmetric division does not allow the stem cell compartment to expand [91, 92]. The argument runs that in situations such as injury, where the rate of cellular turnover must be largely increased in order to regenerate the affected tissue, the size of the SC pool should undergo a marked expansion. This hints that asymmetric division might not be the full solution.

Experimental evidence points out to the fact that SCs in some tissues, such as the central neural system [50] and the epidermis [74], can divide symmetrically. Symmetric SC division consists of both daughter cells sharing the same fate: SC or differentiated. In this way, the number of cells is regulated by the frequencies of (symmetric) divisions producing SCs or differentiated cells. Since this division modality allows for expansion of the SC compartment, an alternative model arises [91] where most SCs can divide both symmetrically and asymmetrically with the balance between these two proliferation modes controlled by environmental signals to produce the appropriate number of SCs and differentiated cells. However, it has been recognised that, whilst symmetric division confers the capability of enhanced growth and increased regenerative capacity, it also increases the likelihood of cancer. This view is supported by findings according to which the cellular machinery involved in asymmetric division has been evolutionary conserved with a role in tumour suppression, the gene products that promote symmetric SC division also function as oncogenes [91].

Our aim is to analyse the stochastic dynamics of cell differentiation cascades where both modes of SC proliferation occur. We will study optimality strategies where by a trade-off between symmetric division (which enhances adaptability) and asymmetric division (which endows stability).

1.1.3 Stochastic dynamics and extinction of HIV-1 in patients under potent anti-retroviral therapy

HIV infection has been proved to be effectively controlled by administration of anti-retroviral therapy (ART). Despite the great success of of highly-active ART (HAART), the goal of curing, in the sense of completely eradicating, HIV-1 infection is yet to be achieved [105]. Quantitative analysis of the temporal evolution of plasma viral load upon HAART treatment suggests the existence of several phases in the therapy-induced decay of the viral load [102, 69, 111]. After an initial shoulder, reflecting delays associated to both the pharmacokinetics and the production of virus by newly infected cells [101, 55], a first phase of fast exponential decline of the viral load is observed where viral load is reduced by one to two orders of magnitude over a period of time of approximately two weeks. This fast response stage, with half-lime time of the order of days, reflects short half-life time of plasma virus and of productively infected CD4+ T lymphocytes [57, 124, 83]. Following this initial phase of fast decline in plasma viral load, a second stage of slower decay starts with a half-life time between one and four weeks. This phase reflects the contribution to virus load of infected cells with longer half-life time, such as macrophages, and infected CD4+ T cells that exhibit a lower rate of viral replication [99, 58, 126]. After this second stage, plasma virus load has normally fallen below the detection threshold of standard clinical assays ($\sim$ 50 copies RNA/ml). However, following this second phase, HAART appears to fail to completely eradicate the infection. Rather, a third stage ensues with much longer half-life time than the previous ones (of the order of years [69]) in which residual levels of viral load (1-5 copies RNA/ml detectable only by supersensitive assays) persist in plasma as well as in other bodily compartments, such as semen.

The question of what is the source of this residual viral load has triggered much debate which has materialised in several working hypothesis. One of these hypothesis invokes the possibility that HAART is not completely suppressive thus allowing the infection to continue to replicate in anatomical HIV-1 reservoirs [102], in particular within the so-called "drug sanctuaries", i.e. sites of poor drug penetration where the infection is allowed to persist [67].

An alternative model,which is abundantly supported by recent studies, suggests that, although HAART is fully suppressive, a cellular reservoir exists which allows the infection to linger in latent form [102] with residual viral load is the result of the activation of the latently infected cells [102]. Such a latent reservoir is established within the population of infected CD4+ T memory cells [25, 24] and, therefore, they remain in the resting state in the presence of HAART for prolonged periods of time. As a consequence, latently infected cells are able to escape the effect of the drug and immune surveillance due to the fact that they undergo no duplication and, consequently, exhibit very low levels of HIV-1 messenger RNA [111]. However, since latently infected cells release virus when stimulated with the proper antigen, viral rebound will eventually occur when HAART is withdrawn leading to HIV-1 infection recurrence, consistent with a wider scenario of quiescence-induced escape [3].

Once HAART has forced the infection to enter the latent stage, one can observe transient episodes of viremia where the viral load raises above the standard test detection limit (50 copies mRNA/ml) for a brief period of time [33, 104, 54, 95]. These episodes are referred to as *blips*. The origin and clinical relevance of these blips remains unclear and a number hypothesis have been formulated [111].

Given the inability of HAART to hit latently infected cells, combined therapies sup-

pressing the latent reservoir has been proposed [105]. A promising avenue in this direction consists of combining HAART with agents that specifically activate latently effective cells, thus rendering them susceptible to attack by HAART. The rationale for this combined therapy is that increasing the activation rate of the latently infected cells the size of this compartment should decay rapidly and, due stochastic fluctuations, these cells eventually will be suppressed taking all the infected population with them.

1.2 Mathematical framework

Generally speaking, the problem we address in this thesis concerns the stochastic dynamics of populations with different cell types. The framework most suited for dealing with such problem is that of population dynamics. Since during the latent state numbers of individuals are low, we need to model our populations in terms of stochastic processes, in particular of Markov processes [44]. The Markov process for the population dynamics will be formulated in terms of the corresponding Master Equation. These equations are notoriously difficult to solve exactly and in any practical case one must resort to approximate methods to deal with it.

In some cases we are dealing with small populations, and in other situations we are looking for rare events, for that reason we use the semi-classical approximation, which is a WKB approximation [73] to compute the probabilities of rare events.

We include a detailed explanation of the semi-classical approach in Appendix B. This approximation transforms our problem of dealing with a Master Equation to a problem of classical mechanics with a Hamiltonian with several degrees of freedom, as many as cell types. To compute the invariant manifolds of this system, which usually is the first step in the study of these dynamical system, is not easy and require non-linear approach, techniques such as parametrisation method [17, 18] to obtain high-order expansion. More difficulties associated to such systems appear due to their slow-fast nature. Furthermore, the study of motion near hyperbolic points may be necessary. To integrate the equations of motion, Taylor integrator methods [64] combined with, automatic differentiation techniques [64] allow us to use larger steps achieving higher accuracy than other explicit methods, such as Runge-Kutta, can provide. The Taylor integrator method, is not a symplectic integrator, i.e. it does not preserve the Hamiltonian structure of the equations, however, this is irrelevant, since one can require a local error below the roundof machine error. In Appendix C we explain the methods used to study these Hamiltonian systems.

Although we have made some progress in large-size asymptotic treatment of these problems, we heavily relay in simulation and numerical methods. Our main tool to study the Master Equation will be the Gillespie Stochastic Simulation Algorithm (SSA), which is a numerical Monte Carlo technique based on a reinterpretation of the Master Equation. In Appendix A this methodology is explained in detail. The Gillespie SSA requires large computational times, in particular when (i) large systems are considered and (ii) when separation of time scales appears. In the latter case, time-scale separation can be taken advantage of formulate a more efficient variant of the SSA proposed by Cao et al. [20], this method is explained in detail in Appendix D.

1.3 Aims and objectives

The main aim of this PhD Thesis is to study the effect of fluctuations in coupled populations of biological systems where cells in latent states play a major role. In doing so, we try to put to forward some biologically meaningful aspects of the dynamics of these systems. The specific points we aim to cover and the organisation of the thesis are as follows.

In Chapter 2, we study the behaviour of cell populations with hierarchical structure from the point of view of their stability properties. In particular,

1. Symmetric vs Asymmetric division in the stem cell compartment. We study the robustness of hierarchically-organized populations, depending on whether stem cells divide symmetrically, asymmetrically, or both. We assess how the symmetric division affects the stability of the population, regarding the role of stem cells symmetric division of SC in cancer progression.

2. The competition between population with different modes of stem cell division. This is crucial in order to find optimal architectures to maximize the robustness (long-time survival, resistance to invasion and ability to invade) of hierarchical populations.

3. The influence of parameters such as the duplication and death rate of the stem cells, the average life-time of the fully differentiated cells, the length of the differentiation cascade and the fluctuations of population of stem cells on the robustness and optimality of differentiation cascades.

In Chapter 3, an homogeneous model of combined HAART and latently infected cell activation therapies of the HIV-1 dynamics in the blood stream is presented. We are interested in

1. The effect of the activation rate of the latently infected cells in the extinction time of the infection. In particular we analyse if the therapies based on increase this rate are able to suppress the infection in a reasonable time.

2. The importance of the efficiency of the anti-retroviral therapies, including the limiting case of an efficiency of 100%, in the size of the persistence viral load.

3. The formulation of an asymptotic theory based on the semi-classical quasi-steady state approximation to describe the dynamics of the process. The accuracy of this asymptotic method is compared to the multi-scale SSA proposed by Cao et al.

In Chapter 4, we extend a model proposed by Rong and Perelson [110] to a non-homogeneous model of the HIV-1 dynamics in the blood stream, we consider that cells and virons are not uniform distributed in the blood stream. The specific points we aim to address are:

1. The mechanism for the emergence of transient episodes of viremia, known as viral blips. In particular, we investigate if they are the product of inhomogeneous density fluctuations or another mechanism must be considered.

2. If the appearance of viral blips is affected by laboratory procedures, such as the time elapsed between the blood sample extractions and the observations.

3. Whether the likelihood, amplitude and frequency of the viral blips is affected by the different of possible types of viral production, namely, continue vs burst.

In Chapter 5, we proceed to discuss our results, compare, when possible, with previous models or experimental results, and we give directions for future work.

Details regarding methodological issues, as well as an introduction to the stochastic modelling via the Master Equation, are give in the appendices. For those who are not familiarised with models based on Master Equations, the author recommends read first Appendix A which provides the mathematical background to understand Chapter 2. Appendices B, C and D together with Appendix A provide the necessary mathematical background to follow Chapter 3 and Chapter 4.

Chapter 2

Robustness of differentiation cascades with symmetric stem cell division

Stem cells perform the task of maintaining tissue homeostasis by both self-renewal and differentiation. Whilst it has been argued that stem cells divide asymmetrically, there is also evidence that stem cells undergo symmetric division. Symmetric stem cell division has been speculated to be key for expanding cell numbers in development and regeneration after injury. However, it might lead to uncontrolled growth and malignancies such as cancer. In order to explore the role of symmetric stem cell division, we propose a mathematical model of the effect of symmetric stem cell division on the robustness of a population regulated by a serial differentiation cascade and we show this may lead to extinction of such population. We examine how the extinction likelihood depends on defining characteristics of the population such as the number of intermediate cell compartments. We show that longer differentiation cascades are more prone to extinction than systems with less intermediate compartments. Furthermore, we have analysed the possibility of mixed symmetric and asymmetric cell division against invasions by mutant invaders in order to find optimal architecture. Our results show that more robust populations are those with unfrequent symmetric behaviour.

2.1 Biological Background

There is large body of literature examining the properties of differentiation cascades, in particular in the haematopoietic system [1, 29, 82] and in relation to several kinds of leukaemias and haematological diseases [26, 27, 87, 77]. Marciniak et al. [82] have studied a deterministic model in which they explore the role of regulation in a system with asymmetric SC division. They have found that for their model to exhibit efficient repopulation, regulation by environmental signals must occur at the level of the fraction of self-renewal. Mackey and co-workers [26, 27, 77] have done extensive modelling and analysis of a number of haematological diseases in which circulating cellular blood components exhibit oscillatory behaviour. By means of delay-differential-equation models and exhaustive parameter sensitivity analysis, they have proposed which processes in the haematopoietic differentiation cascade are more likely to be involved in the development of disease. They have

also found that delays in the differentiation cascade are fundamentally linked to the onset of the oscillations, a mechanism akin to the extinction mechanism we explore here. Dingli et al [32] have studied a model of the architecture and dynamics of hematopoiesis to provide estimates of the number of compartments, the size of each compartment, and the corresponding replication rates.

There has also been a number of stochastic models of serial differentiation cascades that tackle evolutionary issues. The model proposed by Pepper et al. [98] deals with a number questions arising when considering which evolutionary purpose can such a costly system (from the energetic point of view) possibly serve. The conclusion of their study is that differentiation cascades provides with intrinsic protection against somatic mutations leading to malignancies such as cancer. Evolution towards malignant behaviour and cancer has been studied, for example, by Sun & Komarova [119] and Rodriguez-Brenes et al. [106, 107], where the mechanisms of regulation of normal tissues are studied in detail to ascertain how can they be subverted in order to produce cancer. Other related work is the symmetric stem cell division models proposed by Dingli et al. [31], were a Moran process is proposed to study the competition between a population of normal stem cells and a population of cancer stem cells. They observed that a larger duplication rate in the invader (cancer) stem cells increases the probability of invasion.

Michor and co-workers [39, 75, 87, 88, 86] have modelled the dynamics of myleoid leukemia using models consisting of hierarchical differentiation cascades. It has been found that cancer initiation requires only a single mutation. Their models suggest that imatinib is a potent inhibitor of the production of differentiated leukemic cells, but does not deplete leukemic stem cells. Lenaerts et al [78] have shown that although imatinib, does not eradicate chronic myleoid leukemic, due to the stochastic nature of hematopoiesis, leukemic stem cells undergo extinction. This result shows the importance of stochastic effects on the dynamics of hierarchical cell populations.

Zhao et al. [127] have proposed a linear model for colonic epithelial cells, that explicitly takes into account the proliferation kinetics of a cell as a function cell position within the crypt, They have observe that those cells with mitotic activities concentrated near the stem cells delay the rate of mutation accumulation in colonic stem cells.

Mutations in hierarchically structured populations have been previously studied by Werner et al. [125], they modelled a general hierarchically organized multi-compartment tissue, allowing any number of mutations in a cell. They showed that these tissues strongly suppress the cells that are carrying multiple mutations. Traulsen et al [120] have studied the effect of different kinds of mutations and showed that although neutral mutations often leads to clonal extinction, disease is still possible, and in this case, it may become difficult to eliminate neutral mutations with therapy.

Also related to the context of this section, a mechanism for stochastic evolutionary escape and its consequences for drug resistance based on the presence of a quiescent, drug-resistant population has been recently described [3]. Since quiescent cancer stem cells have been recently found in intestinal crypts [16], this escape mechanism can be relevant to ascertaining the efficacy of therapies targeting cancer stem cells.

The aim of this chapter is to address some of the issues arising from the consideration of symmetric SC division in serial differentiation cascades, in particular those regarding the evolution of uncontrolled growth and the risk of cancer. To do so, we consider a stochastic mathematical model of the serial differentiation cascade and use it to address two problems (i) the long-term viability (stability) of a population of cells maintained by a

differentiation cascade whose SCs undergo symmetric division only, and (ii) the likelihood of invasion of a mutant population with increased symmetric SC division in competition with a population with asymmetric SC division (robustness). Regarding the former, we show that serial differentiation cascades with symmetric SC differentiation exhibit an intrinsic instability mechanism which induce extinctions with high likelihood. Thus, these cascades seem to have an in-built fail-safe mechanism against excessive symmetric SC division. The competition model allows us to estimate *optimality* conditions in, in the sense of maximum robustness, for the rate of symmetric division in terms of maximising its chance to take over another population with less symmetric-division capability whilst minimising its chances of undergoing extinction.

The organisation of the section is as follows. Section 2.2 is devoted to presenting our model of a differentiation cascade with symmetric SC division in detail and discussing its underlying hypothesis. In Section 2.3, we present simulation results for this model and discuss the emergence of a mechanism of extinction induced by symmetric SC division. In Section 2.4, we analyse the robustness of the different division strategies by formulating a model for the competition between populations using different such strategies and extract conclusions regarding their optimality. Finally, in Section 2.5, we summarise our results.

2.2 Stochastic modelling of a serial differentiation cascade with symmetric SC division

In this section we proceed to present and discuss our stochastic model of a hierarchically-organised cell population. Our aim is to formulate a regulated stochastic model which, by incorporating symmetric SC division, can lead to changes in the size of SC compartment. Regulation is achieved by means of a cytokine which is produced by the MC compartment which controls the rate of apoptosis of the stem cells.

The stochastic approach is justified by the small number of stem cells, typically present in their host organism. For example, according to [91], in the haematopoietic system only a 0.003 % of the cells are SCs. Given these small numbers in the SC compartment, we expect random effects to be important if not dominant.

2.2.1 Model description

We consider a compartmental model of the serial differentiation cascade with symmetric SC division. As shown in Fig 2.1 each compartment corresponds to a stage in the cascade: from the SC compartment to the MC compartment with a number of intermediate TAC compartments. We further introduce in our model the secretion of a cytokine by the MCs which regulates the size of the SC compartment. We study the dynamics of the population of cells in each compartment. In particular, we examine the behaviour of a differentiation cascade of length $n+1$, with stem cells, $n-1$ partially-differentiated, transient amplifying cells, and mature cells: x_0 represents the number of SCs, x_i with $i = 1, ..., n-1$, the number of TACs at differentiation stage i, and x_n, the number of MCs. Furthermore, x_{n+1} represents the amount of a cytokine which regulates the size of the SC compartment through a negative-feedback [81, 26, 27, 118]. Such cytokine is secreted at a rate wich is proportional to the number of fully-mature cells. Therefore, this negative feedback accounts for the mature-cell regulation of the size of the SC compartment which has been incorporated, for example, in models of haematopoeitisis [82].

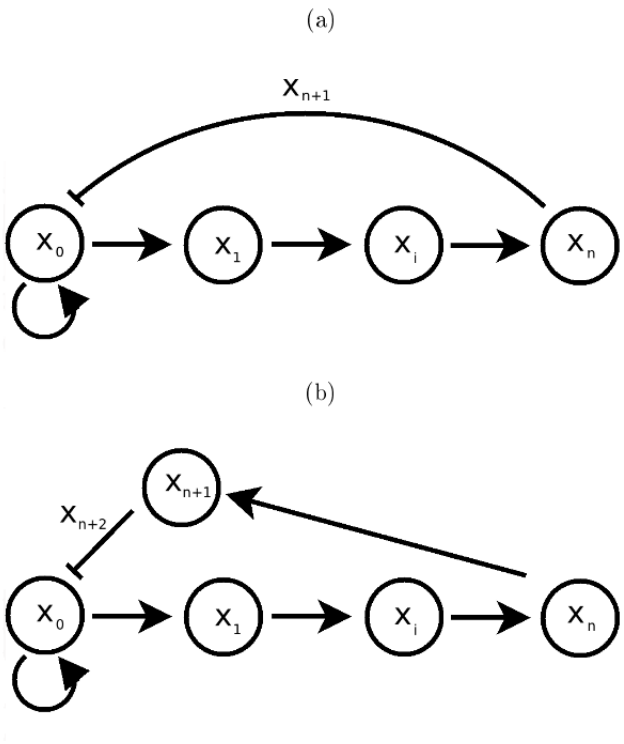

Figure 2.1: Diagrammatic representation of the hierarchic differentiation cascade. x_0 represents the population of the SC compartment, x_i the population of TAC cells at i stage, x_n the population of the MC compartment and x_{n+1} represents the amount of cytokine. Plot (a) corresponds to the well-stirred scenario, whereas plot (b) corresponds to the delayed scenario (see main text for details).

Transition rate	$r_j = (\Delta x_0^j, \Delta x_1^j, ..., \Delta x_{n+2}^j)$	Description
$W_1 = px_0$	$(1, 0, ..., 0)$	SC self-renewal
$W_2 = d_0 x_0$	$(-1, 2, 0, ..., 0)$	SC differentiation
$W_3 = \lambda_0 x_0 x_{n+1}$	$(-1, 0, ..., 0, -1, 0)$	SC apoptosis
$W_{2+2i} = \lambda_i x_i$	$(0, ..., -1, ..., 0)$	TAC apoptosis
$W_{3+2i} = d_i x_i$	$(0, ..., -1, 2, 0, ..., 0)$	TAC differentiation
$W_{2+2n} = \lambda_n x_n$	$(0, 0, ..., -1, 0, 0)$	MC apoptosis
$W_{3+2n} = sx_n$	$(0, 0, ..., 0, 1, 0)$	Cytokine secretion
$W_{4+2n} = \lambda_{n+1} x_{n+1}$	$(0, 0, ..., 0, -1, 0)$	Cytokine clearance (well-stirred scenario)
$W_{5+2n} = s_2 x_{n+1}$	$(0, 0, ..., 0, -1, +1)$	Cytokine transport
$W_{6+2n} = \lambda_{n+2} x_{n+2}$	$(0, 0, ..., 0, -1)$	Cytokine clearance (delayed scenario)
$W_{7+2n} = \lambda_0 x_0 x_{n+2}$	$(-1, 0, ..., 0, -1)$	SC apoptosis

Table 2.1: Transition rates corresponding to the stochastic model of the serial differentiation cascade with symmetric stem cell division. A description of the corresponding elementary population-dynamical processes is given in Section 2.2.1. We choose $d_0 = 1-p$ day^{-1}, to have that stem cells divide, in average, once per day, $\lambda_i = 0.01$ day^{-1} and $d_i = 1 - \lambda_i$ day^{-1} for $i = 1, ..., n-1$. s is fixed in the following way: from equation (2.5), at the steady state we have $0 = s\overline{x_n} - \lambda_{n+1}\overline{x_{n+1}} - \lambda_0 \overline{x_0 x_{n+1}}$, this implies $s = \frac{\lambda_{n+1}\overline{x_{n+1}} + \lambda_0 \overline{x_0 x_{n+1}}}{\overline{x_n}}$.

Our stochastic model is formulated in terms of the corresponding master equation [122, 44]:

$$\frac{\partial P(X,t)}{\partial t} = \sum_j \left(W_j(X - r_j, t)P(X - r_j, t)) - W_j(X,t)P(X,t)\right) \tag{2.1}$$

where $X = (x_0, \ldots, x_n, x_{n+1})$ and $P(X,t)$ is the probability of the population vector to have value X at time t. For full specification of our stochastic models, we need to prescribe the transition rates, $W_j(X,t)$, corresponding to the probability per unit time of the process j. These rates are modelled in terms of the law of mass action [47]. r_j is the change in X when elementary process j occurs, i.e. $X(t + \Delta t) = X(t) + r_j$ with probability $W_j \Delta t$.

We will consider two different scenarios schematically represented in Fig. 2.1. The first one, corresponding to Fig. 2.1.(a) and which will be referred to as the well-stirred scenario, the cytokine which controls the size of stem cell compartment is assumed to be instantaneously transported to the it. By contrast, the second scenario, corresponding to Fig. 2.1.(b) and to be referred to as the delayed scenario, the cytokine requires a finite amount of time to reach the stem cell compartment. We have modelled this by introducing a compartment where, upon secretion, the cytokine is transported to at a certain rate. The elementary processes involved in our model are:

- SCs divide symmetrically, so that they can undergo:
    1. Self-renewal. Both daughter cells share the SC fate of the mother with transition rate W_1 (see Table 2.1)
    2. Differentiation. Both daughter cells differentiate to first-stage TAC with transition rate W_2 (see Table 2.1)

3. Apoptosis with cytokine-regulated transition rate W_3 if we are considering the well-stirred scenario or W_{7+2n}, otherwise (see Table 2.1)

- Stage-i, $i = 1, \ldots, n-1$, TACs can undergo:

  1. Differentiation. Both daughter cells differentiate to either the next TAC stage (if $i < n-1$) or to the MC compartment (if $i = n-1$) with transition rate W_{2+2i} as given in Table 2.1
  2. Apoptosis with transition rate W_{3+2i} as given in Table 2.1

- MCs can undergo:

  1. Release cytokine with transition rate W_{3+2n} as defined in Table 2.1
  2. Apoptosis with transition rate W_{2+2n} as defined in Table 2.1

- Cytokines can undergo:

  1. Clearance with transition rate W_{4+2n} if we are considering the well-stirred scenario, or W_{6+2n}, otherwise (see Table 2.1)
  2. Transport to the intermediate compartment (x_{n+2} in Fig. 2.1.(b)) with transition rate W_{5+2n} if we are considering the delayed scenario (see Table 2.1).

We will analyse this system by means of numerical Monte-Carlo simulations using the Gillespie stochastic simulation algorithm [47, 48]. The mean-field limit of the model also provides useful information. For the model described by Eq. (B.1) and Table 2.1, corresponding to the well-stirred scenario , the mean-field model is given by the following system of ODEs:

$$\dot{x}_0 = px_0 - d_0x_0 - \lambda_0x_0x_{n+1}, \tag{2.2}$$
$$\dot{x}_i = 2d_{i-1}x_{i-1} - \lambda_ix_i - d_ix_i,\ i = 1, ..., n-1, \tag{2.3}$$
$$\dot{x}_n = 2d_{n-1}x_{n-1} - \lambda_nx_n, \tag{2.4}$$
$$\dot{x}_{n+1} = sx_n - \lambda_{n+1}x_{n+1} - \lambda_0x_0x_{n+1}, \tag{2.5}$$

which has two fixed points. The trivial (unstable) equilibrium $(0, 0, ..., 0)$, which corresponds to the extinction of the system, a positive equilibrium fixed point, P_S

$$P_S = \left(\frac{\lambda_1x_1 + d_1x_1}{2d_0}, ..., \frac{\lambda_{j+1}x_{j+1} + d_{j+1}x_{j+1}}{2d_j}, ..., \frac{\lambda_nx_n}{2d_{n-1}}, x_n, \frac{p-d_0}{\lambda_0}\right) \tag{2.6}$$

We will fix the number of x_n cells at the metastable state. We denote as $\overline{x_i}$, the number of cells in the i compartment at the metastable state.

Our model assumes that the signal is produced by the mature cells, we do this assumption instead of consider that the signal is produced by, for example, the transient amplifying cells in position k. In this case the signal producing rate s, should be of the form:

$$s = \frac{\lambda_{n+1}\overline{x_{n+1}} + \lambda_0\overline{x_0x_{n+1}}}{\overline{x_k}}. \tag{2.7}$$

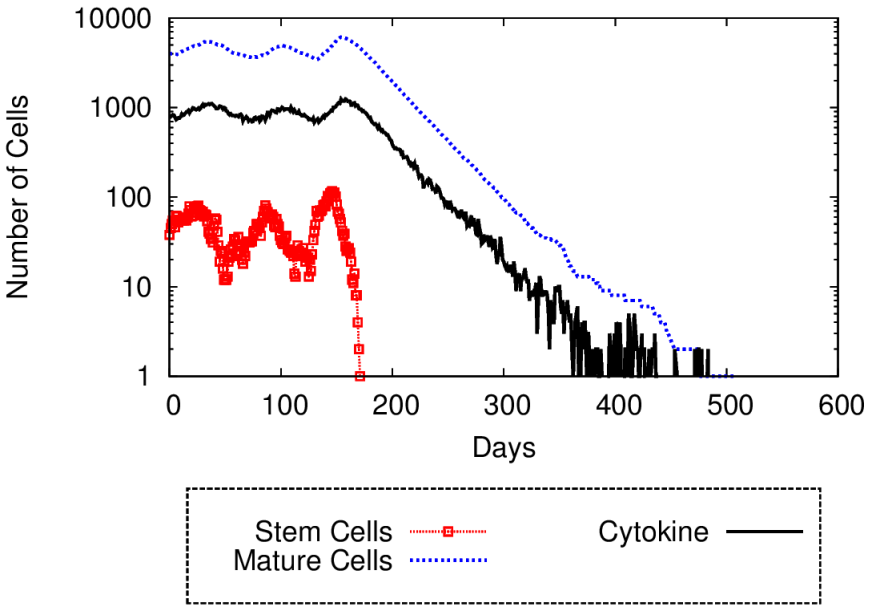

Figure 2.2: Gillespie simulation of a system with some parameter values that kill in a short time the population. The black line corresponds to the x_0 population and red and to x_n and x_{n+1} respectively. $p = 0.6$ day^{-1}, $\lambda_n = 0.03$ day^{-1}, $\lambda_{n+1} = 1$ day^{-1}, $\lambda_0 = \frac{1}{4000}$ day^{-1}, the Length of the differentiation cascade is 4.

The signal producing rate necessary to the cells in each compartment to keep the amount of signal necessary to control the population. We see that the only efficient possibility is that the signal is generated by the mature cells. However, this possibility of TAC cells producing signal is not out of our study. If the signal is produced by the x_k cells, the new system is equivalent to a system described above with length k taking as a new λ'_k (the death rate of the new mature cells) the value of $\lambda_k + d_k$, since the $x_{k+1}, ...x_n$ cells has no effect on the system.

In the scenario (b), that is, the cytokine is not transported immediately to the stem cells compartment, we consider another compartment, x_{n+2}, and the reactions $x_{n+1} \xrightarrow{s_2} x_{n+2}$ and $x_{n+2} \xrightarrow{\lambda_{n+2}} \emptyset$. changing $x_0 + x_{n+1} \to \emptyset$ by $x_0 + x_{n+2} \to \emptyset$. In the Section 2.3 we will see the effect of this change in function of the transport rate s_2.

2.3 Extinction induced by symmetric SC division

We now proceed to analyse the stochastic model described in Section 2.2.1 and describe an extinction mechanism intrinsic to the structure of a serial differentiation cascade with symmetric cell division. We interpret this mechanism as an anti-cancer mechanism inherent to the hierarchical structure of serial differentiation cascades.

2.3.1 Delay-induced extinction in serial differentiation cascades with symmetric SC division

In order to proceed with our analysis, we perform numerical simulations of our model by means of the Gillespie stochastic simulation algorithm [47, 48]. This algorithm is based on an exact reformulation of the stochastic process described by the master equation Eq. (B.1) which allows us to generate exact sample paths or realisations of the underlying process. An example of such a realisation which illustrates the extinction mechanism in our model with symmetric SC division is illustrated in Fig. 2.2.

Fig. 2.2 shows simulation results where the population has been initially set to be equal to the (stable) positive equilibrium of the mean-field limit Eqs (2.2)-(2.5). This particular example is illustrative of the mechanism through which extinction occurs. Initially a fluctuation in the system induces an increase in the number of SCs. This increase in SC population propagates through the differentiation cascade and it eventually reaches the MC compartment which starts expanding. Such expansion in MC numbers induces an increase in cytokine concentration, which, in turn, leads to decay in the size of SC compartment. As a consequence, oscillatory behaviour ensues. However, since the system, specially the SC compartment, is subject to fluctuations and these are amplified by the length of the differentiation cascade (an increase of one cell in the size of the SC compartment induces an increase $O(2^n)$ in the MC compartment), the amplitude of the oscillations grow until the SC compartment size hits the absorbing barrier at which point the population undergoes extinction.

Since delays appear to be instrumental for this extinction pathway, we are interested in the effects of altering the balance between the x_{n+1}/x_n cells life-time and the replenish rate via x_0 on the average extinction time. To carry on this analysis, we compute the extinction time as a function of the SC proliferation rate, p, and the death rate of the MCs, λ_n. Our results are shown in Figure 2.3.

Fig. 2.3 shows that there is a region in the λ_n-p-plane where the average extinction time, T_E, is such that $T_E > 10^4$ days. For all other values of these two parameters, the waiting time for extinction to occur becomes much shorter. It is relatively straightforward to see that the effect of these two parameters within the region of the parameter space where $T_E > 10^4$ is to cancel the effect of the delay between the SC and MC compartments due to the length of the differentiation cascade. Large values of the MCs death rate, λ_n, stabilises the system via a dissipative-like effect, namely, it impairs the ability of the MC compartment to expand in response to fluctuations in the SC compartment size. It also weakens the effect of the feed-back between the MC and SC compartments, as it effectively reduces the concentration of cytokine.

The effect of varying the value of the self-renewal rate, p, is slightly different. When $\frac{p}{d_0} \gtrsim 1$, the SC compartment cannot grow, on the contrary, under the effect of SC apoptosis and random fluctuations, it will dwindle and the population will become extinct. As p grows, its effect is strongly coupled to λ_n. If λ_n is small, i.e. the MC life expectancy is increased, the effects of fluctuations and delay are reinforced and the population undergoes rapid extinction. If, on the contrary, λ_n is large, we observe two regimes: A regime of intermediate values of p where the effects of fluctuations and delay are cancelled by the rapid death of the MCs (see above), and a regime of high values of p where MC death is not fast enough to compensate for the increased effects of fluctuations in the SC compartment which take over and produce short survival times.

Another model parameter that has an obvious effect on the delay is the length of the

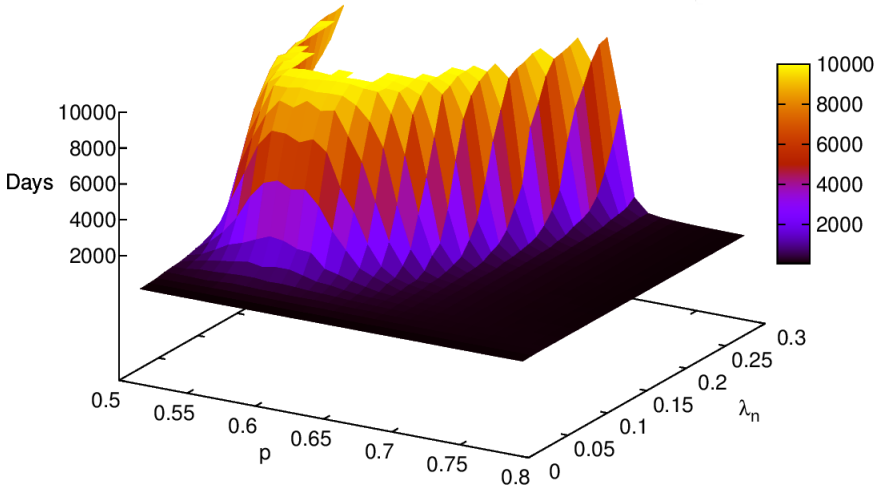

Figure 2.3: This plot represents the extinction time of the system depending on the parameters λ_n and p. The length of the differentiation cascade is $n = 5$, the x-axis is the death rate of the mature cells, the y-axis is the duplication probability of the stem cells, the z-axis is the days needed to get an extinction, the white color means that more than 10000 days ($\sim$ 30 years) are needed to get an extinction. $\lambda_{n+1} = 1$ day^{-1}, The number of mature cells at the metastable state is $\overline{x_n} = 5000$, $\lambda_0 = \frac{1}{2500}$ day^{-1}.

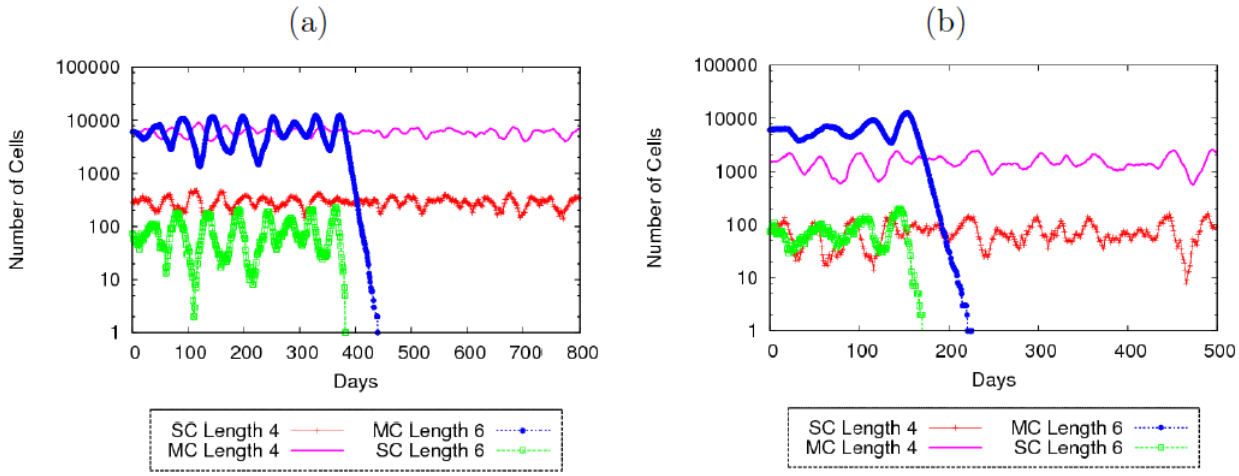

Figure 2.4: Sample paths of the dynamics of our serial differentiation cascade model obtained by means of the stochastic simulation algorithm. Plot (a) corresponds two different cascades with length $n = 4$ and length $n = 6$ with the same number of MCs. Plot (b), idem fixing the number of SCs, instead. We observe that, in both cases, shorter cascades ($n = 4$) are more stable that longer ones ($n = 6$). $\lambda_{n+1} = 1$ day^{-1}, $\lambda_0 = \frac{1}{6000}$ day^{-1}, $\lambda_n = 0.25$ day^{-1}, $p = 0.6$.

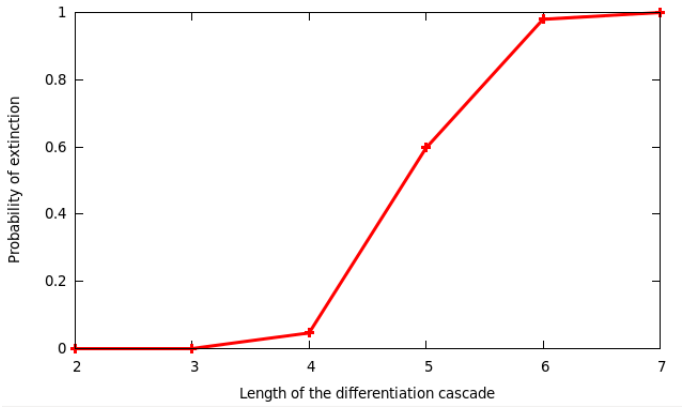

Figure 2.5: Simulation results corresponding to the dependence on the length of the differentiation cascade, n, of the probability of extinction within a time window $(0, T_E)$, $P_E(T_E)$, with $T_E = 1000$ days. $p = 0.53$ day^{-1}, $\lambda_n = 0.25$, $\lambda_{n+1} = 1$, $\overline{x_n} = 26000$, $\lambda_0 = \frac{1}{26000}$ day^{-1}.

differentiation cascade, n. Longer chains promote the effect of the delay and therefore favours extinctions. This is illustrated in Fig. 2.4, where we show sample paths of our model for different values of n. We see that indeed longer differentiation cascades destabilise the system and favour extinction. This is further explored in Fig. 2.5, where we show the extinction probability within the time window of time of duration $(0, T_E)$, $P_E(T_E)$, as a function of n. Fig. 2.5 shows a sharp increase in this quantity as n increases.

2.3.2 Delayed cytokine scenario

In this section we consider the delayed cytokine scenario where:

- The secreted cytokine, x_{n+1}, is transported to x_{n+2}, that is, $x_{n+1} \xrightarrow{s_2} x_{n+2}$, with transition rate transition rate $W_{5+2n} = s_2 x_{n+1}$
- The cytokine in x_{n+2} is degraded, that is, $x_{n+2} \xrightarrow{\lambda_{n+2}} \emptyset$, with transition rate transition rate $W_{6+2n} = \lambda_{n+2} x_{n+1}$
- The size of the SC compartment is controlled by x_{n+2}, that is $x_0 + x_{n+2} \to \emptyset$, with transition rate transition rate $W_{7+2n} = \lambda_0 x_0 x_{n+2}$

We start by analysing the mean-field behaviour of the system:

$$\dot{x}_0 = p x_0 - d_0 x_0 - \lambda_0 x_0 x_{n+1}, \tag{2.8}$$
$$\dot{x}_i = 2 d_{i-1} x_{i-1} - \lambda_i x_i - d_i x_i, \ i = 1, ..., n-1, \tag{2.9}$$
$$\dot{x}_n = 2 d_{n-1} x_{n-1} - \lambda_n x_n, \tag{2.10}$$
$$\dot{x}_{n+1} = s x_n - \lambda_{n+1} x_{n+1} - s_2 x_{n+1}, \tag{2.11}$$
$$\dot{x}_{n+2} = s_2 x_{n+1} - \lambda_{n+2} x_{n+1} - \lambda_0 x_0 x_{n+2}, \tag{2.12}$$

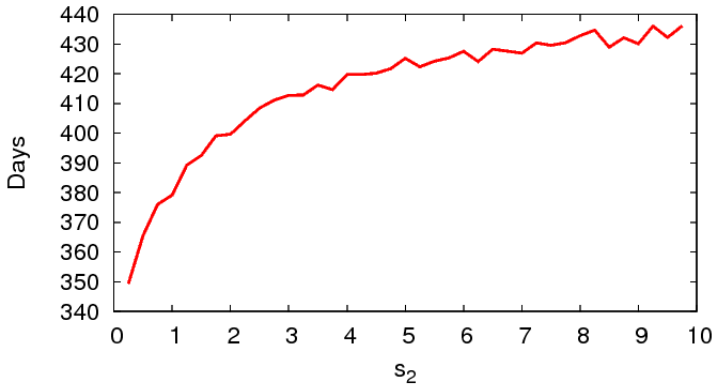

Figure 2.6: Extinction time in function of the transport rate s_2. $p = 0.6$ day^{-1}, $\lambda_n = 0.03$, $\lambda_{n+1} = 1$, $\lambda_{n+2} = 1$, $\overline{x_n} = 10000$, $\lambda_0 = \frac{1}{10000}$ day^{-1}, $n = 5$.

which implies that the secretion rate, s, is now determined by

$$s = \frac{(s_2 + \lambda_{n+1})(\lambda_{n+2}\overline{x_{n+2}} + \lambda_0\overline{x_0 x_{n+2}})}{\overline{x_n} s_2}, \tag{2.13}$$

and the positive equilibrium is of the form:

$$P_S = \left(\frac{\lambda_1 x_1 + d_1 x_1}{2d_0}, ..., \frac{\lambda_{j+1}x_{j+1} + d_{j+1}x_{j+1}}{2d_j}, ..., \frac{\lambda_n x_n}{2d_{n-1}}, x_n, \frac{\lambda_{n+2}x_{n+2} + \lambda_0 x_0 x_{n+2}}{s_2}, \frac{p - d_0}{\lambda_0} \right). \tag{2.14}$$

Note that if $\lambda_{n+2} = \lambda_{n+1}$, we recover the previous model when $s_2 \to \infty$.

We are interested in how the dependence of the behaviour of population on the cytokine delay, which is controlled by s_2. Fig 2.6 shows the extinction time as a function of s_2. In Fig 2.7, we have plotted s as a function of s_2, as given by Eq 2.13. Taken together, these two results show that a decrease in s_2 contributes to destabilise the population, since this contributes to increase the delay between cytokine secretion and SC response. Moreover, more cytokine needs to be produced to maintain the SC compartment size.

2.4 Robustness of populations with asymmetric SC division

So far, we have focused on the study of differentiation cascades with symmetric stem cell division. We have uncovered that symmetric stem cell division may induce extinction of the population, specially in long differentiation cascades where the delays in the regulation of stem cells by mature cells are more important. This result points out that utilisation of symmetric stem cell alone may not be an optimal strategy.

In normal situations, stem cell division is commonly believed to be mostly asymmetric with symmetric division being a rare event [71]. However, it has also been put forward that symmetric SC division could also play an important role, specially in situations, such as wound repair, where the SC compartment must be allowed to expand in order to compensate for an increased demand in cellular turnover [74]. In view of our results regarding the induction of instabilities by symmetric SC division, one could ask the question of how frequent symmetric SC division can be before anomalies in the population start to appear.

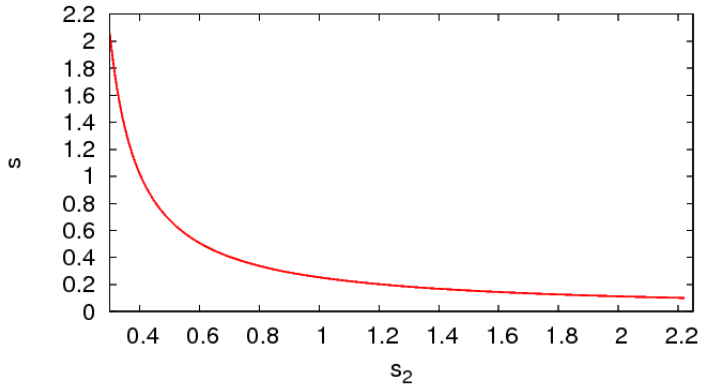

Figure 2.7: Value of s according to Eq. 2.13 in function of s_2. $p = 0.6$ day^{-1}, $\lambda_n = 0.03$, $\lambda_{n+1} = 1$, $\lambda_{n+2} = 1$, $\overline{x_n} = 10000$, $\lambda_0 = \frac{1}{10000}$ day^{-1}.

The aim of this section is to address these two issues, namely, whether symmetric SC division is an optimal strategy and the frequency of symmetric SC division, as well as ascertaining which are the generic features of an optim, i.e. maximally robust, differentiation cascade.

2.4.1 Stochastic modelling of a differentiation cascade with asymmetric stem cell division

Our first step is to present our stochastic model for a differentiation cascade with asymmetric stem cell division. We formulate our model in terms of the transition rates that go into the corresponding master equation Eq. (B.1), which are shown in Table 2.2. Model formulation is very similar to the one for the differentiation cascade with symmetric SC division: we consider the same $n + 2$ different cell and chemical species, i.e. SC, $n - 1$ TACs, MCs, and the MC-secreted cytokine.

The dynamics of this system is essentially the same as in the symmetric SC division case (see Table 2.1) except for the SC cell dynamics. Following Knoblich [71], we assume that SCs divide asymmetrically with occasional symmetric cell division is a rare event. We thus consider that SCs divide asymmetrically with probability $1 - e$. We further consider than the rate of asymmetric division is regulated (inhibited) by a cytokine produced by the mature cells [82]. These two factors are summarised in the transition rate W_1, Table 2.2. With probability e, SCs behave as a symmetrically-dividing cell, whose behaviour is characterised by transition rates W_1, W_2, and W_3, Table 2.2, i.e. a SC which behave as a symmetrically-dividing cell can (i) self-renew, (ii) differentiate, or (iii) undergo apoptosis, with probability rates W_1, W_2, and W_3, respectively. In our study, the parameters a and b will be chosen to have the same division rate as in the symmetric division model at the metastable state, that is, $\frac{(1-e)a}{b+\overline{y_{n+1}}} + ep + ed_0 = p + d_0$.

The mean-field behaviour of the model is described by the following system of law-of-mass action ODEs:

Reacting rate	$r_j = (\Delta y_0^j, \Delta y_1^j, ..., \Delta y_{n+1}^j)$	Description
$W_1 = \frac{(1-e)a}{b+y_{n+1}} y_0$	$(0, 1, ..., 0)$	asymmetric division–differentiation
$W_2 = epy_0$	$(1, 0, ..., 0)$	symmetric self-renewal
$W_3 = ed_0 y_0$	$(-1, 2, 0, ..., 0)$	symmetric differentiation
$W_4 = e\lambda_0 y_0 y_{n+1}$	$(-1, 0, ..., 0, -1)$	SC apoptosis
$W_{3+2i} = \lambda_i y_i$	$(0, ..., -1, ..., 0)$	TAC apoptosis
$W_{4+2i} = d_i y_i$	$(0, ..., -1, 2, 0, ..., 0)$	TAC differentiation
$W_{3+2n} = \lambda_n y_n$	$(0, 0, ..., -1, 0)$	MC apoptosis
$W_{4+2n} = sy_n$	$(0, 0, ..., 0, 1)$	Cytokine secretion
$W_{5+2n} = \lambda_{n+1} y_{n+1}$	$(0, 0, ..., 0, -1)$	Cytokine clearance

Table 2.2: Reaction rates corresponding to the stochastic dynamics of a differentiation cascade with both symmetric and asymmetric division. Symmetric division is considered to be a rare event which occurs with probability e [72]. We choose $d_0 = 1 - p$ day^{-1}, $\lambda_i = 0.01$ day^{-1} and $d_i = 1 - \lambda_i$ day^{-1} for $i = 1, ..., n-1$. s is fixed in the following way: from equation (2.19), at the steady state we have $0 = s\overline{y_n} - \lambda_{n+1}\overline{y_{n+1}} - e\lambda_0\overline{y_0 y_{n+1}}$, this implies $s = \frac{\lambda_{n+1}\overline{y_{n+1}} + e\lambda_0\overline{y_0 y_{n+1}}}{\overline{y_n}}$.

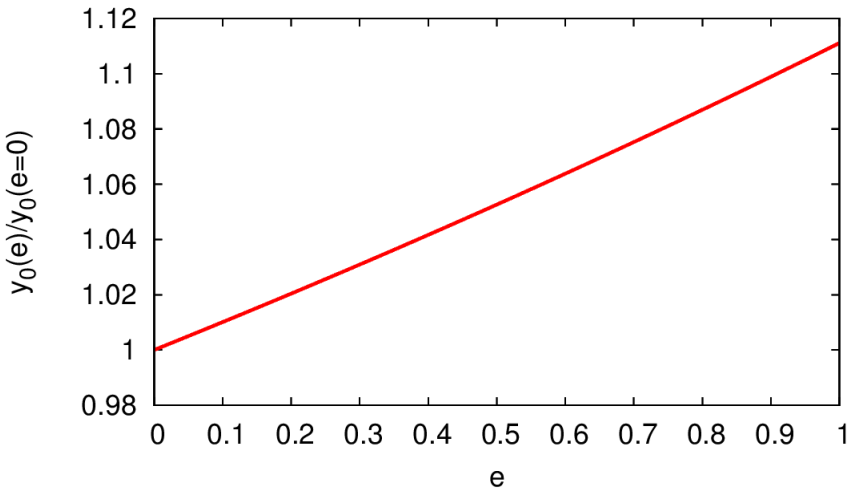

Figure 2.8: Relative size of the stationary average size SC compartment at the metastable state in function of e, $y_0(e)/y_0(e=0)$, as determined by Eq. 2.20. We have normalised with $y_0(e=0)$. Parameter values: $a = 1000$, $b = 700$, $\lambda_0 = \frac{1}{10000}$ day^{-1}, $\overline{y_n} = 10000$, $p = 0.55$ day^{-1}, $\lambda_n = 0.05$ day^{-1}, $\lambda_{n+1} = 1$ day^{-1}, the Length of the differentiation cascade is 4.

$$\dot{y}_0 = epy_0 - ed_0y_0 - e\lambda_0y_0y_{n+1} \tag{2.15}$$

$$\dot{y}_1 = \frac{(1-e)a}{b+y_{n+1}}y_0 + 2ed_0y_0 - \lambda_1y_1 - d_1y_1 \tag{2.16}$$

$$\dot{y}_i = 2d_{i-1}y_{i-1} - \lambda_iy_i - d_iy_i \qquad i = 2, ..., n-1 \tag{2.17}$$

$$\dot{y}_n = 2d_{n-1}y_{n-1} - y_n\lambda_n \tag{2.18}$$

$$\dot{y}_{n+1} = sy_n - \lambda_{n+1}y_{n+1} - e\lambda_0y_0y_{n+1} \tag{2.19}$$

Where y_i is the number of cells in the compartment i. The variables and parameters are described in the Table 2.2. Eqs. (2.15)-(2.19) have a positive equilibrium given by:

$$P_A = \left(\frac{\lambda_1y_1 + d_1y_1}{\frac{(1-e)a}{b+y_{n+1}} + 2ed_0}, ..., \frac{\lambda_{j+1}y_{j+1} + d_{j+1}y_{j+1}}{2d_j}, ..., \frac{\lambda_ny_n}{2d_{n-1}}, y_n, \frac{p-d_0}{\lambda_0} \right) \tag{2.20}$$

Fig. 2.8 shows the average stationary size of the stem cell compartment as predicted by Eqs. (2.15)-(2.19). We observe that, whilst an increase in the size of the SC compartment is obtained as e is let to grow, the magnitude of such increase, for the chosen set of parameter values, of the order of a 10 %.

Regarding the behaviour of the stochastic model, the main difference with respect to the symmetric cell division model (Table 2.1) involves the lack of delay-induced extinction behaviour exhibited by differentiation cascade model with pure symmetric SC division. This behaviour is illustrated in Fig. 2.9 where two typical sample paths are shown for different values of the probability of symmetric division, e. If the probability of symmetric division, e, is small, the variation in size of the SC compartment is bounded, which renders the system resilient to the effect of the delay-induced oscillations that, in the pure symmetric SC division system, eventually lead to extinction of SC compartment followed by the extinction of the whole population. Fig. 2.10, we have plotted the extinction probability of a differentiation with asymmetric SC division as a function of e and show that, indeed, differentiation cascades with small probability of symmetric division are impervious to the delay-induced extinction mechanism.

2.4.2 Competition between populations

We now move on to study of the robustness of the asymmetric population, that is, whether it can withstand attempts of invasion by other populations using different strategies. In what follows, such strategies will refer to variations of two parameters: The probability of symmetric division, e and the rate of symmetric self-renewal p. Our aim is to ascertain criteria of evolutionary optimality based on our results regarding the outcome of competition between populations characterised by different values of these parameters.

Asymmetric vs symmetric population

We start by studying the competition between a resident population generated by differentiation cascade with asymmetric SC division, hereafter referred to as A, and a symmetric-SC-division invader, referred to as S, whose population dynamics is given by the model described in Section 2.2.

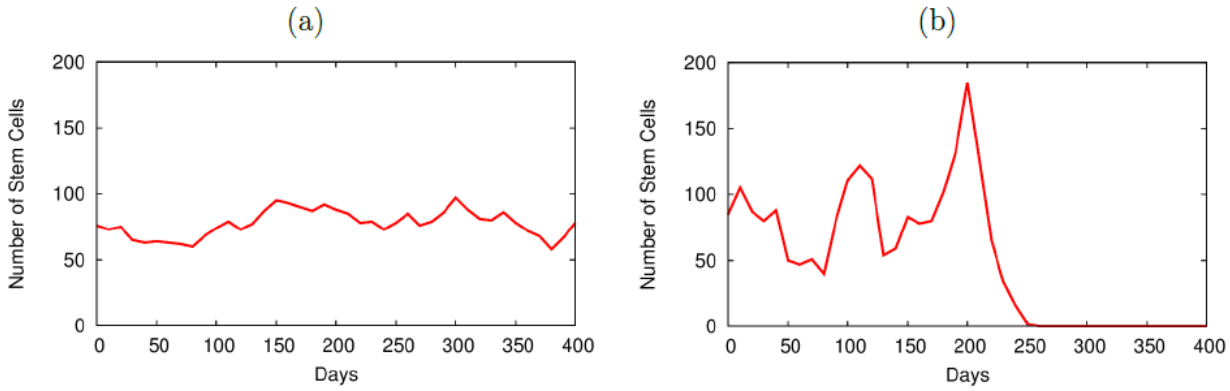

Figure 2.9: Sample paths showing the time evolution of the number of SCs for different values of e. Panel (a) corresponds to $e = 0.05$ whereas panel (b) shows a realisation with $e = 1$. Parameter values: $a = 1000$, $b = a - \overline{x_{n+1}}$, $\lambda_0 = \frac{1}{5000}$ day^{-1}, $p = 0.55$ day^{-1}, $\lambda_n = 0.03$ day^{-1}, $\lambda_{n+1} = 1$ day^{-1} $n = 4$, $\overline{x_n} = 5000$. We can see that the population with symmetric stem cells division becomes extinct much faster than the asymmetric.

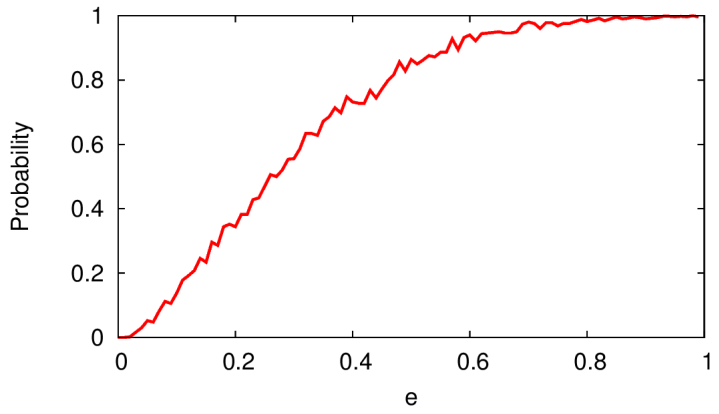

Figure 2.10: Simulation results corresponding to the dependence on the non asymmetric division probability of stem cells e, of the probability of extinction within a time window $(0, \tau)$, $P_E(\tau)$, with $\tau = 1000$ days. $p = 0.55$ day^{-1}, $\lambda_n = 0.03$, $\lambda_{n+1} = 1$, $\overline{x_n} = 6000$, $\lambda_0 = \frac{1}{6000}$ day^{-1} $a = 1000$, $b = a - \overline{x_{n+1}}$.

Mean-field behaviour. In order to proceed further, we start by giving some results regarding the behaviour of the mean-field limit using qualitative theory of ODEs. For simplicity, we will assume that both populations of mature cells are producing the same cytokine.

Let y_0 (x_0) be the size of SC compartment of the asymmetric (symmetric) division population. The mean-field behaviour of the model of competition between the populations A and S is described by the following system of law-of-mass action ODEs:

$$\dot{y}_0 = epy_0 - ed_0y_0 - e\lambda_0y_0x_{n+1} \tag{2.21}$$
$$\dot{y}_1 = \frac{(1-e)a}{b+y_{n+1}}y_0 + 2ed_0y_0 - \lambda_1y_1 - d_1y_1 \tag{2.22}$$
$$\dot{y}_i = 2d_{i-1}y_{i-1} - \lambda_iy_i - d_iy_i \qquad i = 2, ..., n-1 \tag{2.23}$$
$$\dot{y}_n = 2d_{n-1}y_{n-1} - \lambda_ny_n \tag{2.24}$$
$$\dot{x}_0 = e'p'x_0 - e'd_0'x_0 - e'\lambda_0'x_0x_{n+1} \tag{2.25}$$
$$\dot{x}_1 = \frac{(1-e')a'}{b'+x_{n+1}}x_0 + 2ed_0'x_0 - \lambda_1'x_1 - d_1'x_1 \tag{2.26}$$
$$\dot{x}_i = 2d_{i-1}'x_{i-1} - \lambda_i'x_i - d_i'x_i \qquad i = 2, ..., n-1 \tag{2.27}$$
$$\dot{x}_n = 2d_{n-1}'x_{n-1} - \lambda_n'x_n \tag{2.28}$$
$$\dot{x}_{n+1} = sy_n + s'x_n - \lambda_{n+1}x_{n+1} - e\lambda_0x_{n+1}y_0 - e'\lambda_0'x_{n+1}x_0 \tag{2.29}$$

Let the quantities r and r' be defined as:

$$r = \frac{p-d_0}{\lambda_0}$$
$$r' = \frac{p'-d_0'}{\lambda_0'} \tag{2.30}$$

i.e. r and r' are the ratios between the net SC growth rate and the SC differentiation rate for each of the competing populations, which coincide with steady-state value of the mean-field cytokine concentration for each of the populations.

From Eq. (2.21) we see that $\dot{y}_0 > 0$, i.e. y_0 grows in time, if $x_{n+1} \in (0,\, r)$. On the contrary y_0 decreases as time progresses if $x_{n+1} \in (r, \infty)$. Similarly, Eq. (2.25) implies that x_0 is increasing with time when $x_{n+1} \in (0, r')$ and decreasing when $x_{n+1} \in (r', \infty)$. Moreover, according to Eqs. (2.21) and (2.25), when $t \to \infty$, the stationary level of cytokine is given by $x_{n+1} \to \max(r, r')$. We thus consider three possible scenarios for the mean-field limit:

- $r > r'$. The S population becomes extinct: as $t \to \infty$ $x_{n+1} \to r$ which implies that, as $t \to \infty$, $\dot{y}_0 = 0$ and $\dot{x}_0 \leq 0$ with the equality in the latter holding for $x_0 = 0$ only.
- $r = r'$. Both populations coexist: as $t \to \infty$, $x_{n+1} \to r = r'$ which implies that, as $t \to \infty$, both $\dot{y}_0 = 0$ and $\dot{x}_0 = 0$ hold.
- $r < r'$. By the same reasoning as in the first case, the A population becomes extinct.

Regarding the behaviour of the stochastic system, there are some important differences with respect to its mean-field counterpart. In Figure 2.11, we show that the probability of

invasion as a function of the self-renewal rate, p', and death rate λ_0', of the invader stem cells. Instead of the 3 scenarios that characterise the mean-field limit, we have:

- $r \geq r'$. In this case, extinction of S is the most likely scenario: the population S is forced to evolve under higher on-average cytokine levels which induces upregulation of apoptosis of the S-stem cells. As $r' \to r$, this competitive advantage of A over S weakens. However, at that point, the delay-induced extinction mechanism for S takes over. Since we are considering e to be small, delays have little effect on the population A, which leads to eventual extinction of S. This behaviour is illustrated in Fig. 2.11, which shows that the probability of S to invade A vanishes in this regime.

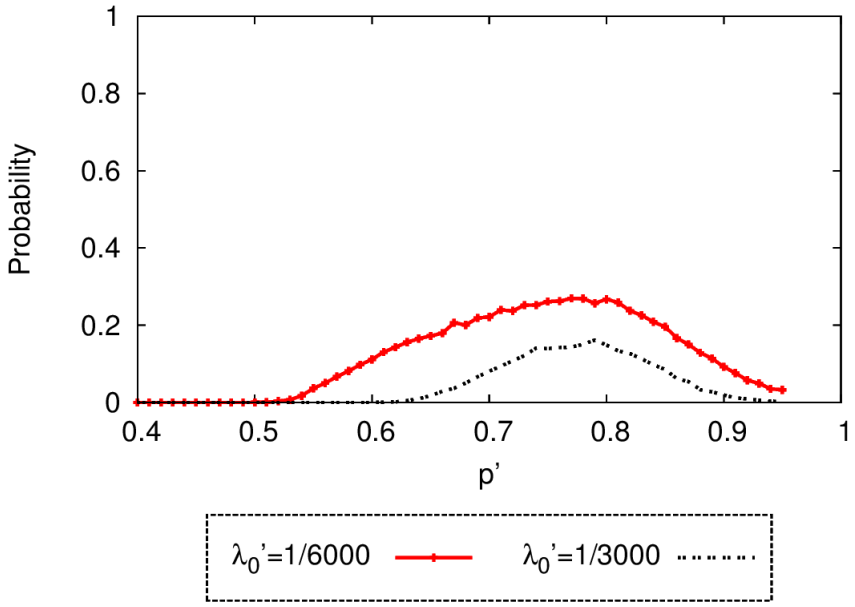

Figure 2.11: Probability invasion of the competition of two populations, one with asymmetric division with $e = 0.1$, and the other with pure symmetric division, $e' = 1$, and we plot the probability of invasion in function of the duplication rate of the invader population and for 2 different values of invader stem cells death. $a = 1000$, $b = a - \overline{y_{n+1}}$, $\lambda_0 = \frac{1}{6000}$ day^{-1}, $\overline{y_n} = 6000$, $p = 0.55$ day^{-1}, $\lambda_n = 0.03$ day^{-1}, $\lambda_{n+1} = 1$ day^{-1}.When $\lambda_0' = \frac{1}{6000}$, $r' = r$ for $p' = 0.55$, $\lambda_n' = 0.03$ day $^{-1}$, $\lambda_{n+1}' = 1$ day $^{-1}$, $a' = 1000$, $b' = a - \overline{x_{n+1}}$ when $\lambda_0' = \frac{1}{3000}$, $r' = r$ for $p' = 0.6$. $x_0(0) = 1$, $x_i(0) = 0 \quad \forall i \neq 0$.

- $r < r'$. Under these conditions, the population A is the one which evolves under *excess of cytokine* conditions, as the average steady-state concentration of cytokine is higher than the one the A population would have in the absence of the population S. As a consequence, the probability of S invading A is now positive, as shown in Fig. 2.11. We also observe that the probability of invasion as a function of r' reaches a maximum value and then starts decreasing. This behaviour is again due to delay-induced extinctions: as the relative net growth rate of the S-stem cells increases the probability of delay-induced extinction of the S population also increases (as shown in Fig. 2.3).

In order to further explore the behaviour of the stochastic competition model in the $r < r'$ regime, we have done simulations to compute the probability of invasion and the probability of extinction of both populations as a function of e, i.e. the probability of asymmetric behaviour of A-stem cells, and the rate of (symmetric) self-renewal of S-stem cells. The results are shown in Fig. 2.12. We observer (Fig. 2.12(a)) that there is a threshold value of e below which the resident A-type population cannot be invaded by a S-type invader, regardless of the value of p'. If the A-type resident has an e above this threshold, then two outcomes are possible: invasion, for moderately high values of p', or extinction of the symmetric invader (see also Fig. 2.11), for even higher values of p'. Furthermore, as e grows, Fig. 2.12(b) shows that the more likely outcome is both populations be extinct. This is due to the fact that for larger values of e the symmetric component becomes dominant in population A as well as S, and consequently the A-population starts to becoming affected by the effects of the corresponding delays. The probability of long term coexistence is negligible, according to our simulations.

Optimal differentiation cascades

Finally, we tackle the issue of examining the optimality properties of differentiation cascades. In this context, we define optimality of a differentiation cascade in terms of its resilience to invasion, namely, optimal differentiation cascades are those which are maximally resilient to invasion.

In order to address this issue, we again consider the competition between two populations generated by differentiation cascades characterised by different values of the probability of symmetric behaviour, e, and the self-renewal rate, p. We study the ability of the resident population to withstand invasion as a function of the values of these parameters for both populations. We have chosen these two particular quantities as the focus of our analysis, as the are directly related to the ability for adaptive behaviour of differentiation cascades, which has been argued to be at the root of symmetric cell division [91].

We start by analysing the optimal strategy regarding the probability of symmetric behaviour, e. To this end, we have ran simulations of the competition between a resident with probability of symmetric behaviour, e, and an invader with probability of symmetric behaviour, e'. All the other parameters are taken to be equal for both populations. Results are shown in Fig. 2.13.

In the light of our results regarding delay-induced extinction for higher values of e, i.e. when the symmetric part of the dynamics dominates, we expect that there exists a trade-off between resilience to invasion and long-term survival and elevated frequency of SC symmetric behaviour (which favours adaptive responses). This expectation is confirmed by the simulations results shown in Figs. 2.13(a), which show the probability of invasion. We can observe that resident populations with $e \ll 1$ are very stable and resilient to invasion. As e increases, so that a faster and more efficient adaptive response be possible, an invader with $e' \leq e$ is likely to wipe out the resident population (see Fig. 2.13(a)).

We have also investigated the effect of the rate of self-renewal on the resilience against invasion of an A-type population. Our results are reported in Fig. 2.14 where we have plotted the probability of invasion (Fig. 2.14(a)), the probability of extinction (Fig. 2.14(b)), and the probability of coexistence after a time T_F has elapsed (2.14(c)). These simulations have been done for $e = 0.1$ and $e' = 0.05$, which correspond to the region of parameter values where, according to Fig. 2.13, the probability of invasion is positive. The results shown in Fig. 2.14 indicate that if $p > p'$, i.e. if the rate self-renewal of the resident is

(a)

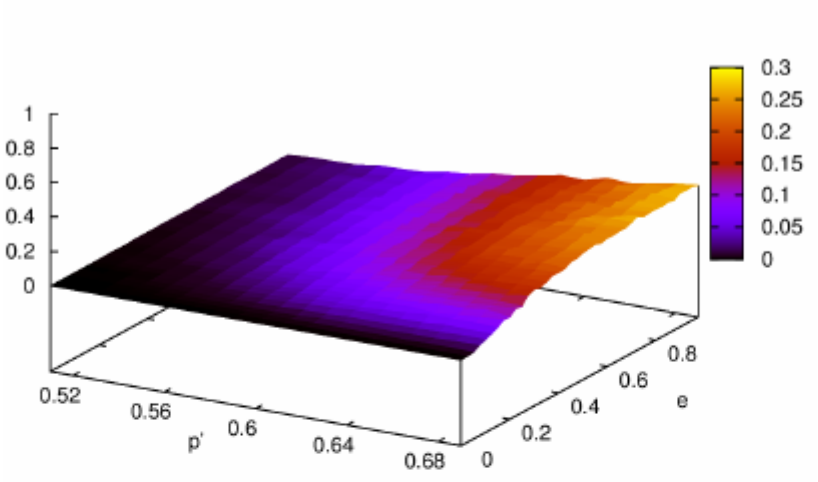

(b)

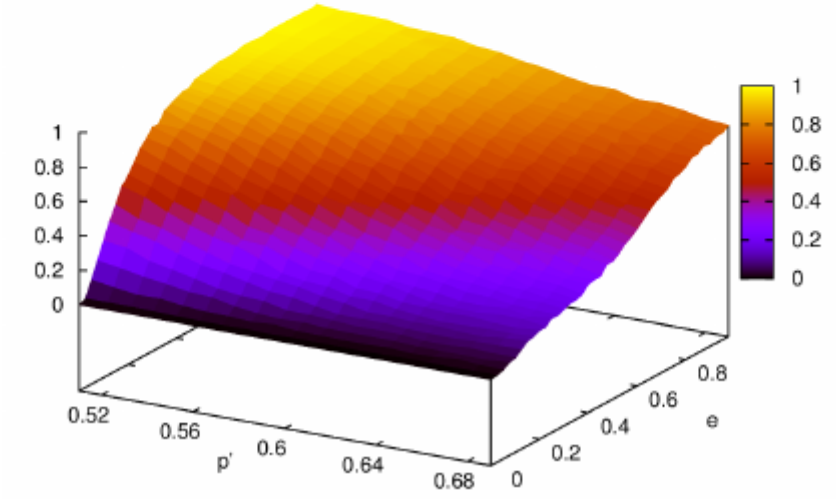

Figure 2.12: Simulation results for the competition between a resident with mixed asymmetric division, i.e. $0 < e < 1$, and an invader with pure symmetric division, i.e. $e' = 1$. Plot (a) and plot (b) show, respectively, the probability of invasion and the probability of extinction of both populations as a function of the duplication rate of the symmetric division and the probability of symmetric-like division of the asymmetric population, e. $a = 1000$, $b = a - \overline{y_{n+1}}$, $\lambda_0 = \frac{1}{3000}$ day^{-1}, $\overline{x_n} = 6000$, $p = 0.55$ day^{-1}, $\lambda_n = 0.03$ day^{-1}, $\lambda_{n+1} = 1$ day^{-1}. We run simulations until a final time= 6000 days. $e' = 1$, $\lambda'_0 = \frac{1}{3000}$ day^{-1}, $\overline{x_n} = 6000$, $p' = 0.55$ day^{-1}, $\lambda'_n = 0.03$ day^{-1}, $\lambda'_{n+1} = 1$ day^{-1}. $x_0(0) = 1$, $x_i(0) = 0 \quad \forall i \neq 0$.

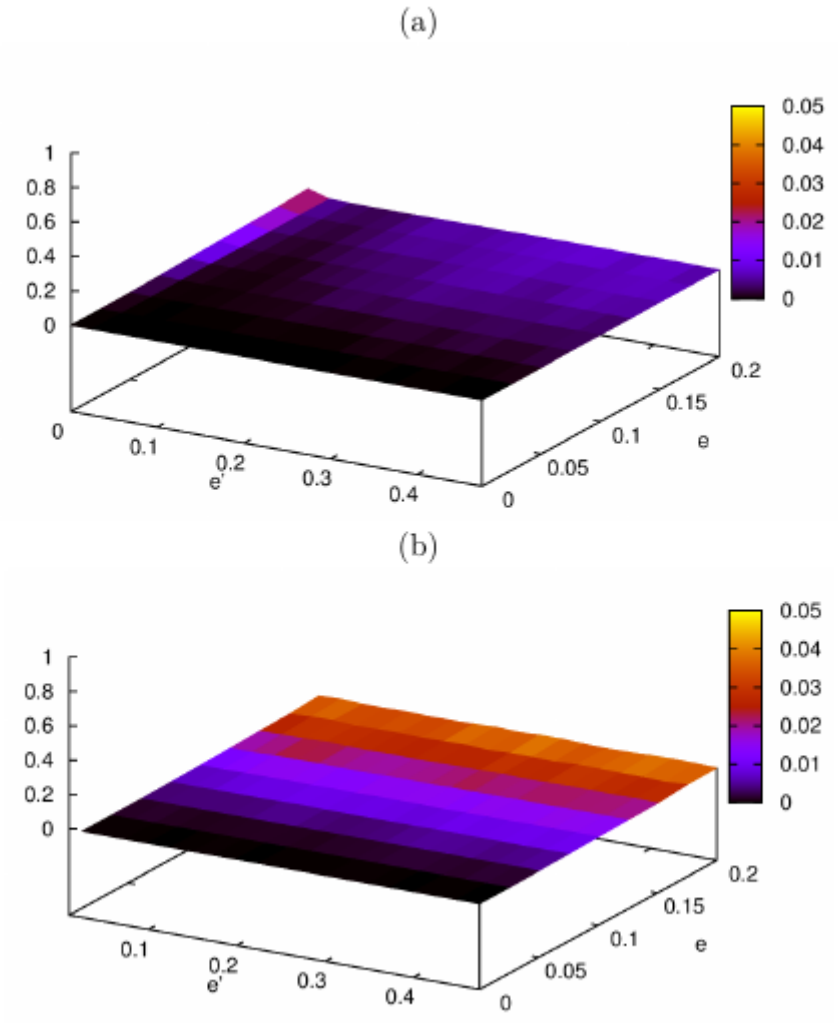

Figure 2.13: Simulation results for the competition between two A-type populations. Plot (a) and (b) show the probability of invasion and extinction of both populations, respectively. We have plotted these three quantities as a function of the probability of symmetric behaviour of the resident, e, and the invader e'. $a = 1000$, $b = a - \overline{y_{n+1}}$, $\lambda_0 = \frac{1}{3000}$ day^{-1}, $\overline{y_n} = 6000$, $p = 0.55$ day^{-1}, $\lambda_n = 0.05$ day^{-1}, $\lambda_{n+1} = 1$ day^{-1}, $a' = 1000$, $b' = a' - \overline{x_{n+1}}$, $\lambda'_0 = \frac{1}{3000}$ day^{-1}, $\overline{x_n} = 6000$, $p' = 0.55$ day^{-1}, $\lambda'_n = 0.05$ day^{-1}, $\lambda'_{n+1} = 1$ day^{-1}, We run simulations until a final time= 6000 days. $x_0(0) = 1$, $x_i(0) = 0 \quad \forall i \neq 0$.

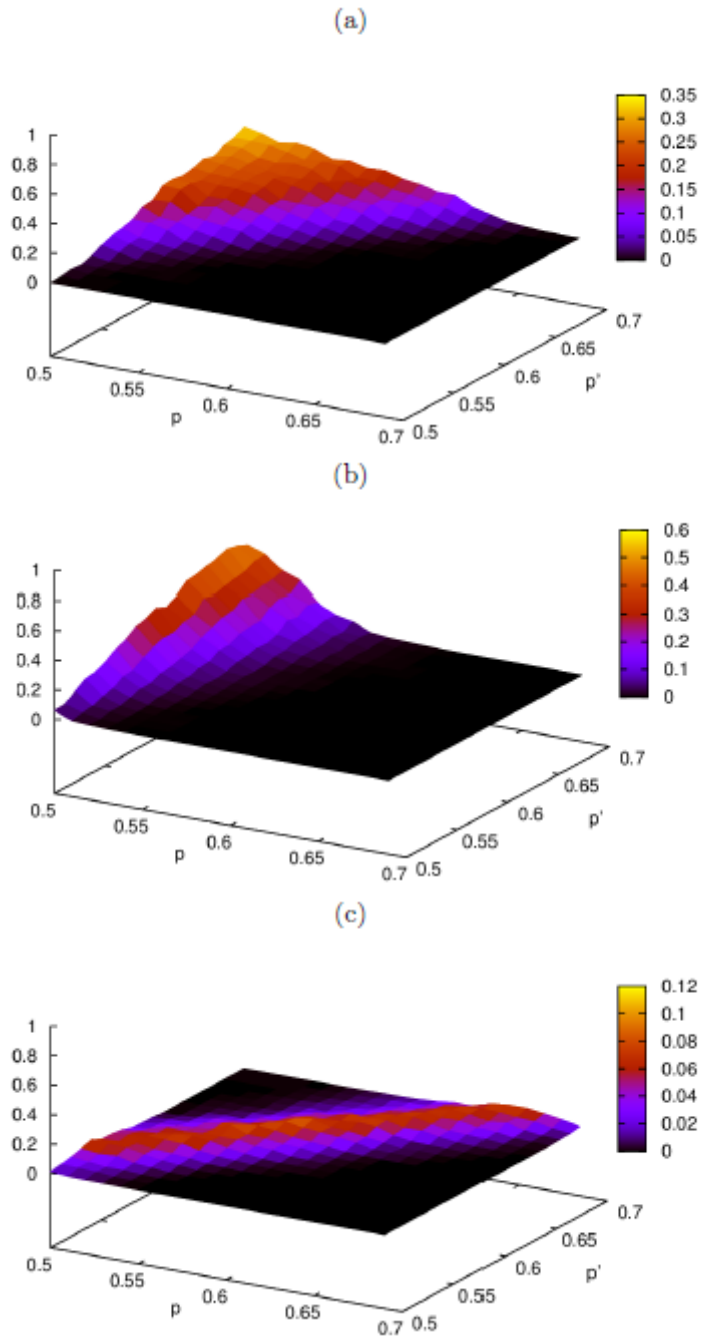

Figure 2.14: Simulation results for the competition between two A-type populations. Plot (a), (b), and (c) show the probability of invasion, extinction of both populations, and probability of coexistence, respectively. We have plotted these three quantities as a function of the probability of the stem cells duplication resident, p, and the invader p'. $a = 1000$, $b = a - \overline{y_{n+1}}$, $\lambda_0 = \frac{1}{3000}$ day^{-1}, $\overline{y_n} = 6000$, $e = 0.1$ day^{-1}, $\lambda_n = 0.05$ day^{-1}, $\lambda_{n+1} = 1$ day^{-1}, $a' = 1000$, $b' = a' - \overline{x_{n+1}}$, $\lambda'_0 = \frac{1}{3000}$ day^{-1}, $\overline{x_n} = 6000$, $e' = 0.05$ day^{-1}, $\lambda'_n = 0.05$ day^{-1}, $\lambda'_{n+1} = 1$ day^{-1}, We run simulations until a final time $T_F = 6000$ days. $x_0(0) = 1$, $x_i(0) = 0 \quad \forall i \neq 0$.

larger than that of the invader, the resident population is resilient to invasion.

Taken together, the results shown in Figs. 2.13 and 2.14 show that the optimal trade-off between resilience to invasion and capability for adaptive behaviour is realised by populations with small probability of symmetric behaviour, e, and large value of the self-renewal rate.

2.5 Conclusions

In this chapter, we have presented an analysed stochastic models of differentation cascades to study the effect of symmetric and asymmetric stem cell division. Our model is a compartmental model in which each compartment corresponds to a different differentiation stage, we have considered stem cells, transient amplifying cells, fully differentiated cells and a cytokine, produce by the FD cells which regulates the size of the stem cell compartment. In particular, we have deduced from our model some protection mechanism of the hierarchically structured cell populations. We have proposed a new extinction mechanism in which, the delay between the changes due noise fluctuations in the stem cell compartment, and the cytokine compartments, unstablises the whole population and eventually leads the system to extinction. Moreover, we have investigated a more realistic situation in which both, symmetric and asymmetric stem cell division are present, and we have looked for optimal strategies to be robust against invasion.

Chapter 3

Antigen-stimulation induced eradication of the HIV-1 infection in patients under highly active anti-retroviral therapy

HIV-1 patients under potent anti-retroviral develop a small reservoir of latent cells which persists and that anti-retroviral therapies are unable to eliminate, which hinders the total eradication of the infection. Recent research activity has been focused on formulating strategies aimed at removing the latent infection [121, 113, 65, 71]. One such proposal consists of elevating the rate of activation of the latently infected cells. We present a stochastic model of dynamics of the HIV-1 infection and study the effect of the rate of latently infected cell activation on the expected extinction time of the infection. We analyse our model by means of an asymptotic approximation using the semi-classical quasi steady state approximation (QSS). We also present a lower bound of the extinction reducing our stochastic problem to an easier 1-dimensional system which, in some cases, is a good approximation of the original one. We test the accuracy of our asymptotic results by means of a hybrid multi-scale stochastic simulation algorithm.

3.1 Introduction

HIV-1 infected patients are effectively treated with highly active anti-retroviral therapy (HAART). Whilst HAART is successful in keeping the disease at bay with average levels of viral load well below the detection threshold of standard clinical assays, it fails to completely eradicate the infection [63]: the infection persist in form of a latent a reservoir with a half-life time of years. This implies that life-long administration of HAART is, at the moment, necessary for HIV-1-infected patients, which is prone to drug resistance and cumulative side effects as well as imposing a considerable financial burden on developing countries, those more afflicted by HIV, and public health systems [121].

The latent reservoir consists of a population of latently infected T cells (probably, memory cells) which host, but do not produce the virus. Since virion production is not occurring within latently infected cells, they are immune to effects of HAART [110]. During their life-cycle, latently infected cells can undergo activation thus becoming active infected

cells with the ability to produce virus. The latently infected cell population is replenished by both active infected cell proliferation and also by slow, density-dependent homeostatic proliferation of the memory CD4+ T memory cells (and, therefore, of the latently infected cell compartment), which, according to [23], drives persistence and determines the size of the latent reservoir. This cycle is able to maintain positive, albeit small levels of viral load for very long time.

The presence of this latent infection has been recognised as major barrier for complete eradication of HIV-1 infection and the search for combination therapies, i.e. HAART plus specific agents that tackle the latent reservoir, has become a very active field of research [121, 113, 65, 66]. One of such potential approaches consist using agents that activate latently infected cells: by activating the cells in the latent reservoir, they would be rendered sensitive to HAART. This would, at least theoretically, clear the latent reservoir and, eventually, the infection. Early studies regarding reactivation of the latent reservoir used interleukins (IL-2, IL-3, and IL-7) in combination with specific antibodies (CD3). These attempts failed because it increased the absolute count of T cells [121, 113]. More recent studies have focused on the use of small molecules that reactivate latent virus production without inducing global T cell activation, in particular several histone deacetylases (HDAC) and other chromatin modifiers [121]. Here, we focus on modelling the efficiency of the latter type of therapy in combination of HAART. In particular, our aim is to analyse how the average extinction time of the infected cell population (both active and latent) changes as the activation rate of latently infected cells is increased.

We perform a WKB asymptotic analysis of the partial differential equation for the probability generating function associated to the Master Equation which describes stochastic population dynamics. This method relays on the solution of a variational problem for the optimisation of an action functional, which effectively reduces the problem to the analysis of the associated Hamilton equations [73, 35]. In order to make further progress, we take advantage of the multiplicity of time scales in the system, to perform a quasi-steady state approximation (QSSA) on the Hamilton equations, thus reducing the dimensionality of the problem [2]. We further used advanced numerical techniques to analyse the multi-dimensional Hamiltonian system: computation of invariant manifolds [53] and Taylor integration method [64] together with automatic differentiation techniques [64], which are used to obtain high accuracy and larger time steps. Our asymptotic results are tested by means of multi-scale stochastic simulations [20].

The organisation of the chapter is as follows. Section 3.2 is devoted to presenting our model of the HIV-1 dynamics under HAART in detail and discussing its underlying hypothesis. In Section 3.3 we present an asymptotic analysis of our stochastic process, which transforms it into a classical mechanics problem via the semi-classical approximation. We perform a time-scale analysis of the resulting Hamilton-Jacobi equations to use a Quasi steady state approximation to reduce the dimension of the problem. Moreover, we present a simplification of the model which allows us to reduce the system to an easy handle 1-dimensional system which gives us a lower bound of the extinction time. In Section 3.4 we present the results obtained via the different methods presented and a comparison of them. Finally, in Section 3.5 we summarise our results.

Transition rate	$r_j = (\Delta T, \Delta L, \Delta T^*, \Delta V)$	Description
$W_1 = \lambda\Omega$	$(1,0,0,0)$	Recruitment of T cells
$W_2 = d_T T$	$(-1,0,0,0)$	Death of T
$W_3 = \eta(1-\epsilon)kVT\Omega^{-1}$	$(-1,1,0,-1)$	Infection $T+V \implies L$ cell
$W_4 = (1-\eta)(1-\epsilon)kVT\Omega^{-1}$	$(-1,0,1,-1)$	Infection $T+V \implies T^*$ cell
$W_5 = rL$	$(0,1,0,0)$	Proliferation $L \implies 2L$
$W_6 = \frac{r}{L_{max}}\frac{L*(L-1)}{2}\Omega^{-1}$	$(0,-2,0,0)$	$L+L \implies \emptyset$
$W_7 = d_0 L$	$(0,-1,0,0)$	Death of L_i
$W_8 = a_L L$	$(0,-1,1,0)$	Activation $L \to T^*$
$W_9 = \delta T^*$	$(0,0,-1,0)$	Death of T^*
$W_{10} = cV$	$(0,0,0,-1)$	Clearance of virus
$W_{11} = p_v T^*$	$(0,0,0,1)$	Production of virus by T^*
$W_{12} = \epsilon kVT\Omega^{-1}$	$(0,0,0,-1)$	Infection failed

Table 3.1: Transition rate corresponding to the stochastic model of HIV dynamics. A description of the corresponding elementary population-dynamical processes is given in Section 3.2.

3.2 Stochastic Model

Our model is a stochastic generalisation of the model proposed by Rong and Perelson [110]. It takes into account 4 different variables: T represents the number of $CD4^+$ T-cells that are susceptible to HIV-1 infection, L, which stands for the number of latently infected cells that cannot produce virus. L cells can be activated by stimulation with their recall antigens. Finally, T^* and V represent productively infected cells, i.e. those that can produce virus particles, and the total viral load, respectively.

Our stochastic model is formulated in terms of the corresponding master equation [122, 44]:

$$\frac{\partial P(X,t)}{\partial t} = \sum_j \left(W_j(X - r_j, t)P(X - r_j, t)) - W_j(X,t)P(X,t)\right) \tag{3.1}$$

where $X = (x_1, x_2, x_3, x_4) = (T, L, T^*, V)$ and $P(X,t)$ is the probability of the population vector to have X particles at time t. For full specification of our stochastic model, we need to prescribe the transition rates, $W_j(X,t)$, corresponding to the probability per unit time of the elementary processes j to occur. These rates are modelled in terms of the law of mass action [47]. r_j is the change in X when elementary process j occurs, i.e. $X(t+\Delta t) = X(t) + r_j$ with probability $W_j\Delta t$: $P(X(t+\Delta t) = X(t) + r_j | X(t)) = W_j\Delta t$.

The elementary processes involved in our model are:

- Recruitment of new CD4+T cells with transition rate W_1 (see Table 3.1).
- CD4+T cells can undergo:

Parameter	Description	Value
T_0	CD4+T cells at the metastable state	599999 cells ml^{-1}
L_0	Latently infected cells at the metastable state	0.934778 cells ml^{-1}
T_0^*	Productively infected cells at the metastable state	0.115067 cells ml^{-1}
V_0	Viral load 10 copies ml^{-1} at the metastable state	
T_1	CD4+T cells 600000 cells ml^{-1} at the extinction	
L_1	Latently infected cells at the extinction	0 cells ml^{-1}
T_1^*	Productively infected cells at the extinction	0 cells ml^{-1}
V_1	Viral load at the extinction	0 copies ml^{-1}
λ	Recruitment rate of T cells	10000 ml^{-1} day^{-1}
d_T	Death rate of T cells	0.0166 day^{-1}
k	infection rate	$2.4 \cdot 10^{-8}$ ml day^{-1}
ϵ	Drug efficacy	0.85
η	Fraction resulting in latency	0.001
d_L	Death rate of latently infected cells	0.001 day^{-1}
a_L^s	Standard rate of transition from latently to productively	0.1 day^{-1}
a_L	rate of transition from latently to productively	varied
σ	death rate of productively infected cells	1 day^{-1}
c	clearance rate of free virus in blood stream	23 day^{-1}
p_v	Viral production rate	2000 day^{-1}
r	proliferation rate of activated cells	0.2 day^{-1}
L_{max}	Carrying capacity density of latent cells	1.888 cells ml^{-1}
Ω	System size	5000 ml

Table 3.2: Parameter values of the different rates

1. Apoptosis with transition rate W_2 (see Table 3.1).

- Latently infected cells L_i can undergo:

1. Homeostatically balanced proliferation. Following [110], we account for homoeostatic control of proliferation by means of a combination of branching ($L_i \to 2L_i$) with binary annihilation ($L_i + L_i \to \varnothing$). It has been shown (see e.g. [35]) that this combination is an stochastic counterpart of the standard logistic growth. The corresponding transition rates are W_3 for branching and W_4 for binary annihilation (see Table 3.1).
2. Death. We assume a simple linear decay with transition rate W_5 as shown in Table 3.1.
3. Activation. By means of this process a latently infected cell becomes an active infected cell $L_i \to T_i^*$. The corresponding transition rate is W_6, see Table 3.1.

- Active infected cells, T_i^*, cell are subjected to:

1. Apoptosis with transition rate W_7 (see Table 3.1).
2. Virion production. Contrary to latently infected cells, active infected cells synthesise and release new virions. In general, viral production can occur in a continuous fashion over the life span of an infected cell or in a burst which kills the cell. For the HIV infection both modes have been proposed [97]. Transition rate W_9 (Table 3.1) corresponds to continuous production. Later in the chapter, we consider an additional scenario, in which both continuous and burst production occur.

- Finally, virus, V_i, can:

1. Infect a healthy T cell producing a latently infected cell. In patients under HAART, the infection process is hindered by the presence of an anti-retroviral drug. The efficiency of such drug is measured by a parameter, ϵ, which takes values between 0 and 1, the latter (former) corresponding to a maximally (in)efficient drug. $(1 - \epsilon)$ is interpreted as the proportion of virions capable of infection under HAART treatment. We also assume that, upon infection, the cell can become latently infected with probability η or active with probability $(1 - \eta)$. Therefore the corresponding transition rate W_8 is proportional to $\eta(1 - \epsilon)$ as shown in Table 3.1.
2. Infect a healthy T cell producing an active infected cell. In this case, the corresponding transition rate W_2 is proportional to $(1 - \eta)(1 - \epsilon)$ (see Table 3.1).
3. Undergo clearance. Virions are removed from the blood, and we model this process as a simple linear decay with transition rate W_8 as per Table 3.1.
4. Fail to infect and being eliminated by the drug with transition rate W_{10} (see Table 3.1).

The parameter values used in our analysis are based on current estimates available in the literature. They are summarised in Table 3.2.

As a first approach to the dynamics, one can study the mean-field behaviour of this system, which is given by the set of ordinary differential equations (3.2), (3.3), (3.4) and (3.5).

$$\frac{d}{dt}T(t) = \lambda - d_T T - (1-\epsilon)kVT \tag{3.2}$$

$$\frac{d}{dt}L(t) = \eta(1-\epsilon)kVT + rL(1-\frac{L}{L_{max}}) - d_0 L - a_L L \tag{3.3}$$

$$\frac{d}{dt}T^*(t) = (1-\eta)(1-\epsilon)kVT - \delta T^* + a_L L \tag{3.4}$$

$$\frac{d}{dt}V(t) = N\delta T^* + p_v T^* - cV - kVT \tag{3.5}$$

The mean-field system has two fixed points. The point with coordinates $(T_1, 0, 0, 0)$, i.e. the disease-free equilibrium associated to extinction of the infection, is a repeller fixed point. The other fixed point, of the form (T_0, L_0, T_0^*, V_0) with $L_0, T_0^*, V_0 \neq 0$, is a global attractor. When noise is considered, the latter equilibrium becomes a metastable state, whereas the former becomes an absorbing state [35]. From Eqs. (3.2)-(3.5), we obtain that this metastable state exists as long as $a_L < a_L^*$, where:

$$a_L^* = \frac{r - d_0}{1 - \left(\frac{\eta(1-\epsilon)kT_1}{\delta(c+kT_1)pv^{-1} - (1-\eta)(1-\epsilon)kT_1)}\right)} \tag{3.6}$$

3.3 Asymptotic analysis and numerical methods

In this section we study the stochastic dynamics described by Eq. (3.1). We follow the methodology presented in [2] and we use the semi-classical approximation, but performing a time-scale analysis on the resulting Hamilton equations to simplify to reduce the dimension of the resulting problem. A multi-scale stochastic simulation method, which takes advantage of the separation of time scales to produce fast simulations, is used to test our results.

3.3.1 Semi-classical approximation

In Appendix B we have included all details of the semi-classical approximation, in this section we apply that methodology to our specific problem.

Consider the generating function associated to the probability distribution Eq. (3.1).

$$G(p_1, p_2, p_3, p_4, t) = \sum_{n=0}^{\infty} p_1^{x_1} p_2^{x_2} p_3^{x_3} p_4^{x_4} P(x_1, x_2, x_3, x_4, t). \tag{3.7}$$

The evolution of the generating function is determined by a partial differential equation

(PDE), which is derived from the Master Equation (3.1):

$$\begin{aligned}\frac{\partial G}{\partial t} &= -\lambda(p_1-1) - d_T(1-p_1)\frac{\partial G}{\partial p_1} - (1-\eta)(1-\epsilon)k(p_3-p_1p_4)\frac{\partial G}{\partial p_1}\frac{\partial G}{\partial p_4} \\ &\quad -\eta(1-\epsilon)k(p_2-p_1p_4)\frac{\partial G}{\partial p_1}\frac{\partial G}{\partial p_4} - r(p_2^2-p_2)\frac{\partial G}{\partial p_2} - \frac{r}{2L_{max}}(1-p_2^2)\frac{\partial^2 G}{\partial p_2^2} \\ &\quad -d_L(1-p_2)\frac{\partial G}{\partial p_2} - a_L(p_3-p_2)\frac{\partial G}{\partial p_2} - p_v(p_3p_4-p_3)\frac{\partial G}{\partial p_3} - \delta(1-p_3)\frac{\partial G}{\partial p_3} \\ &\quad -c(1-p_4)\frac{\partial G}{\partial p_4} - \epsilon k(p_1-p_1p_4)\frac{\partial G}{\partial p_1}\frac{\partial G}{\partial p_4}. \end{aligned} \tag{3.8}$$

Which can be interpreted as a Schrödinger equation,

$$\frac{\partial}{\partial t}G = -\hat{H}G, \tag{3.9}$$

where the Hamiltonian operator, $\hat{H}$, in the $\hat{p}$ (momentum) representation is

$$\begin{aligned}\hat{H}(\hat{p_1},\hat{p}_2,\hat{p}_3,\hat{p}_4,\hat{q}_1,\hat{q}_2,\hat{q}_3,\hat{q}_4) &= \lambda(\hat{p}_1-1) + d_T(1-\hat{p}_1)\hat{q}_1 + (1-\eta)(1-\epsilon)k(\hat{p}_3-\hat{p}_1\hat{p}_4)\hat{q}_1\hat{q}_4 \\ &\quad +\eta(1-\epsilon)k(\hat{p}_2-\hat{p}_1\hat{p}_4)\hat{q}_1\hat{q}_4 + r(\hat{p}_2^2-\hat{p}_2)\hat{q}_2 + \frac{r}{2L_{max}}(1-\hat{p}_2^2)\hat{q}_2^2 \\ &\quad +d_L(1-\hat{p}_2)\hat{q}_2 + a_L(\hat{p}_3-\hat{p}_2)\hat{q}_2 + p_v(\hat{p}_3\hat{p}_4-\hat{p}_3)\hat{q}_3 + \delta(1-\hat{p}_3)\hat{q}_3 \\ &\quad +c(1-\hat{p}_4)\hat{q}_4 + \epsilon k(\hat{p}_1-\hat{p}_1\hat{p}_4)\hat{q}_1\hat{q}_4 \end{aligned} \tag{3.10}$$

where $\hat{q}_i \equiv -\frac{\partial}{\partial \hat{p}_i}$. The operators $\hat{p}_i$ and $\hat{q}_i$ satisfy the commutation relation $[\hat{p}_i, \hat{q}_j] = \delta_{i,j}$.

From Eq. (3.9), we formulate an Ansatz where $G = \exp(-S)$. When the system size, Ω, is big, one may employ the WKB approximation and consider a $\bar{S}$ with S of the form $S = -\Omega\bar{S}$ expanding up to order $O(\Omega^{-1})$ (neglecting $O(\Omega^{-2})$ terms), one obtains the classical Hamilton-Jacobi equations

$$\frac{\partial S}{\partial t} = H\left(p, \frac{\partial S}{\partial p}\right), \tag{3.11}$$

Instead of directly tackling with the Hamilton-Jacobi equation, which, in general, we do not know how to solve, we exploit the analogy of the Shrödinger equation and use a Feynman path-integral representation we obtain a solution of (3.8), that is

$$G(p,t) = \int_0^t \left(\exp\left(-S(p,q)\right)Dq(s)Dp(s)\right)ds + p^{x_0}, \tag{3.12}$$

with

$$S(p,q,t) = \int_0^t \left(-H(p,q) + \sum_{i=1}^{n} q_i(s)\dot{p}_i(s)\right)ds. \tag{3.13}$$

The semi-classical approximation consists of approximating the path integral (B.13) by

$$G(p,t) \approx \exp\left(-S(p,t)\right), \tag{3.14}$$

where p_i are the solution of the Hamilton equations of the (classical) Hamiltonian

$$\begin{aligned}H(p,q) &= \lambda(p_1-1) + d_T(1-p_1)q_1 + (1-\eta)(1-\epsilon)k(p_3-p_1p_4)q_1q_4 \\ &\quad +\eta(1-\epsilon)k(p_2-p_1p_4)q_1q_4 + r(p_2^2-p_2)q_2 + \frac{r}{2L_{max}}(1-p_2^2)q_2^2 \\ &\quad +d_L(1-p_2)q_2 + a_L(p_3-p_2)q_2 + p_v(p_3p_4-p_3)q_3 + \delta(1-p_3)q_3 \\ &\quad +c(1-p_4)q_4 + \epsilon k(p_1-p_1p_4)q_1q_4. \end{aligned} \tag{3.15}$$

This implies, in particular (B.6) corresponds to the classical Lagrangian action related to (3.15). The equations of motion are given by $dq_i/dt = \partial H/\partial p_i$, $dp_i/dt = -\partial H/\partial q_i$ [6], that is

$$\begin{aligned}
\frac{dp_1}{dt} &= d_T(p_1-1) + (1-\eta)(1-\epsilon)k(p_1p_4-p_3)q_4 + \eta(1-\epsilon)k(p_1p_4-p_2)q_4 + \epsilon k(p_1p_4-p_1)q_4,\\
\frac{dp_2}{dt} &= r(p_2-p_2^2) + \frac{r}{L_{max}}(p_2^2-1)q_2 + d_L(p_2-1) + a_L(p_2-p_3),\\
\frac{dp_3}{dt} &= p_v(p_3-p_3p_4) + \delta(p_3-1),\\
\frac{dp_4}{dt} &= (1-\eta)(1-\epsilon)k(p_1p_4-p_3)q_1 + \eta(1-\epsilon)k(p_1p_4-p_2)q_1 + c(p_4-1) + \epsilon k(p_1p_4-p_1)q_1,\\
\frac{dq_1}{dt} &= \lambda - d_Tq_1 - (1-\epsilon)kp_4q_1q_4 + \epsilon k(1-p_4)q_1q_4,\\
\frac{dq_2}{dt} &= \eta(1-\epsilon)kq_1q_4 + r(2p_2-1)q_2 - \frac{r}{L_{max}}p_2q_2^2 - d_Lq_2 - a_Lq_2,\\
\frac{dq_3}{dt} &= (1-\eta)(1-\epsilon)kq_1q_4 + a_Lq_2 + p_v(p_4-1)q_3 - \delta q_3,\\
\frac{dq_4}{dt} &= -kp_1q_1q_4 + p_vp_3q_3 - cq_4.
\end{aligned} \tag{3.16}$$

These equations are formally solved with boundary conditions

$$\begin{aligned}
q_i(0) &= x_i(0),\\
p_i(t) &= p_i.
\end{aligned} \tag{3.17}$$

3.3.2 Quasi-steady state approximation

In this section, we proceed to formulate a quasi-steady approximation, that allows us to simplify the system Eq. (3.16). We proceed by re-scaling our variables in such a way to make explicit the separation of time scales and simplify the model according to the quasi-steady state approximation. For clarity, we perform this analysis in two steps. We start by defining the following set of re-scaled (dimensionless) quantities:

In this section, we proceed to re-scale variables so that we can analyse the intrinsic time scales of each of the variables involved and simplify the model according to the quasi-steady state approximation. For clarity, we perform this analysis in two steps. We start by defining the following set of re-scaled (dimensionless) quantities:

$$\begin{aligned}
\hat{q}_1 &= \frac{q_1}{T_0},\\
\hat{q}_2 &= \frac{q_2}{L_0},\\
\hat{q}_3 &= \frac{q_3}{T_0^*},\\
\hat{q}_4 &= \frac{q_4}{V_0},\\
s &= kV_0t.
\end{aligned} \tag{3.18}$$

Parameter	Order of magnitude
$\kappa_1 = \frac{\lambda}{kT_0V_0}$	$O(10^5)$
$\kappa_2 = \frac{d_T}{kV_0}$	$O(10^5)$
$\kappa_3 = \frac{rL_0}{kV_0T_0}$	$O(10^0)$
$\kappa_4 = \frac{d_LL_0}{kV_0T_0}$	$O(10^{-2})$
$\kappa_5 = \frac{a_LL_0}{kV_0T_0}$	$O(10^0)$
$\kappa_6 = \frac{p_vT_0^*}{kV_0T_0}$	$O(10^3)$
$\kappa_7 = \frac{\delta T_0}{kV_0T_0}$	$O(10^0)$
$\kappa_8 = \frac{c}{kT_0}$	$O(10^3)$

Table 3.3: Re-scaled parameters following the re-scaling of variables shown in Eq. 3.18

In this re-scaled variables, the Hamiltonian can be written as

$$H(p,x) = kT_0V_0H_\kappa(p,x), \tag{3.19}$$

where $H_\kappa(p,q)$ is given by

$$\begin{aligned} H_\kappa(p,q) &= \kappa_1(p_1-1) + \kappa_2(1-p_1)q_1 + (1-\eta)(1-\epsilon)(p_3-p_1p_4)q_1q_4 \\ &\quad +\eta(1-\epsilon)(p_2-p_1p_4)q_1q_4 + \kappa_3(p_2^2-p_2)q_2 + \kappa_3\frac{L_0}{2L_{max}}(1-p_2^2)q_2^2 \\ &\quad +\kappa_4(1-p_2)q_2 + \kappa_5(p_3-p_2)q_2 + \kappa_6(p_3p_4-p_3)q_3 + \kappa_7(1-p_3)q_3 \\ &\quad +\kappa_8(1-p_4)q_4 + \epsilon(p_1-p_1p_4)q_1q_4, \end{aligned} \tag{3.20}$$

and where, for simplicity of the notation, we have dropped the hats of the re-scaled variables $\hat{q}_i$. The parameters κ_i are given in Table 3.3.

The Hamiltonian equations for the re-scaled variables read as follows

$$\begin{aligned} kV_0T_0\frac{dq_1}{ds} &= kV_0T_0\frac{\partial H_\kappa}{\partial p_1}, & kV_0\frac{dp_1}{ds} &= -\frac{kV_0T_0}{T_0}\frac{\partial H_\kappa}{\partial q_1}, \\ kV_0L_0\frac{dq_2}{ds} &= kV_0T_0\frac{\partial H_\kappa}{\partial p_2}, & V_0\frac{dp_2}{ds} &= -\frac{kV_0T_0}{L_0}\frac{\partial H_\kappa}{\partial q_2}, \\ kV_0T_0^*\frac{dq_3}{ds} &= kV_0T_0\frac{\partial H_\kappa}{\partial p_3}, & kV_0\frac{dp_3}{ds} &= -\frac{kV_0T_0}{T_0^*}\frac{\partial H_\kappa}{\partial q_3}, \\ kV_0^2\frac{dq_4}{ds} &= kV_0T_0\frac{\partial H_\kappa}{\partial p_4}, & kV_0\frac{dp_4}{ds} &= -\frac{kV_0T_0}{V_0}\frac{\partial H_\kappa}{\partial q_4}, \end{aligned} \tag{3.21}$$

and, therefore,

$$\begin{aligned} \frac{dq_1}{ds} &= \frac{\partial H_\kappa}{\partial p_1}, & \frac{dp_1}{ds} &= -\frac{\partial H_\kappa}{\partial q_1}, \\ \frac{L_0}{T_0}\frac{dq_2}{ds} &= \frac{\partial H_\kappa}{\partial p_2}, & \frac{L_0}{T_0}\frac{dp_2}{ds} &= -\frac{\partial H_\kappa}{\partial q_2}, \\ \frac{T_0^*}{T_0}\frac{dq_3}{ds} &= \frac{\partial H_\kappa}{\partial p_3}, & \frac{T_0^*}{T_0}\frac{dp_3}{ds} &= -\frac{\partial H_\kappa}{\partial q_3}, \\ \frac{V_0}{T_0}\frac{dq_4}{ds} &= \frac{\partial H_\kappa}{\partial p_4}, & \frac{V_0}{T_0}\frac{dp_4}{ds} &= -\frac{\partial H_\kappa}{\partial q_4}. \end{aligned} \tag{3.22}$$

In order to proceed further with our time-scale analysis, we note that the dynamical equations for q_1 and q_4 are dominated by the terms in κ_1 and κ_2, which, according to Table 3.3, are $O(10^5)$, and κ_6 and κ_8, which are $O(10^3)$, respectively. On the contrary, the dominant terms in the equations for q_2 and q_3 are $O(1)$. In view of this, we re-scale the dimensionless time s as

$$T = \kappa_1 s. \tag{3.23}$$

In terms of the re-scaled time T, our Hamilton equations are given by

$$\begin{array}{rclrcl} \dfrac{dq_1}{dT} &=& \dfrac{1}{\kappa_1}\dfrac{\partial H_\kappa}{\partial p_1}, & \dfrac{dp_1}{dT} &=& \dfrac{1}{\kappa_1}\dfrac{\partial H_\kappa}{\partial q_1}, \\ \epsilon_1\dfrac{dq_2}{dT} &=& \dfrac{\partial H_\kappa}{\partial p_2}, & \epsilon_1\dfrac{dp_2}{dT} &=& \dfrac{\partial H_\kappa}{\partial q_2}, \\ \epsilon_2\dfrac{dq_3}{dT} &=& \dfrac{\partial H_\kappa}{\partial p_3}, & \epsilon_2\dfrac{dp_3}{dT} &=& \dfrac{\partial H_\kappa}{\partial q_3}, \\ \epsilon_3\dfrac{dq_4}{dT} &=& \dfrac{1}{\kappa_6}\dfrac{\partial H_\kappa}{\partial p_4}, & \epsilon_3\dfrac{dp_4}{dT} &=& \dfrac{1}{\kappa_6}\dfrac{\partial H_\kappa}{\partial q_4}, \end{array} \tag{3.24}$$

where $\epsilon_1 = \kappa_1\frac{L_0}{T_0} = O(10^{-1})$, $\epsilon_2 = \kappa_1\frac{T_0^*}{T_0} = O(10^{-2})$, and $\epsilon_3 = \frac{\kappa_1}{\kappa_6}\frac{L_0}{T_0} = O(10^{-3})$, and all the right hand sides of the Hamilton equations are now $O(1)$. In view of this separation of time scales, we can assume that q_1 is a slow variable which will remain roughly constant in relation to q_2, and q_3 (and similarly q_4) is a fast variable which can be considered to be at equilibrium with the rest of the system. Therefore, the quasi-steady state Hamilton (QSSH) equations read

$$\begin{array}{rclrcl} \dfrac{dq_1}{dT} &=& \dfrac{\partial H_\kappa}{\partial p_1}, & \dfrac{dp_1}{dT} &=& -\dfrac{\partial H_\kappa}{\partial q_1}, \\ \epsilon_1\dfrac{dq_2}{dT} &=& \dfrac{\partial H_\kappa}{\partial p_2}, & \epsilon_1\dfrac{dp_2}{dT} &=& -\dfrac{\partial H_\kappa}{\partial q_2}, \\ \epsilon_2\dfrac{dq_3}{dT} &=& \dfrac{\partial H_\kappa}{\partial p_3}, & \epsilon_2\dfrac{dp_3}{dT} &=& -\dfrac{\partial H_\kappa}{\partial q_3}, \\ \epsilon_3\dfrac{dq_4}{dT} &=& \dfrac{1}{\kappa_6}\dfrac{\partial H_\kappa}{\partial p_4}, & \epsilon_3\dfrac{dp_4}{dT} &=& -\dfrac{1}{\kappa_6}\dfrac{\partial H_\kappa}{\partial q_4}. \end{array} \tag{3.25}$$

In following sections we consider two different approximations. In both approximations we assume that the healthy cells are constant, that is $p_1 = 1$ and $q_1 = 1$, this hypothesis holds since if we project on the plane (p_1, q_1), the stochastic extinction and the metastable state are very close, the distance is $O(10^{-5})$, and that the equations for p_1 and q_1 are essentially linear in p_1 and q_1 plus a small perturbation in the other variables. The first approximation consists in considering $\epsilon_2 = 0$ and $\epsilon_3 = 0$, we refer this as Strong QSS. The other option consists in considering only $\epsilon_3 = 0$, this approximation is refereed as Weak QSS. In this particular problem, the Strong QSS and the Weak QSS lead us to a very similar solutions, see Figure 3.4. However, in other cases their results could be different, for this reason we give tools to study the Weak QSS and to compare them.

Strong QSS

The so-called strong QSSA consists of applying QSS conditions to the equations for q_3, p_3, q_4 and p_4:

$$\begin{array}{rclcrcl} \frac{dq_1}{dT} & = & 0, & & \frac{dp_1}{dT} & = & 0 \\ \frac{dq_2}{dT} & = & \frac{\partial H}{\partial p_2}, & & \frac{dp_2}{dT} & = & -\frac{\partial H}{\partial q_2} \\ 0 & = & \frac{\partial H}{\partial q_3}, & & 0 & = & \frac{\partial H}{\partial q_4}, \\ 0 & = & \frac{\partial H}{\partial p_3}, & & 0 & = & \frac{\partial H}{\partial p_4}. \end{array} \tag{3.26}$$

That is,

$$\begin{aligned} \frac{dp_2}{dT} &= \frac{1}{\epsilon_1}\left(-\kappa_3(p_2^2 - p_2) - \kappa_3\frac{L_0}{L_{max}}(1-p_2^2)q_2 - \kappa_4(1-p_2) - \kappa_5(p_3 - p_2)\right), \\ \frac{dq_2}{dT} &= \frac{1}{\epsilon_1}\left(\eta(1-\epsilon)q_1q_4 + \kappa_3 q_2(2p_2^2 - 1) - \kappa_3\frac{L_0}{L_{max}}p_2q_2^2 - \kappa_4 q_2 - \kappa_5 q_2\right), \end{aligned} \tag{3.27}$$

where

$$\begin{aligned} p_1 &= 1, \\ q_1 &= 1, \\ p_3 &= \frac{\kappa_6 - \kappa_7 - C\kappa_6 - B\kappa_6 p_2 \pm \sqrt{(\kappa_6 - \kappa_7 - C\kappa_6 - B\kappa_6 p_2)^2 - 4\kappa_7\kappa_6 A}}{2\kappa_6 A}, \\ q_3 &= \frac{-\kappa_5}{(1-\eta)(1-\epsilon)q_1 D p_3 + \kappa_6(Ap_3 + Bp_2 + C) - \kappa_7 q_3}q_2, \\ p_4 &= \frac{-(1-\eta)(1-\epsilon)q_1p_3 - \eta(1-\epsilon)p_2q_1 - \kappa_8 - \epsilon p_1q_1}{-(1-\eta)(1-\epsilon)q_1p_1 - \eta(1-\epsilon)p_1q_1 - \kappa_8 - \epsilon p_1q_1} \\ q_4 &= \frac{\kappa_6}{p_1q_1 + \kappa_8}p_3q_3, \end{aligned}$$

with

$$\begin{aligned} A &= \frac{-(1-\eta)(1-\epsilon)q_1}{-(1-\eta)(1-\epsilon)p_1q_1 - \eta(1-\epsilon)p_1q_1 - \kappa_8 - \epsilon p_1q_1} \\ B &= \frac{-\eta(1-\epsilon)p_2q_1}{-(1-\eta)(1-\epsilon)p_1q_1 - \eta(1-\epsilon)p_1q_1 - \kappa_8 - \epsilon p_1q_1} \\ C &= \frac{-\kappa_8 - \epsilon p_1q_1}{-(1-\eta)(1-\epsilon)p_1q_1 - \eta(1-\epsilon)p_1q_1 - \kappa_8 - \epsilon p_1q_1} \\ D &= \frac{\kappa_6}{p_1q_1 + \kappa_8}. \end{aligned}$$

We can discard the positive branch of p_3 for continuity. A phase portrait of the Strong QSSA is shown in Figure 3.1.

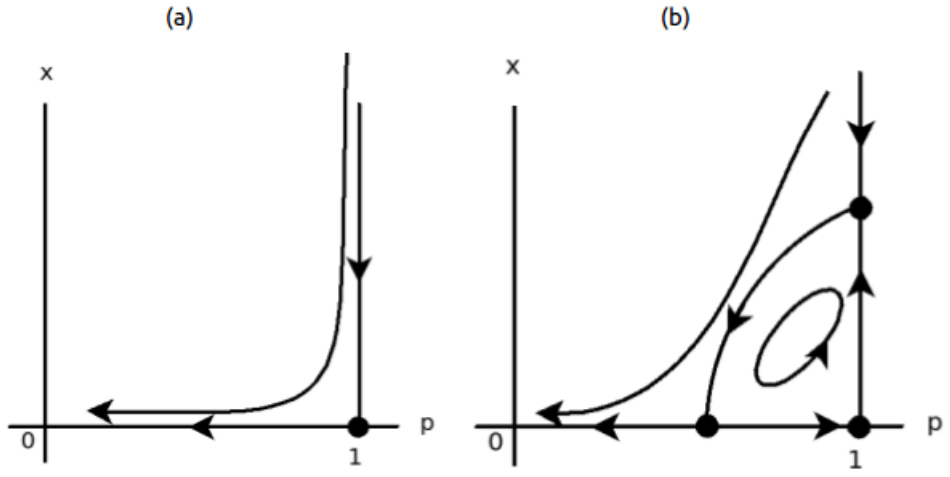

Figure 3.1: Phase diagram of the equations of motions with the Strong QSS assumption in the supercritical case (left) and the subcritical case (right).

Weak QSS

The Weak QSS equations in which quasi-steady state conditions are applied only to the equations for p_4, q_4 reads

$$\begin{aligned}
\frac{dp_2}{dT} &= \frac{1}{\epsilon_1}\left(-\kappa_3(p_2^2-p_2)-\kappa_3\frac{L_0}{L_{max}}(1-p_2^2)q_2-\kappa_4(1-p_2)-\kappa_5(p_3-p_2)\right),\\
\frac{dq_2}{dT} &= \frac{1}{\epsilon_1}\left(\eta(1-\epsilon)q_1q_4+\kappa_3q_2(2p_2^2-1)-\kappa_3\frac{L_0}{L_{max}}p_2q_2^2-\kappa_4q_2-\kappa_5q_2\right),\\
\frac{dp_3}{dT} &= \frac{1}{\epsilon_2}\left(-\kappa_6(p_3p_4-p_3)-\kappa_7(1-p_3)\right),\\
\frac{dq_3}{dT} &= \frac{1}{\epsilon_2}\left((1-\eta)(1-\epsilon)q_1q_4+\kappa_5q_2+\kappa_6(p_4-1)q_3-\kappa_7q_3\right),
\end{aligned} \tag{3.28}$$

where

$$\begin{aligned}
p_1 &= 1,\\
q_1 &= 1,\\
p_4 &= \frac{-(1-\eta)(1-\epsilon)q_1p_3-\eta(1-\epsilon)p_2q_1-\kappa_8-\epsilon p_1q_1}{-(1-\eta)(1-\epsilon)q_1p_1-\eta(1-\epsilon)p_1q_1-\kappa_8-\epsilon p_1q_1}\\
q_4 &= \frac{\kappa_6}{p_1q_1+\kappa_8}p_3q_3.
\end{aligned}$$

3.3.3 Heteroclinic orbits and extinction time

As we have seen in Section 3.2, this system has two different regimes: $a_L \geq a_L^*$, in which only the trivial fixed point exists, and $a_L < a_L^*$, where in addition to the trivial fixed point, a positive fixed point (associated to a persistent infection exists. If this metastable

state exists, the mean field behaviour, which is exactly the dynamics along $p_i = 1$, has two different fixed points: an attractor (which corresponds to the metastable state) and a repeller (which corresponds to the extinction).

As time goes to infinity, the trajectories approach the 0 level energy. The action is $S = 0$ on $p_i = 1$ and on $x_2 = x_3 = x_4 = 0$. However, it is positive on the heteroclinic connection between the metastable state and the stochastic extinction, which is of the form $x_2 = x_3 = x_4 = 0$, $0 < p_i < 1$.

Since the trivial fixed point corresponds to the only absorbing state of the stochastic dynamics, and the population can not explode, extinction takes place with probability 1. If the metastable state is of the form $x_i \gg 0$, that is the system size $\Omega \gg 0$, the extinction probability $P_0(t) = G(0,t)$ can be approximated by:

$$G(0,t) \approx 1 - \exp\left(-\frac{t}{\tau}\right), \tag{3.29}$$

We look for τ of the form

$$\tau = A\Omega^B exp(\Omega C), \tag{3.30}$$

where C is the integral of the re-scaled action, $\bar{S}$, along the heteroclinic connection between the metastable state and the stochastic extinction. The semi-classic approximation is valid when $\Omega \gg 0$. We will perform a numerical fit of A and B using the exact solution (computed with Gillespie simulations) of the system for large values of Ω. A full derivation of this approximation is included in Appendix B.

Numerical fit of A and B

It is clear that as $\Omega \to \infty$ the solution of the semi-classical approximation tends to the exact solution of Eq. (3.1), and we can use this fact in our advantage to determine A and B. We also have to notice that we can determine analytically C, as it is the integral of the action along the heteroclinic connection. A direct fit of a function of the form

$$f(\Omega) = A\Omega^B \exp\left(C\Omega\right)$$

can be very unstable. We rather analyse

$$g(x) = \frac{1}{\Omega} log f(\Omega) = \hat{A}x + \hat{B}x \log\left(x\right) + \hat{C},$$

with $x = \dfrac{1}{\Omega}$, which is more favourable, since first we are interested in C, therefore we want to have C alone with small terms suppressed by Ω. Our procedure is as follows,

1 Given a a_L we select an initial Ω and we compute τ using stochastic simulations (the multi-scale stochastic simulation employed to perform this simulations is explained later).

2 Save $\epsilon_\Omega = \dfrac{1}{\Omega}$ and $\delta_\Omega = \epsilon log\left(\dfrac{1}{\tau}\right)$. Increase Ω and go to 1 until we have some values of $(\epsilon_\Omega, \delta_\Omega)$.

3 using an implementation of the non-linear least-squares (NLLS) Levenberg–Marquardt algorithm [96] fit $g(x) = Ax + Bxlog(x) + C_S$ via A, B, C_S where $x = log(\delta_\Omega)$ and the right-hand term is $\epsilon\delta_\Omega$ with some of the higher values of Ω we have.

4 If $|C_S - C| >$ tol, where C is the one obtained analytically, increase Ω and go to 1.

5 If $|C_S - C| <$ tol we choose $C_S = C$ and we fit again via A and B.

6 As we can expect B of the form $B = \pm\frac{n}{2}$ with $n \in \mathbb{N}$, we choose B as the closest number of this form to B.

7 finally we fit again just via A.

8 As we are interested in $\Omega = 5000ml$, the mean extinction time, obtained with the semi-classical approximation is, $\tau_s = -\left(g\left(\frac{1}{5000}\right)5000\right)$.

Note that we expect B to take this form, since this system exhibits the so-called Stokes phenomenon [6]. Therefore it is natural to expect that there is a singularity in the complex space which is a pole. Moreover, for the binary-Annihilation-decay process, it has been proven that $B = \frac{1}{2}$ [8, 9, 10]. Numerically B approaches $\frac{1}{2}$ (independently of a_L). To obtain analytic expressions for A and B requires a careful analysis of the related Stokes phenomenon [10]. This is postponed for future work.

3.3.4 Lower Bound

We now present another approximation which provides a lower bound to the extinction time. The variable x_2, associated to latently infected cells, is the most important variable since the drug is unable to clear it. It is also the slowest variable and it is affected by the other variables only via the reaction W_3, which is the slowest reaction in the system. Numerical simulations suggest the ratio W_3/W_5 is negligible (see Fig. 3.2). If we consider $W_3 = 0$, only the reactions W_5, W_6, W_7 and W_8 affect x_2. In this case, we can reduce our 4-dimensional stochastic system to a much simpler one dimensional system. The extinction time, τ_{LB}, of the x_2-cells in this reduced system is a lower bound to the extinction time of the x_2-cells in the 4-dimensional system, and provided η is small or ϵ is large enough it is a good approximation. Therefore, we can use it to get a first approximation of the average extinction time.

Note that, to study the extinction probability of the latently infected cells, this lower bound is equivalent to consider either a perfect efficacy of the drug ($\epsilon = 1$) or $\eta = 0$, since in these cases $W_3 = 0$.

Under this assumption, our system is described by the following master equation

$$\begin{aligned}\frac{\partial P(L,t)}{\partial t} &= (W_5(L - r_j, t)P(L - r_j, t)) - W_5(L,t)P(L,t)) + \\ &+ (W_6(L - r_j, t)P(L - r_j, t)) - W_6(L,t)P(L,t)) + \\ &+ (W_7(L - r_j, t)P(L - r_j, t)) - W_7(L,t)P(L,t)) + \\ &+ (W_8(L - r_j, t)P(L - r_j, t)) - W_8(L,t)P(L,t)),\end{aligned} \tag{3.31}$$

whose mean field behaviour is described by the equation

$$\dot{x}_2 = rx_2(1 - \frac{x_2}{L_{max}}) - d_0x_2 - a_Lx_2. \tag{3.32}$$

We can proceed as in Section 3.3.3,to obtain an asymptotic approximation of the extinction time for the reduced system Eq. (3.31). For simplicity x and p will denote x_2 and p_2 respectively.

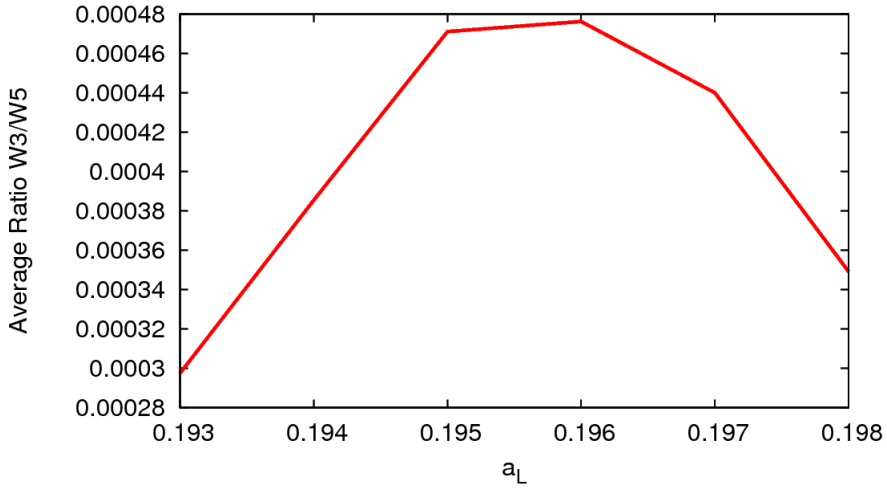

Figure 3.2: Average of the ratio W_3/W_5 computed with 1000 Gillespie simulations, for different values of a_L.

$$H_{LB}(p,x) = r(p^2-p)x + \frac{r}{2L_{max}}(1-p^2)x^2 + (a_L+d_L)(1-p)x \tag{3.33}$$

The associated Hamilton equations are:

$$\begin{aligned} \frac{dx}{dt} &= \frac{\partial H_{LB}}{\partial p} = r(2p-1)x - \frac{r}{L_{max}}px^2 - (a_L+d_L)x \\ \frac{dp}{dt} &= -\frac{\partial H_{LB}}{\partial p} = -r(p^2-p) - \frac{r}{L_{max}}(1-p^2)x - (a_L+d_L)(1-p) \end{aligned} \tag{3.34}$$

3.3.5 Multi-scale stochastic simulations

In order to test the accuracy of our asymptotic analysis, we need to carry out numerical simulations of the stochastic model. The direct simulation method proposed by Gillespie becomes very inefficient for systems with separation of time scales. To address this issue, we use the methodology proposed by Cao et al. [20] to perform faster simulations. A detailed explanation of this method is presented in Appendix D.

Before proceeding with the multi-scale stochastic simulations, we notice that, in this particular case, the number of healthy cells, x_1, is big enough so that their dynamics are essentially determined by the mean-field dynamics (i.e. we can assume there is no noise).

The main idea of the multi-scale simulation method is to produce stochastic simulations for the slow variables and assume that the fast variables are in "stochastic equilibrium", that is, in an state in which birth and death rates are balanced.

How to decide which are the fast and the slow reactions, in general, is an open question, and usually the best way to determine them is to run few simulations of the Gillespie algorithm and decide. However, in this case we can use the results of Section 3.3.2. In this section we consider that x_2 is the slow variable, x_3, x_4 are fast variables and, as before, x_1 follows the ordinary differential equation (2.2). The algorithm is summarised as follows.

1. Set initial conditions at $t = t_0$, $x_1 = x_1(t_0), x_2 = x_2(t_0), x_3 = x_3(t_0), x_4 = x_4(t_0)$.
2. Choose the next step size, Δt, and reaction channel, r_j, according to the Multi-scale simulation algorithm for x_2, x_3, x_4.
3. Update x_1, which is evolving according to Equation (3.2), with x_2, x_3, x_4 constants from t to $t + \Delta t$.
4. Update $t = t + \Delta t$ and x_2, x_3, x_4 according to r_j.
5. If $t < t_f$ go to 2.

Note that x_2, x_3 and x_4 are considered constant in step 3 because the next reaction channel does not occur until $t + \Delta t$.

3.4 Results

In this section we show how the probability of extinction and the average extinction time of the infection changes as the activation rate of the latently infected cells varies. We analyse the system behaviour in two different regimes (subcritical and supercritical), via the different methods explained in the previous section. Finally, we study a possible side effect of the therapy.

3.4.1 Subcritical case

In this section we show the results for the subcritical case, that is, when a metastable state exists, that is $a_L < a_L^*$, using the different methods explained in Section 3.3.

Stochastic Simulation Methods

Performing simulations of this system by means of the regular stochastic simulation algorithm [47] requires a huge amount of computational time. In order to reduce the computation time, we propose two different numerical methods. One method consists of using a multi-scale stochastic simulation method. An alternative method is to perform Gillespie simulations in a reduced 1-dimensional system, in which we have neglected the effect of the virus infection in the latently infected cells. This second method provides a lower bound of the average extinction time (see Section 3.3.4). In Fig 3.3 we compare the average extinction time obtained from these two methods. Good agreement between both methods is observed, which provides evidence of the suitability of the multi-scale simulation method to perform simulations in this problem. We use this method, as it allows us to reach a wider range of values of a_L. The extinction times obtained from the lower bound appears to underestimate slightly the results from the other methods. This difference increases as a_L is close to a_L^*, since the metastable state for the reduced systems disappears earlier.

Weak vs Strong QSSA

The probability of extinction at a given time is given by $G(0, t)$, in previous section we have derived an expression for the semi-classical approximation of G, using it we can approximate $G(0, t)$ by

$$G(0, t) = 1 - \exp\left(-t/\tau\right) \tag{3.35}$$

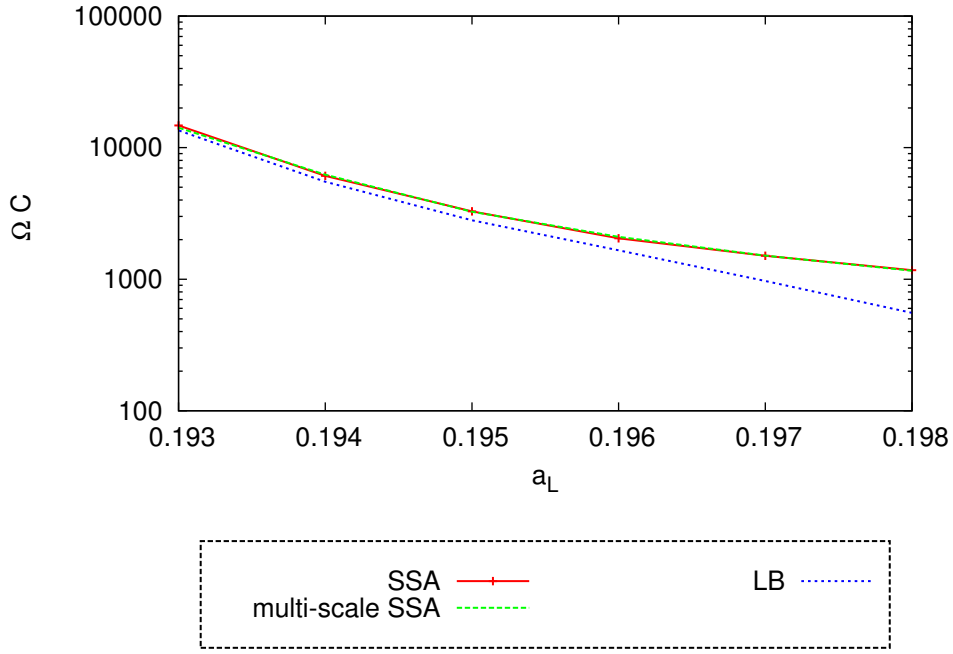

Figure 3.3: Average over 1000 simulations of the extinction time of the system described by Eq. (3.1) computed with the Gillespie SSA, the multi-scale SSA and Gillespie SSA for the Lower Bound system (Eq. (3.31)) for different values of a_L.

with

$$\tau = A\sqrt{\Omega}e^{\Omega C}. \tag{3.36}$$

where ΩC is the integral of the re-scaled Lagrangian action, $\bar{S}$, along the heteroclinic connection between the stochastic extinction and the metastable state. Computing this heteroclinic connection is, in general, very hard. To reduce the dimensionality of the problem, we have performed a QSSA on the Hamilton equations. In Figure 3.4 we compare ΩC for different values of a_L computed with the Weak and the Strong QSSA, as a_L increases the difference between both tends to 0, then for large values of a_L we can use the Strong QSSA. In Figure 3.5 we show the heteroclinic connection, projected on the (p_2, q_2) plane, computed with the Strong QSSA and the Weak QSSA.

Lower Bound

Using the reduced system described by Eq (3.31), the computation of the heteroclinic is trivial. In this case the metastable state has the form

$$(p, x) = \left(1, L_{max}\frac{r - a_L - d_L}{r}\right), \tag{3.37}$$

and the stochastic extinction is

$$(p, x) = \left(\frac{a_L + d_L}{r}, 0\right). \tag{3.38}$$

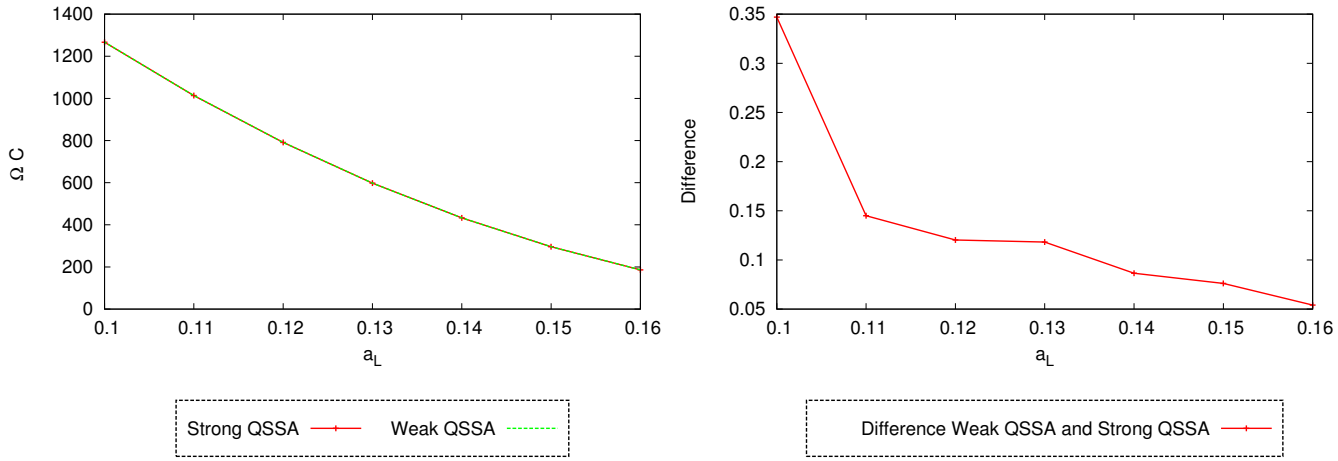

Figure 3.4: ΩC computed with the Strong QSSA and the Weak QSSA (left), a difference between them (right), for different values of a_L.

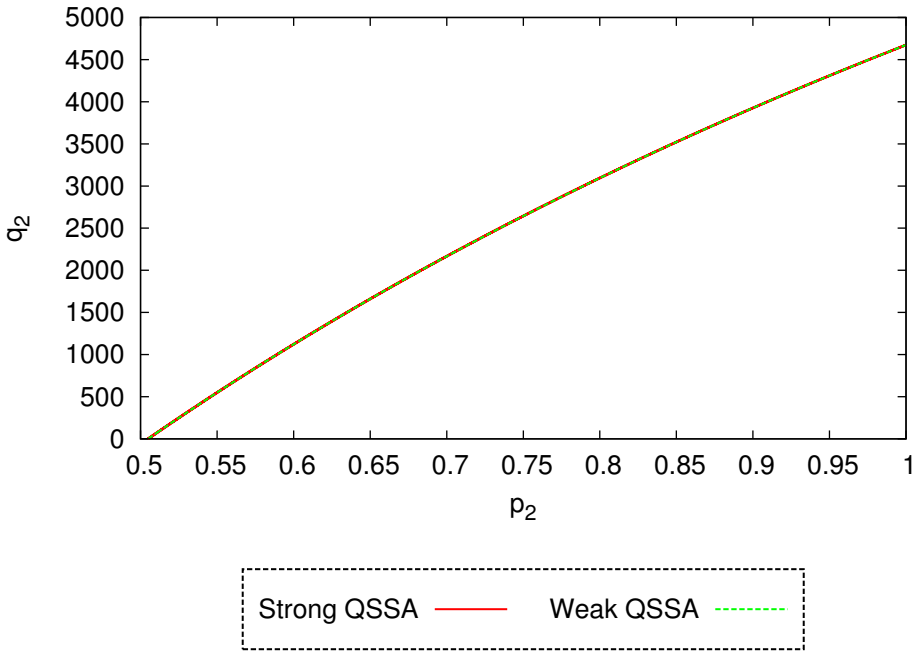

Figure 3.5: Projection on the $(p_2, q_2)-$plane of the heteroclinic connection between the metastable state and the stochastic extinction, computed with the Strong QSSA and the Weak QSSA. $a_L = a_L^s$.

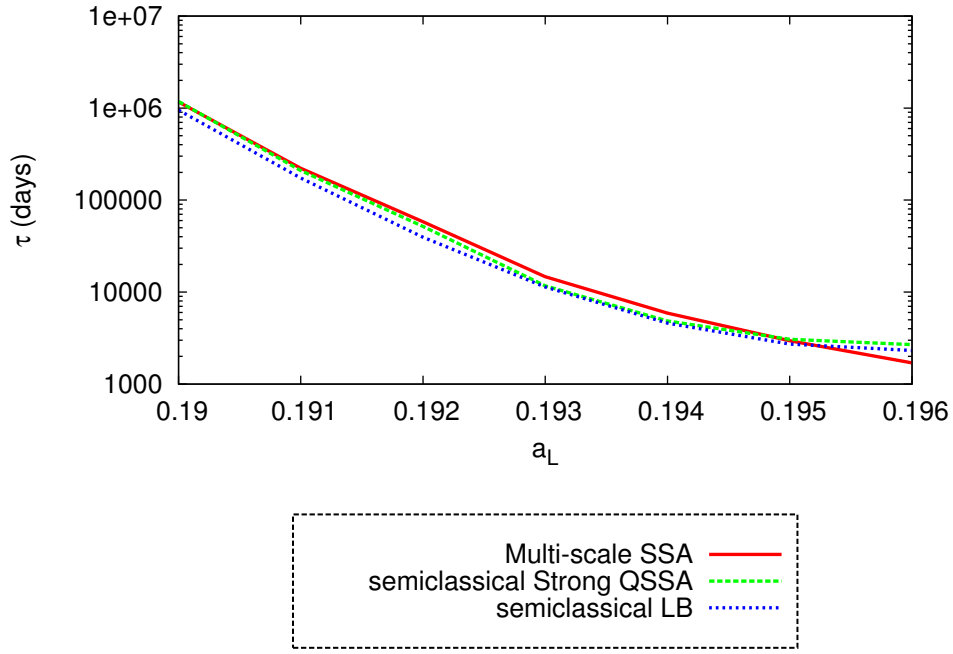

Figure 3.6: Mean extinction time for different values of a_L obtained via the semi-classical approximation with the Strong QSSA, the semi-classical approximation for the reduced (Lower Bound) system. Average is done over 1000 realisations of the multi-scale stochastic simulation algorithm

From Eq. (3.33), using the fact that the energy is preserved ($H = 0$), we obtain an analytic expression for the heteroclinic connection

$$x(p) = 2L_{max}\frac{r(p^2-p)+(a_L+d_L)(1-p)}{r(p^2-1)}, \tag{3.39}$$

therefore

$$\begin{aligned}\Omega C_{LB} &= \int_1^{\frac{a_L+d_L}{r}} x(p)dp = \int_1^{\frac{a_L+d_L}{r}} 2L_{max}\frac{r(p^2-p+(a_L+d_L)(1-p)}{r(p^2-1)}dp \\ &= 2L_{max}\,\frac{rp-log(p+1)(r+a_L+d_L)}{r}\Big|_1^{\frac{a_L+d_L}{r}}.\end{aligned} \tag{3.40}$$

In Figure 3.6 we show a comparison between the mean extinction time, and the probability of extinction at a given time computed via stochastic simulations, the semi-classical approximation with the Strong QSSA and the semi-classical approximation for the reduced (lower bound) system. We observe good agreement between the semi-classical and the exact solution, except in a neighbourhood of a_L^* where the number of latently infected cells is given in a small number and, in this case, the system size is not large enough, therefore the semi-classical approximation is not accurate.

3.4.2 Supercritical case

We are interested in the probability of extinction in a certain time, t, which is given by $G(0,t)$. Of particular interest is the case that the initial condition is the metastable state with $a_L = a_L^s$.

For $a_L \geq a_L^*$ the phase diagram is sketched in Figure 3.1 left. The main feature is that there is no metastable state. We approximate $G(p,t) \approx \exp(-S(p,t))$. A full derivation of this approximation is given in Appendix B.

Given a time T_f, the action is given by

$$\begin{aligned} S(p,T_f) &= HT_f - \int_0^{T_f} (q_1,q_2,q_3,q_4)(\dot{p}_1,\dot{p}_2,\dot{p}_3,\dot{p}_4)dt \\ &\quad -(n_1(0),n_2(0),n_3(0),n_4(0))(\log(p_1(0)),\log(p_2(0)),\log(p_3(0)),\log(p_4(0))), \end{aligned} \tag{3.41}$$

where $n_i(0) = p_i(0)q_i(0)$ is the initial condition. To obtain the probability of extinction, $P_0(t) = G(0,t)$, we proceed as follows:

- Choose initial conditions $(p(0),q(0))$ satisfying $p_i(0)q_i(0) = n_i(0)$,
- Integrate the equations (3.26) up to $p_2(T) = 0$, from this we will obtain a time T and a trajectory γ.
- Compute S_γ the action S along that trajectory γ.
- Then, approximate $P_0(T_f) = G(0,T_f) \approx exp(-S_\gamma(0,T_f))$.

A different way to approximate $G(0,t)$ should be to study only the extinction time of the latently infected cells, and assume that the dynamics of the other variables are described by the mean-field behaviour. This assumption is equivalent to consider $p_1 = p_3 = p_4 = 1$ and look for $G(1,0,1,1,t)$.

The same procedure is applicable for the 1-dimensional system described by Eq. (3.31).

Figure 3.7 shows the probability of extinction as a function of time, for different values of a_L, computed according to these methods. For comparison purposes, we also represent the results obtained by multi-scale stochastic simulations. In this case, the semi-classical approximation provides values of the extinction probability slightly below the numerical values.

3.4.3 Side effects: viral blips

Any increment of a_L reduces the viral load of the metastable state, however this does not give us information on the short time. In this subsection we study the short time effect of the antigen stimulation on the viral load and we will show that this stimulation could produce viral blips [110].

We observe that for a short time after the antigen stimulation, the viral load increases (Fig. 3.8). This is because the more x_2 cells are activated, the more x_3 cells appear in the system, therefore the amount of virus, x_4, increases as well.

Starting at the metastable state for $a_L = a_L^s = 0.1$ day^{-1}, we perform different simulations for different values of $a_L > a_L^s$. We observe, see results in Fig 3.8 (left), that for any a_L there is a peak of the viral load peak and then decays. The mean field behaviour also shows the same evolution pattern, as can be seen in Fig. 3.8 (right), and it gives us a good approximation of the solution of (3.1). In all our tests cases the peak in viral load stays within a few times the detection limit of standard assays (50 RNA copies/ml).

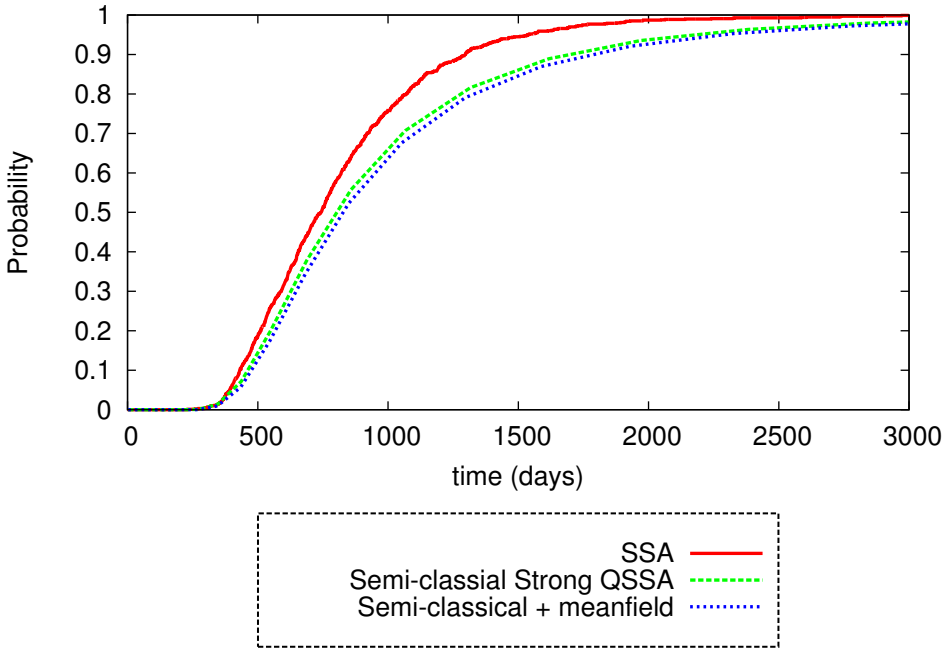

Figure 3.7: Probability of extinction as a function of time comparing three different approximations: assuming $p_1 = p_3 = p_4 = 1$(blue), Multi-scale stochastic simulations (red), semi-classical approximation for the QSSA (green)

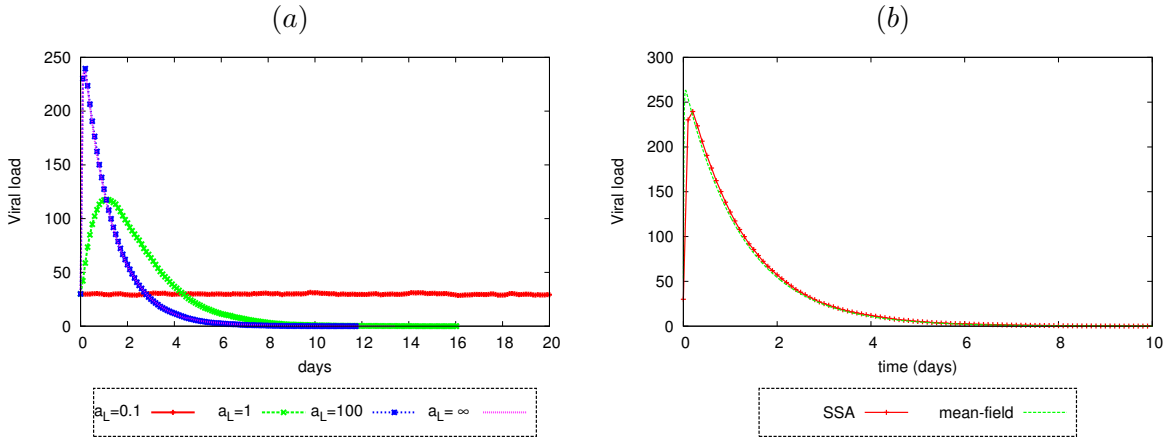

Figure 3.8: Gillespie simulations of the viral dynamics for different values of a_L. As initial condition we take the value of the variables at the metastable state before the antigen stimulation, that is $a_L = a_L^s$ (left). A comparison between a Gillespie simulation and the mean-field behaviour of the viral dynamics. As initial condition we take the value of the variables at the metastable state before the antigen stimulation, that is $a_L = a_L^s$, and we choose $a_L = 100$. (right)

3.5 Conclusions

In this chapter we have presented and analysed a stochastic model of HIV-1 dynamics in the blood stream under anti-retroviral therapy to study of the survival probability in a certain time of the viral load. We have investigated how the extinction probability depend on the activation rate of the latently infected cells using stochastic simulations and analytic approximations. Furthermore we have presented some reductions of the system which has given a lot of tractability to the problem without losing accuracy in the solution. From a medical point of view, according to this model, this therapy can reduce the average extinction of the infection to a few years.

Chapter 4

Stochastic modelling of viral blips in HIV-1-infected patients: Effects of inhomogeneous density fluctuations

An stochastic model of HIV-1 infection dynamics under HAART is proposed in order to analyse the origin and dynamics of the so-called viral blips, i.e. episodes of transient viremia that occur in the phase of where the disease remains in a latent state during which the viral load raises above the detection limit of standard clinical assays. Based on prior work in this subject, we consider an infection model in which latently infected cell compartment sustains a residual (latent) infection over long periods of time and, unlike previous models, we include the effects of inhomogeneities in cell and virus concentration in the blood stream. We further consider the effect of burst virion production. By comparing with the experimental results obtained during an study in which intensive sampling was carried out on HIV-1-infected patients undergoing HAART over a long period of time, we conclude that our model supports the hypothesis that viral blips are consistent with random fluctuations around the average viral load. We further conclude that agreement between our simulation results and the blip statistics obtained in the aforementioned study improves when burst virion production is considered. We also study the effect of sample manipulation artifacts on the results produced by our model, in particular, that of the post-extraction handling time, i.e. the time elapsed between sample extraction and actual test. Our results support the notion that the statistics of viral blips can be critically affected by such artifacts.

4.1 Introduction

An early hypothesis regarding the origins of viral blips, whose emergence was, at the time, suspected of heralding imminent virological failure, was that they are due to the appearance of new, drug-resistant viral variants [80]. However, a number of studies have compiled evidence against viral blips being correlated with virological failure [54, 89, 95], thus weakening the case of viral blips being early warnings related to viral evolution leading to drug resistant strains of the virus. Further to the hypothesis of blips being originated by

viral evolution, other mechanisms have been proposed which include antigen-driven CD4+ T cell activation due to vaccination or secondary infections [37, 52, 41, 40, 43, 61, 62]. It has also been shown that activation of latently infected cells may play a role in the emergence of viral blips. For example, Jones & Perelson have proposed a model in which increased activation of latently infected cells can lead to a burst in viral load [63]. The possibility that asymmetric division of activated latently infected cells may help to explain the decay kinetics of the latent compartment and intermittent viral blips has been in explored in [109]. Recently, Rong & Perelson [111] have formulated a model in which stochastic activation of latently infected cells can maintain viral blips without completely depleting the latent reservoir, thus maintaining long-term, low-level viremia. They also developed a model which incorporated density-dependent homeostatic proliferation of the memory CD4+ T memory cells (and, therefore, of the latently infected cell compartment), which, according to [23], drives persistence and determines the size of the latent reservoir.

Alongside all these models which postulate that viral blips have a physiological origin, there is an alternative school of thought which claims that most viral blips are random occurrences of probabilistic origin related to the small number of virus mRNA in the latent phase as well as being partly produced by laboratory artefacts during the processing of the samples [76, 94]. According to this view, viral blips are mostly uncorrelated with virological failure, virus evolution, vaccination, or non-adherence to treatment regimen [95, 76, 94] and, therefore, only a small fraction of such occurrences are of clinical significance. Conway & Coombs [28] have proposed a model to analyse the stochastic viral dynamics in treated patients. This model treats viral blips as random events occurring every time the viral load reaches the standard detection limit (i.e. 50 mRNA/ml). Although this model reproduces many of the features of HIV-1 viral dynamics and provides a detailed description of its stochastic dynamics, there are several properties of the statistics of viral blips in which [28] appears to depart from experimental observation. One such departure refers to the frequency of blips. According to the model formulated in [28], blip frequency decreases exponentially in time which disagrees with the results by DiMascio et al. [30] where a constant blip rate is reported. Conway & Coombs [28] claim that this difference is due to the fact that, whilst theirmodel accounts only for blips of small amplitude caused by fluctuations, [30] inlcude in their statistics blips of both small and large amplitude. Therefore, Conway & Coombs implicitly assume that large blips must have a biological origin. Similarly, the data collected by Nettles et al. [95], where intensive sampling was carried out on HIV-1-infected patients with samples collected every 2-3 days over a period of 3 to 4 months, reported that blips were observed in 9 out of 10 patients with an average of two blips per patient. The blip statistics produced by the model formulated in [28] appears to predict that blips be too rare to be comparable to the experimental data, even in conditions of elevated virus rate production and latent cell activation. It can be argued that the rationale for this discrepancy is the same as before: Nettles et al. [95] measure the full range of blips (both small and large amplitudes) whilst Conway & Coombs [28] account only for small-amplitude blips. Therefore, according to this model [28], small amplitude blips are consistent with an stochastic model whereas large amplitude blips must be produced by causes other than random fluctuations.

One common feature shared by all of the models discussed in the Introduction, both stochastic and deterministic, is that they all assume that the system is well-mixed, i.e. all the cellular and molecular species are evenly distributed over the volume of blood so that only the number of each species determines the state of the system. For this

modelling assumption to hold, the numbers of each species must be large enough so that their densities remain approximately uniform. The system we are dealing with in this chapter has at least two species, virus and latently infected cells, which are present in very small numbers. As a consequence, their densities can show large fluctuations which would lead to large inhomogeneities in the local numbers of such species. The effect of this inhomogeneity can be rather sizeable, specially since measurements of viral load are performed by extracting small samples of blood which are then analysed.

The aim of this chapter is to ascertain whether density fluctuations affect the stochastic dynamics of the viral load in HAART-treated patients beyond the predictions of reference [28] and investigate if an stochastic model which includes density fluctuations is capable of a more faithfull reproduction of the experimental results reported in [30, 95]. To this end we formulate an stochastic compartmental model [13] where volume of blood is divided in small compartments (whose volume is assumed of the order of the volume of one blood sample taken for analysis). Within each of this compartment, the system is assumed to be well-mixed but we consider that differences may arise between compartments thus accounting for density fluctuations [46, 34, 35, 36, 79, 117]. Furthermore, in order to address the issue of whether laboratory artefacts alter the statistics of viral blips we have designed an *in silico* blood extraction procedure that allows us to study, at least partially, this aspect of the problem.

This chapter is organised as follows. Section 4.2 is devoted to a detailed explanation of the model assumptions and formulation. In Section 4.3 we conduct extensive simulations of our model and present our results. Finally, in Section 4.4 we proceed to discuss our results.

4.2 Model formulation

We now proceed to present our compartmental model of stochastic viral dynamics. Our model is based on the modelling approach whereby spatially inhomogeneous systems are dealt with by compartmentalising the domain where the system lives into small compartments [13]. Within each of these compartments all of the species participating in the dynamics of the system are assumed to be well-mixed, so that our resolution to measure spatial variations is of the order of the compartment size. The local, well-mixed, within-compartment stochastic dynamics is supplemented by stochastic transitions that allow for transport of species between compartments. This approach has been widely applied to many situations in which spatial heterogeneity is essential, in particular, reaction-diffusion systems [46, 34, 35, 36, 79, 117]. This setting will allow us to ascertain the effect of density fluctuations on stochastic viral dynamics.

Further to our compartmental model, we also formulate an *in silico* blood analysis model, which intends to follow as closely as possible the intensive sampling procedure designed by Nettles et al. [95] to analyse the dynamics and statistics of viral blips in HIV-1-infected patients under HAART.

4.2.1 Compartmental Model

In order to account for density fluctuations, we consider a compartmental model, schematically shown in Fig. 4.1. We will assume that, in an attempt to roughly imitate the structure of the blood stream, compartments are arranged on a one dimensional, closed

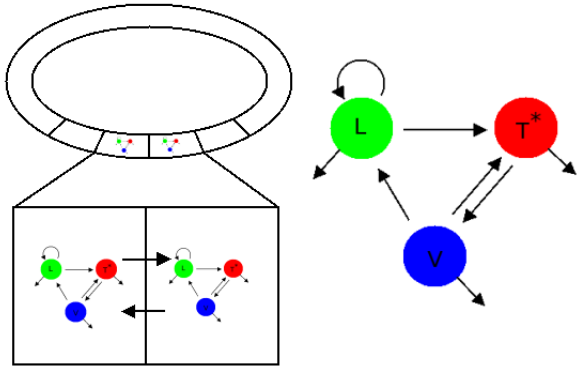

Figure 4.1: This figure depicts an schematic diagram of our compartmental model. Our model represents the circulatory system in a very simplistic way as a one dimensional closed circuit of adjacent compartments. Within each compartment we model the (local) cellular dynamics of an HIV-1-infected T-cell population with latency [110, 28]: We consider the dynamics of the HIV-1 virus load (V), active infected T-cells (T^*), and latently infected cells (L). Virus capsides, V, are released by active infected cells and infect uninfected T-cells. We consider that the number of uninfected T-cells is so much larger than that of infected cells that we consider them as a reservoir. Latently infected cells can become active upon estimulation with proper antigens. In addition to this within-compartment cellular dynamics, we consider random movement of both latently and active infected cells and virus capsides between compartments.

Transition rate	$r_{j+(i-1)R_L} = (\Delta L_i, \Delta T_i^*, \Delta V_i)$	Description
$W_{1+(i-1)R_L} = \eta(1-\epsilon)kV_iT_i\Omega^{-1}$	$(1,0,-1)$	Latent infection $T_i + V_i \to L_i$ cell
$W_{2+(i-1)R_L} = (1-\eta)(1-\epsilon)kV_iT_i\Omega^{-1}$	$(0,1,-1)$	Active infection $T_i + V_i \to T_i^*$ cell
$W_{3+(i-1)R_L} = rL_i$	$(1,0,0)$	Latent cell proliferation $L_i \to 2L_i$
$W_{4+(i-1)R_L} = \frac{r}{L_{max}}\frac{L_i*(L_i-1)}{2}\Omega^{-1}$	$(-2,0,0)$	Latent cell binary annihilation $L_i + L_i \to \emptyset$
$W_{5+(i-1)R_L} = d_0L_i$	$(-1,0,0)$	Latent cell clearance L_i
$W_{6+(i-1)R_L} = a_LL_i$	$(-1,1,0)$	Activation $L_i \to T_i^*$
$W_{7+(i-1)R_L} = \delta T_i^*$	$(0,-1,0)$	Active cell death
$W_{8+(i-1)R_L} = cV_i$	$(0,0,-1)$	Virion clearance
$W_{9+(i-1)R_L} = p_vT_i^*$	$(0,0,1)$	Continuous virion production
$W_{10+(i-1)R_L} = \epsilon kV_iT_i\Omega^{-1}$	$(0,0,-1)$	Failed infection

Table 4.1: Transition rates corresponding to the stochastic model of viral blip generation. See text (Section 4.2) for details. $R_L = 10$. T_i, the number of uninfected cells is taken to be constant [28]. Ω is the compartment size.

(i.e. with periodic boundary conditions) lattice (see Fig. 4.1). In each compartment, we consider three types of interacting species, namely, active infected cells, latently infected cells, and virus. The number of each of these species in compartment i is referred to as T_i^*, L_i, and V_i, respectively, where $i = 1, \ldots, N_c$ with N_c is the number of compartments. We further introduce the vector $X(t) \equiv (T_1^*(t), L_1(t), V_1(t), \ldots, T_{N_c}^*(t), L_{N_c}(t), V_{N_c}(t))$ whose components correspond to the number of cells of of each species at site $i = 1, \ldots, N_c$ and time t. We will find convenient to define $x_i(t) \equiv (T_i^*(t), L_i(t), V_i(t))$, so that the vector $X(t)$ can be written as $X(t) = (x_1(t), \ldots, x_{N_c})$.

The stochastic dynamics of our system is described by the corresponding Master Equation [122, 79, 44]:

$$\frac{\partial}{\partial t}P(X,t) = \sum_{i=1}^{N_c}\sum_{j=1}^{R_L}\left(W_{j+(i-1)R_L}(X - r_{j+(i-1)R_L})P(X - r_{j+(i-1)R_L}) - W_{j+(i-1)R_L}(X)P(X)\right) \sum_{i=1}^{N_c}\sum_{j=1}^{R_T}\left(\omega_{j+(i-1)R_T}(X - \rho_{j+(i-1)R_T})P(X - \rho_{j+(i-1)R_T}) - \omega_{j+(i-1)R_T}(X)P(X)\right)$$

where we have splitted the Master Equation in a purely local part, corresponding to the population dynamics within each compartment, and a transport part, which accounts for transport of species between adjacent compartments. R_L and R_T are the number of local and transport events, respectively, that can affect the state, x_i, of each compartment. The transition rates are defined in Tables 4.1 and 4.2.

In order to facilitate later formulation of our *in silico* blood extraction protocol and its comparison with [95], we will consider compartments of volume $V_c = 8.5$ ml each, which is the volume of blood sampled extracted for analysis in the study reported in [95]. We will consider that an average individual has 5 litres of blood so we need to consider $N_c = 588$ compartments.

The within-compartment stochastic viral dynamics model is based on previous works by Rong & Perelson [110] and Conway & Coombs [28] and it is schematically shown in Fig. 4.1. Following the latter, we assume that, due to the large numbers in which CD4+

Transition rate	$\rho_{j+(i-1)R_T}$	Description
$\omega_{1+(i-1)R_T} = \mu_{L+}L_i$	$(0,...,0,-1,0,0,1,0,...)$	$L_i + L_{i+1} \to L_i - 1 + L_{i+1} + 1$
$\omega_{2+(i-1)R_T} = \mu_{L-}L_i$	$(0,...,0,1,0,0,-1,0,...))$	$L_i + L_{i-1} \to L_i - 1 + L_{i-1} + 1$
$\omega_{3+(i-1)R_T} = \mu_{T^*+}T_i^*$	$(0,...,0,-1,0,0,1,0,...))$	$T_i^* + T_{i+1}^* \to T_i^* - 1 + T_{i+1}^* + 1$
$\omega_{4+(i-1)R_T} = \mu_{T^*-}T_i^*$	$(0,...,0,1,0,0,-1,0,...)$	$T_i^* + T_{i-1}^* \to T_i^* - 1 + T_{i-1}^* + 1$
$\omega_{5+(i-1)R_T} = \mu_{V+}V_i$	$(0,...,0,-1,0,0,1,0,...)$	$V_i + V_{i+1} \to V_i - 1 + V_{i+1} + 1$
$\omega_{6+(i-1)R_T} = \mu_{V-}V_i$	$(0,...,0,1,0,0,-1,0,...)$	$V_i + V_{i-1} \to V_i - 1 + V_{i-1} + 1$

Table 4.2: Transition rate corresponding to the stochastic model of viral blip generation. A detailed is given in the main text (Section 4.2). $R_T = 6$.

T uninfected cells are present, they are unaffected by fluctuations and their number is taken as constant. We assume that two types of infected cells exist, latenly infected cells, L_i, which carry the virus but do not synthesize new virions, and active infected cells, T_i^*, which produce and release new virions. As a consequence, active infected cells are targeted by HAART whereas latently infected cells are immune to its effects. Both types of infected cells are produced by infection of uninfected T cells. Furthermore, latently infected cells can become active, for example, by estimulation with appropriate antigens. Both latently and active infected cells are assumed to die at a certain rate and blood-borne virions are assumed to be cleared off at a constant rate. We also account for experimental results showing that the latently infected cells are maintained by homeostatic proliferation [23], by means of a phenomenological model which includes branching and binary annihilation of latently infected cells [110, 35].

The elementary events involved in our spatial model of stochastic viral dynamics are as follows.

- Latenly infected cells L_i can undergo:

    1. Homeostatically balanced proliferation. Following [110], we account for homoeostatic control of proliferation by means of a combination of branching ($L_i \to 2L_i$) with binary annihilation ($L_i + L_i \to \varnothing$). It has been shown (see e.g. [35]) that this combination is an stochastic counterpart of the standard logistic growth. The corresponding transition rates are $W_{3+(i-1)R_L}$ for branching and $W_{4+(i-1)R_L}$ for binary annihilation (see Table 4.1).
    2. Death. We assume a simple linear decay with transition rate $W_{5+(i-1)R_L}$ as shown in Table 4.1.
    3. Activation. By means of this process a latently infected cell becomes an active infected cell $L_i \to T_i^*$. The corresponding transition rate is $W_{6+(i-1)R_L}$, Table 4.1.
    4. In addition to the processes described above, which have to do with the (within-compartment) population dynamics, we assume that latently infected cells can move between neighbouring compartments. We will assume a coupling between compartments where transitions occur at constant per cell rate, ν_L. In periodic, one dimensional setting, cells in compartment i can move to compartment $i+1$ at rate $\omega_{1+(i-1)R_T}$ or to compartment $i-1$ at rate $\omega_{2+(i-1)R_T}$ as defined in Table 4.2.

- Active infected cells, T_i^*, cell are subjected to:

1. Apoptosis with transition rate $W_{7+(i-1)R_L}$ (see Table 4.1).
2. Virion production. Contrary to latently infected cells, active infected cells synthesise and release new virions. In general, viral production can occur in a continuous fashion over the life span of an infected cell or in a burst which kills the cell. For the HIV infection both modes have been proposed [97]. Transition rate $W_{9+(i-1)R_L}$ (Table 4.1) corresponds to continuous production. Later in the chapter, we consider an additional scenario, in which both continuous and burst production occur.
3. Transport between neighbouring compartments. Just as latently infected cells do, active infected cells can move between compartments at rates $\omega_{3+(i-1)R_T}$ and $\omega_{4+(i-1)R_T}$ as per Table 4.2.

- Finally, virus, V_i, can:

1. Infect a healthy T cell producing a latently infected cell. In patients under HAART, the infection process is hindered by the presence of an antiretroviral drug. The efficiency of such drug is measured by a parameter, ϵ, which takes values between 0 and 1, the latter (former) corresponding to a maximally (in)efficient drug. $(1-\epsilon)$ is interpreted as the proportion of virions capable of infection under HAART treatment. We also assume that, upon infection, the cell can become latently infected with probability η or active with probability $(1-\eta)$. Therefore the corresponding transition rate $W_{1+(i-1)R_L}$ is proportional to $\eta(1-\epsilon)$ as shown in Table 4.1.
2. Infect a healthy T cell producing an active infected cell. In this case, the corresponding transition rate $W_{2+(i-1)R_L}$ is proportional to $(1-\eta)(1-\epsilon)$ (see Table 4.1).
3. Undergo clearance. Virions are removed from the blood, which we model as a simple linear decay with transition rate $W_{8+(i-1)R_L}$ as per Table 4.1.
4. Fail to infect and being eliminated by the drug with transition rate $W_{10+(i-1)R_L}$ (see Table 4.1).
5. Transport between neighbouring compartments. Virions can move between compartments at rates $\omega_{5+(i-1)R_T}$ and $\omega_{6+(i-1)R_T}$ as per Table 4.2).

Numerical methodology We will perform numerical simulations of the Master Equation 4.1 using the methodology proposed by Bernstein [13], which is a straight forward generalisation of the original stochastic simulation algorithm proposed by Gillespie [47].

Parameter values The (default) parameter values used in our simulations are given in Table 4.3. The parameter values corresponding to the model of cellular dynamics of an HIV-1-infected T-cell population with latency are based on estimates available in the literature on the subject.

Random motility between compartments has been modelled as simple diffusion. The transition probability between compartments is therefore given by $\mu_{J+} = \frac{D_J}{h^2}$, where $J = V,\ L,\ T^*$, D_J is the diffusion coefficient of species J, and $h = \sqrt[3]{V_c}$, where V_c is the compartment volume. The magnitude of the diffusion coefficient for several types of viral capsides has been estimated between 1.6 and 30 $\mu\text{m}^2\text{s}^{-1}$ [93]. We consider a typical

Parameter	Rate	Description	Reference
λ	10000 ml^{-1} day^{-1}	Recruitment rate of T cells	[19]
d_T	0.0166 day^{-1}	Death rate of T cells	[90]
k	$2.4 \cdot 10^{-8}$ ml day^{-1}	infection rate	[100]
ϵ	0.85	Drug efficacy	[110]*
η	0.001	Fraction resulting in latency	[63]
d_0	0.001 day^{-1}	Death rate of latently infected cells	[19]
a_L	0.1 day^{-1}	Rate of transition from latently to productively	[110]
σ	1 day^{-1}	death rate of productively infected cells	[83]
c	23 day^{-1}	clearance rate of free virus in blood stream	[104]
p_v	2000 day^{-1}	Viral production rate	[59]
r	0.2 day^{-1}	proliferation rate of activated cells	[110]
L_{max}	See caption	Carrying capacity density of latent cells	[110]
V_c	8.5 ml	Compartment volume	[95]

Table 4.3: Parameter values used in our numerical simulations. The value of L_{max} is let to vary depending on the average viral load we impose on our simulations. For the values of the average viral load considered in Section 4.3, i.e. 10, 12.5, 20, 30, and 40 copies/ml, the corresponding values of $L_{max} = 1.89, 2.36, 3.78, 5.66,$ and 7.55 cells/ml, respectively.

value $D_V = 5$ μm^{2}s^{-1} [56, 12]. Similarly, we take a generic estimate for the diffusion coefficient of a cell $D_L = D_{T^*} = 0.05$ μm^{2}s^{-1} [15]. Furthermore, in order to account for the directionality of blood flow, we assume that $\mu_{J-} = 3\mu_{J+}$.

4.2.2 *In silico* blood sample analysis model

Further to the compartmental model of Section 4.2.1 which allows us to account for density fluctuations in stochastic viral dynamics, we have formulated an *In silico* blood sample analysis model. This additional model has the aim of trying to reproduce the experimental procedure described in [95] as closely as possible. Nettles et al. [95] designed an experimental protocol in which ten HIV-1 infected patients under HAART were intensively sampled (every 2 or 3 days) for a period of 3 to 4 months. Each time blood was extracted, two samples per patient were taken and sent to two different laboratories for analysis. They concluded that blips had short duration (less than 3 days on average) and low amplitude (79 copies/ml on average) with an average of 1.8 blips per patient.

Our procedure is as follows. After running the compartmental dynamics until time t_c, which is chosen to be long enough so that the average properties of the system reach an steady state, we choose two compartments at random i and j among the N_c compartments that compose our system. We then record the corresponding state $x_i(t_c) = (T_j^*(t_c), L_i(t_c), V_i(t_c))$ and $x_j(t_c) = (T_j^*(t_c), L_j(t_c), V_j(t_c))$. Recall that we are assuming that the number of uninfected T cells is assumed to be constant and uniform [28]. In order to account for possible delays between the time of extraction and the actual analysis, we assume that the extracted samples continue to evolve subject to the local (within-compartment) dynamics determined by the rates in Table 4.1 with the transition rates corresponding to between-compartment transitions $\omega_l(X) = 0$. This post-extraction dynamics is ran for a duration t_w.

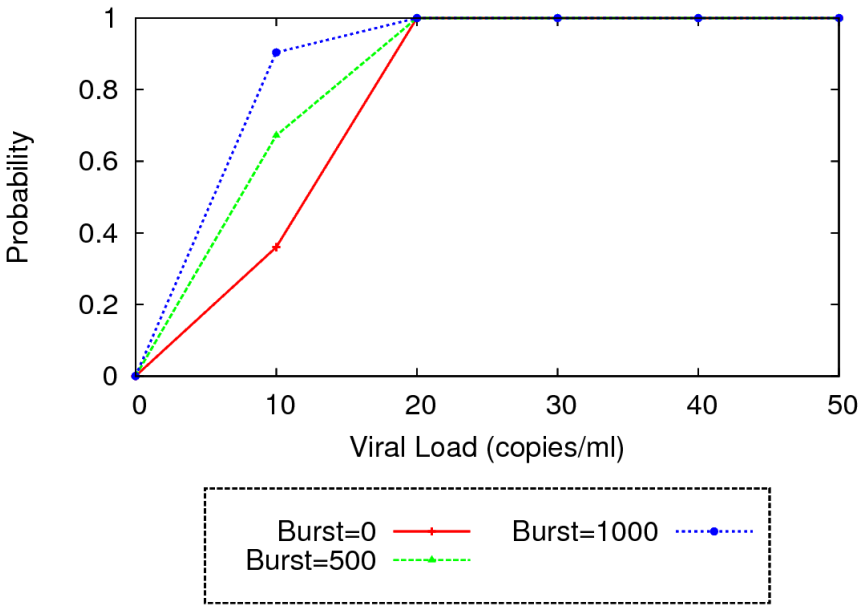

Figure 4.2: Probability of observing at least one blip in our *in silico* blood sample analysis model as a function of the average virus load for different values of the burst size. Nettles et al. [95] in their intensive sampling study showed that 9 out 10 patients underwent at least one viral blip. We observe that, as the average viral load increases the probability of observing at least one blip tends to one. We also observe that as the burst size increases the observation of at least one blip becomes more likely. Note that the rate of continuous virion production has been chosen for each value of the burst size so that the average number of virions produced per active infected cell during its life-time is kept constant. We have fixed an average viral load of 12.5 copies/ml [95]. Parameter values as per Table 4.3. p_v' is taken such that $p_v' + \delta N = p_v$, where N is the burst size and p_v is given in Table 4.3.

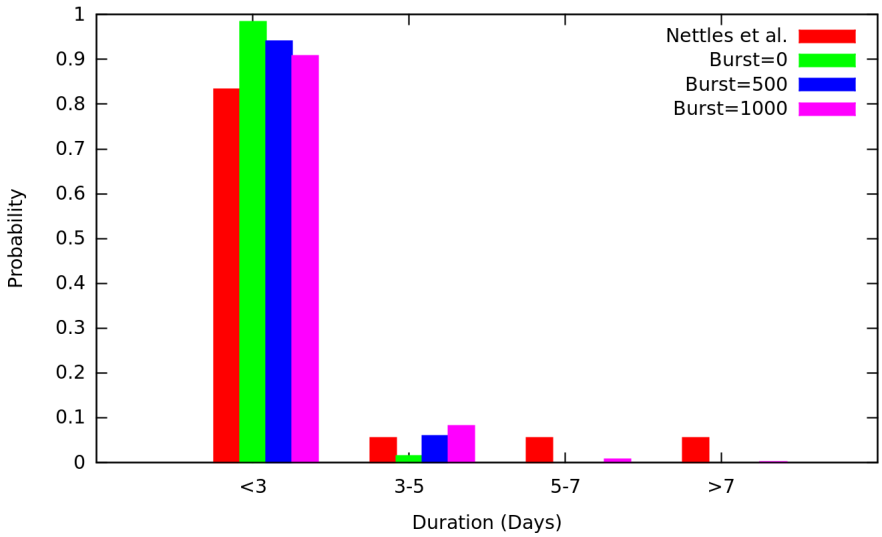

Figure 4.3: Comparison between blips statistics obtained in the study by Nettles et al. [95] and those obtained from our simulations for different burst sizes. This plot shows the probability of observing a blip of a given duration (measured in days). The rate of continuous virion production has been chosen for each value of the burst size so that the average number of virions produced per active infected cell during its life-time is kept constant. We have fixed an average viral load of 12.5 copies/ml [95]. Parameter values as per Table 4.3. p'_v is taken such that $p'_v + \delta N = p_v$, where N is the burst size and pv is given in Table 4.3.

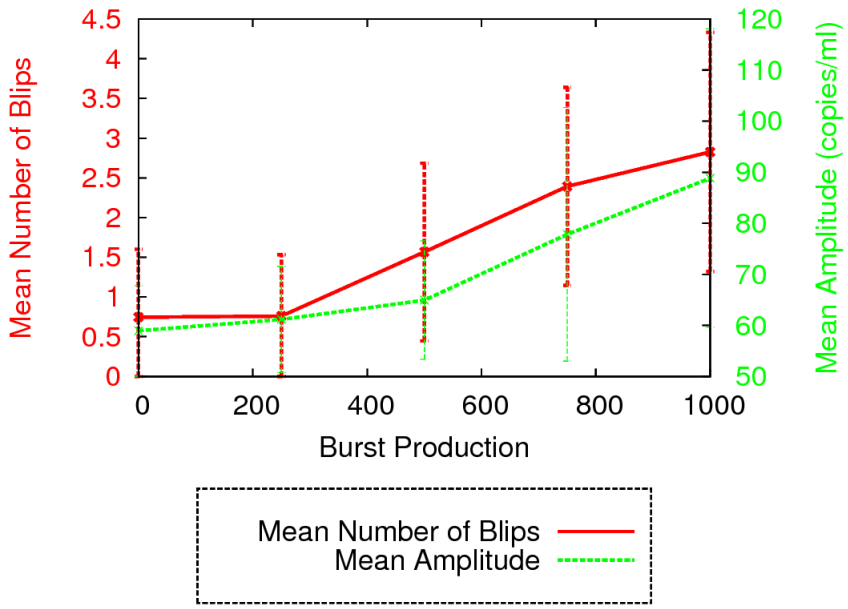

Figure 4.4: This plot shows the average number of blips and median amplitude as a function of the burst size obtained with our model. According to Nettles et al. [95] ,the average number of blips per patient is 1.7 and the median of the amplitude is 79 copies/ml. The rate of continuous virion production has been chosen for each value of the burst size so that the average number of virions produced per active infected cell during its life-time is kept constant. We have fixed an average viral load of 12.5 copies/ml [95]. Parameter values as per Table 4.3. p_v' is taken such that $p_v' + \delta N = p_v$, where N is the burst size and p_v is given in Table 4.3.

4.2.3 Effects of continuous versus burst production of virions

The issue of whether virions are secreted by active infected cells in a continuous way during their lifespan or, on the contrary, they are released in a single burst which, actually, kills the cell remains controversial. Standard models based on mean-field, deterministic systems of ordinary differential cannot distinguish between both production modes, since they predict exactly the same dynamics as long as the total number of virions produced over their lifespan is the same [97]. A recent analysis by Pearson and co-workers has concluded that stochastic models of early infection lead to significantly different results depending on whether virion production is considered as continuous or bursty [97].

Here, we consider this issue regarding its possible influence on the statistics of viral blips. To this end, we consider two models, namely, one in which only continuous virion production is taken into account (given in Table 4.1) and another one in which both modes of virion production, continuous and bursty, are considered. The latter requires an alteration of the process described by Table 4.1. The reaction corresponding to active cell death now reads:

$$W_{7+(i-1)R_L} = \delta T_i^* \text{ and } r_{7+(i-1)R_L} = (0, -1, N) \tag{4.1}$$

which implies that upon active cell death, one active cell death is lost and N virions are realeased. N is the so-called burst size. A further modification needs to be done, this time affecting the rate of continuous virion production:

$$W_{9+(i-1)R_L} = p_v' T_i^* \text{ and } r_{9+(i-1)R_L} = (0, 0, 1) \tag{4.2}$$

where p_v', i.e. the rate of continuous virion production, is now a function of the burst size, N. Given a value of N, we fix p_v' so that the average number of virion produced during the lifespan of am active infected cell is the same as for the purely continuous virion production model (i.e. $N = 0$ as per Table 4.1).

The remaining reactions are left unmodified with respect to those shown in Table 4.1.

4.3 Results

In this section we will use the models presented in section 4.2 to explore the phenomenology associated to our model and obtain statistics of viral blips which can then be compared to the experimental data reported by Nettles et al. [95].

4.3.1 Effect of density fluctuations on blips statistics

We have carried out extensive numerical simulations of our model using the methodology explained in Section 4.2. We start by focusing in our inhomogeneous infection model with continuous virion production as defined by the transition rates given in Tables 4.1, accounting for the local infection dynamics, and 4.2, accounting for diffusion of cells/virions between compartments. Results are included in Figs. 4.2, 4.3 and 4.4.

Nettles et al. [95] reported that 9 out 10 patients who underwent their intensive sampling protocol were observed to exhibit at least one blip. In other words, the probability of detecting at least one blip during the course of their experiments can be estimated to be 90%. By means of numerical simulations of our *in silico* blood sample model, we have computed the probability of detecting at least one blip as a function of the average viral

load (see Fig. 4.2, burst size $N = 0$). Our results show that, as the average viral load grows, so does the probability of detecting at least one blip. According to our results for viral loads bigger that 20 copies/ml, this probability approaches 1, in good agreement with figure reported in [95].

Nettles et al. [95] reported further statistical information, in particular, regarding blip duration (reproduced in Fig. 4.3) by recording the frequency with which blips of a certain duration are observed. They observed the blips with duration of 3 days or shorter accounted for over 80% of the observations. Blips of duration between 3 and 5 days, 5 and 7 days and of 7 days or longer were observed in less than 10% of the cases each. Our simulation results are in good agreement with these observations (see Fig. 4.3). Our model, however, appears to overestimate the frequencies of the shorter blips (duration of 3 days or shorter and between 3 and 5 days) at the expense of the longer ones.

Further information that can be extracted from the data reported in [95] concerns the average number of blips and their average amplitude. According to their experiments, the average number of blips is 1.8 and their average amplitude 79 copies/ml. Regarding these two metrics, our simulation results reported in Fig. 4.4 for burst size equal to zero show that our inhomogeneous infection model with continuous virion production underestimates these quantities by a significant amount.

4.3.2 Effect of burst production of virions

In order to improve the quantitative agreement between the data reported in [95] and our model predictions, we have explored the effect of including both continuous and burst virion production (see Section 4.2.3). In particular, we have analysed the behaviour of our system as a function of the burst size, keeping constant the average number of virions produced by active infected cells during their lifespan.

We have studied the effect of burst production on the statistics concerning viral blips shown in Figs. 4.2, 4.3 and 4.4. Regarding the probability of detecting at least one blip, although its behaviour for positive burst size is qualitatively similar to the burst size $N = 0$ case, our model predicts an increase in the probability of observing at least one blip for lower values of the average viral load (see Fig. 4.2). This increase is proportional to the burst size: The bigger the burst size, the larger the increase in the probability of observing at least one blip.

The discrepancies between experimental data and simulation results concerning the frequency of blip duration tend to be corrected when a positive burst size is considered (see Fig. 4.3). As we have discussed previously, the inhomogeneous infection model with continuous virion production overestimates the frequency of shorter blips at the expense of longer ones. This trend is compensated when we consider burst production of virions: As the burst size is let to increase, shorter blips become less frequent at the expense of longer ones, whose frequency is observed to increase as shown in Fig. 4.3.

Further discrepancies between the data reported in [95] and simulation results of our inhomogeneous infection model with continuous virion production regarding the average number of blips and their average amplitude. Our model with no burst virion production underestimates these quantities. Fig. 4.4 shows that, as burst size increases, the value predicted by our model for these two quantities approaches those reported in [95].

To summarise, although our inhomogeneous infection model with continuous virion production appears to qualitatively capture the blip statistics obtained by Nettles et al.

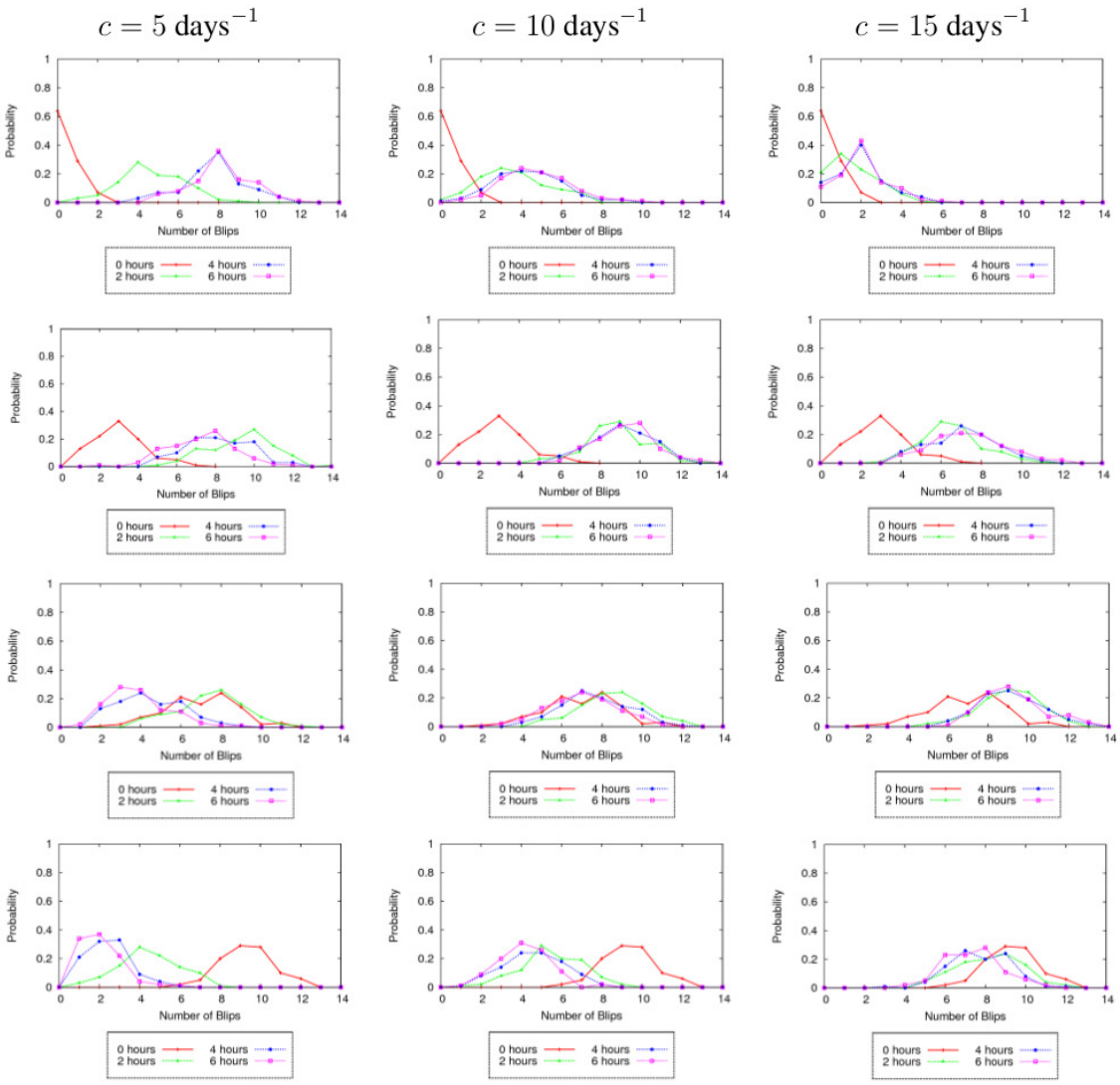

Figure 4.5: Probability of observing n blips within a sample, $P(n)$, as a function of the post-extraction handling time, t_w, and the virus clearance rate, c. We have also considered different value of the average viral load: The first, second, third, and fourth correspond to 10, 20, 30, and 40 copies/ml, respectively. We have considered the continuous virion production only.

[95], better quantitative agreement is obtained when burst production of virions is considered.

4.3.3 Effect of post-extraction handling time

A controversial aspect regarding the origin and clinical significance of viral blips is the claim that their statistics are affected by artifacts related to the sample manipulation process [76, 94]. In order to partially address this issue within the context of our model, we have devised a set of simulations in which we consider the effect of the post-extraction handling time in our *in silico* blood test model, t_w (see Section 4.2.2). This time is assumed to correspond to the time elapsed between extraction of the blood sample and actual analysis at the laboratory. We have considered that t_w is of the order several hours. During this time lapse, the infection dynamics stays running but since the sample is now extracted and therefore isolated there is no between-compartments cell/virion motility (i.e. the dynamics is described by a purely local infection model determined by the rates given in Table 4.1). Extraction of a compartment (sample) and its consequent isolation from the blood stream has the likely effect of reducing the rate at which virus particles are cleared, since it has been isolated from usual removal mechanisms. We have therefore considered the effect of reducing the virus clearance rate with respect to current estimates in the literature (see Table 4.3). Note that all the simulation results presented in Sections 4.3.1 and 4.3.2 correspond to $t_w = 0$.

In order to assess the effects of both the handling time, t_w, and the virus clearance rate, c, we have done numerical simulations to compute the Probability of observing n blips within a sample, $P(n)$, for different values of the average viral load. Our results are reported in Fig. 4.5. For lower values of the average viral load (see Fig. 4.5, 10 and 20 copies/ml), we observe that there is a strong dependence on the average number of blips with t_w: Due to accumulation of virus capsides as time progresses (recall that we are assuming that active infected cells continue to release virions after extraction until such time as the actual count is carried out), the average number of blips increases, as indicated by the fact that the peak of $P(n)$ shifts to larger values of n as t_w increases. Likewise, the position of this peak shifts to larger values of n as the virus clearance rate, c, decreases. For larger values of the average viral load ((see Fig. 4.5, 30 and 40 copies/ml), our simulation results show that the peak of $P(n)$ shifts to smaller values of n as t_w increases. This result is actually an artifact of how blips are defined and counted: A blip is the event whereby the viral load, initially below 50 copies/ml, transiently grows above the detection threshold. When the average viral load is 30 or 40 copies/ml, the duration of these events becomes very long, which has the by-product of reducing the blips count. To illustrate this phenomenon, we show in Fig. 4.6 the number of observations which are above 50 RNA copies/ml. When the viral load is 10 copies/ml, the difference between the number of observations above the detection limit and the number of viral blips is small. However, in the case of 40 copies/ml we see strong discrepancies between both pictures. Although the viral load is most of time above 50 copies/ml, we are considering most of that observations as the same viral blip and, in this case, the number of viral blips is given by the number of observations below the detection limit.

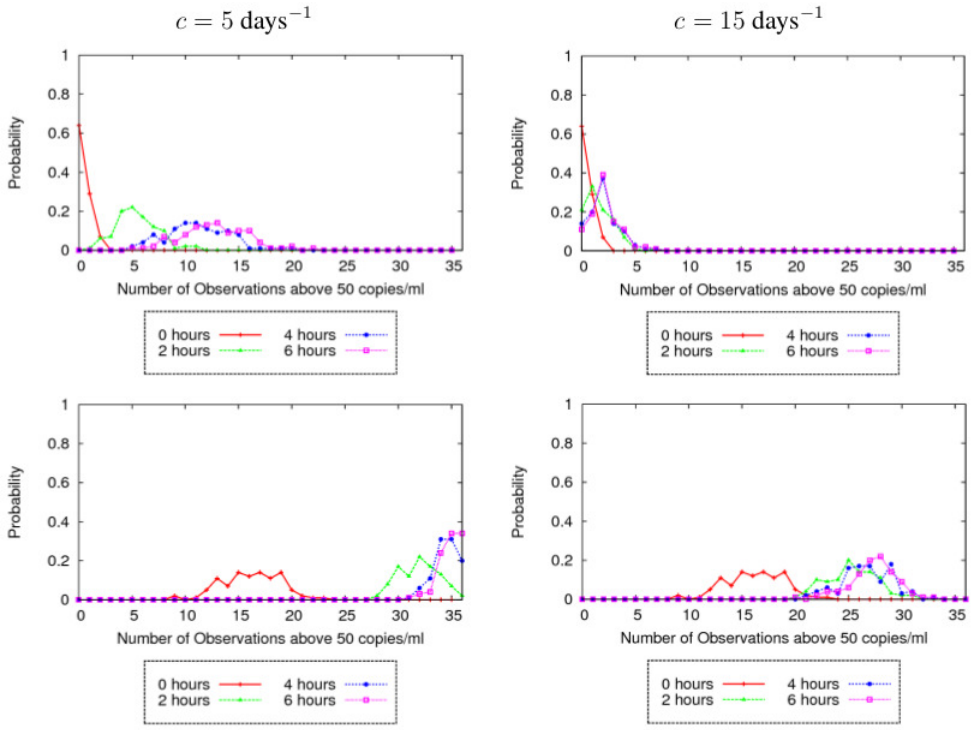

Figure 4.6: Probability of having n observations above the detection limit within a sample, $P(n)$, as a function of the post-extraction handling time, t_w, and the virus clearance rate, c. We have also considered different value of the average viral load: The first, and second correspond to 10 and 40 copies/ml, respectively. We have considered the continuous virion production only.

4.4 Conclusions

In this chapter we have studied if the inhomogeneous density fluctuations, together with experimental artifacts could be the origin of the viral blips, or if an extra assumptions has to be included in the model of chapter 3. To study this we have presented a stochastic model of HIV-1 dynamics in the blood stream, very similar to the model presented in chapter 3 but supplemented with a spatial dependence. To do this we have considered a compartmental model, in each compartment the same dynamics of the model of the previous chapter are considered, supplemented with a random diffusion between compartments. To determine how the experimental protocols can affect the appearance of viral blips we have presented an *in silico* blood test model, to reproduce in a realistic way the experimental protocols and to study if the experimental artifacts can affect the results. Moreover we have shown that the dynamics of the infection in the blood samples, during the time between the extraction and the observation, can play a major role in the appearance of the viral blips. And we have studied how the different virion production (continue vs burst) affect the appearance, the duration and the magnitude of the viral blips.

Chapter 5

Conclusions

The this PhD Thesis we have studied the effect of fluctuations in complex structured populations characterised by the existence of a latent state. In particular we have put light on some questions regarding the dynamics of hierarchically organissed cell populations, and we have investigated the dynamics of HIV-1 in infected patients under anti-retroviral therapy. In this chapter we expose the conclusions of our study.

5.1 Stochastic dynamics of differentiation cascades with regulatory feed-back

The aim of Chapter 2 is to study the robustness of the cell populations with hierarchical structure. To study this we have presented and analysed stochastic models of hierarchical populations governed by differentiation cascades to study the effect of symmetric stem-cell self-renewal on their long-time stability properties as well as their resilience to invasion. The behaviour of these models has given us some insight on intrinsic protection mechanisms, in particular against invasions by malignant, potentially tumorigenic, populations.

Our model of a hierarchically-organised tissue consists of a stochastic compartmental model, where each compartment corresponds to a differentiation stage, with negative-feedback regulating the size of the stem cell compartment. This feedback is assumed to be mediated by a cytokine whose secretion rate is, in turn, modulated by the number of fully-mature cells. The general framework we have used in our model formulation, i.e. in terms of cellular compartments with feedback between the SC and the MC compartments, has been used in a wide variety of studies, ranging from general models of robustness against mutations leading to cancer [98, 106, 107, 119] to more specific models of particular tissues such as the haematopoeitic system [1, 26, 27, 29, 82], epidermis [112] or neurogenesis [7]. Our model formulation is therefore rather generic and the resulting model should be applicable to a wide variety of tissues where hierarchical structure is present.

However, the issue of the cytokine-mediated feedback has more supporting evidence in the haematopoeitic system, where several of these cytokines have been identified which, upon variation in the size of the differentiated cell compartment, regulate the size of the SC compartment by means of negative feedback loop. For example, in the production of white blood cells, the granulocyte colony-stimulating factor (G-CSF) has been demonstrated to mediate a negative feedback [26]. Another example is thrombopoietin, which is involved in negative-feedback regulation in the production of platelets [26]. Erythropoiesis, i.e. the

production of red blood cells, is yet another example in which a negative feed-back is mediated by a cytokine, namely, erithropoietin [81, 118].

In order to investigate the effects of symmetric self-renewal on the robustness of hierarchical populations, we have first formulated a model in which stem cells undergo only symmetric self-renewal. Regarding this model, we have identified a new extinction mechanism in which the coupling between fluctuations that increase the pool stem cells and the delay in stem cell regulation leads to the extinction of the stem cell population and, therefore, to the eventual extinction of the whole: fluctuations in the size of the stem cell compartment propagate along and are amplified by the differentiation cascade in an amount which typically scales as 2^n, where n is the length of the cascade. Since the regulation of stem cell proliferation by the fully differentiated cells has a delay proportional to n, the negative feed-back between both populations may lead to extinction of the stem cells and therefore of the whole population.

The extinction time, T_E, in such symmetric population has been shown to be sensitive to variations of the death rate of the mature cells, λ_n, and the rate of self-renewal, p. We have shown that increasing λ_n leads longer extinction times, whereas populations with larger values of the self-renewal rate p exhibit shorter extinction times. Biologically, these results imply that symmetric stem-cell self-renewal is more likely to be observed in those with shorter delays between the stem cell and mature cells and those where the life-time of the mature cells is shorter and therefore larger cellular turn over is necessary to maintain tissue homeostasis.

We have also explored the possibility that the cytokine is secreted in response to variations in the size of some of TACs compartments. We observe that the behaviour is similar to that of shorter differentiation cascades: If the cytokine is produced at a rate proportional to the number of cells in compartment i, the behaviour of the stem cells is, for all intents and purposes, independent of compartments $i+1, ...m$ which therefore do not affect the system. We have also seen that if the secretion rate of the cytokine were proportional to the number of some of the TACs, the corresponding secretion rate would have to be much larger to maintain the same population of stem cells, as the number of TACs is smaller than the number of MCs (results not shown). These two results suggest that is more likely that the cytokine is produced in response to variations in the size of the mature cells compartment.

In order to proceed further, we have turned our attention to a model which corresponds to a more biologically-realistic situation: a stochastic model of a differentiation cascades where stem cells can proliferate both symmetrically or asymmetrically. In our model, the choice between these two division modes is a random event. Here, we have focused on the robustness of the population generated by a mixed (i.e. with both symmetric and asymmetric stem cell division) differentiation cascade in terms of its resilience against invasion (for example, invasion by a potential tumorigenic differentiation cascade). In particular, we have focused on optimal strategies for a differentiation cascade to be robust against invasions as defined by the values of two parameters: the probability of symmetric behaviour, e, and the rate of symmetric self-renewal, p. Our result show that there exist a trade-off between robustness and the capability of the differentiation cascade for adaptive behaviour in response to some sort of stressful situation (e.g. healing response to injury): Whereas the smallest the value of e, the more robust the population, we have also found that upregulation of symmetric self-renewal, i.e. increased value of p, increases the likelihood of the population to withstand invasion attempts. However, we found that

populations with big values of p are not robust, in the sense that lead the population to extinction due fluctuations and the mechanisms studied in this section.

The issue of the optimal (i.e. *maximally anti-tumour*) architecture of has been recently addressed Rodríguez-Brenes et al. [107]. Comparisons between our results and theirs is difficult as the models are based on slightly different premises. For example, the model considered in [107] does not take regulation into account. In turn, our models do not account for self-renewal of the transient-amplifying cells. In spite of these differences, some of the results of Rodríguez-Brenes et al. [107] are compatible with ours. For example, Rodríguez-Brenes et al. [107] conclude that anti-tumour mechanisms should favour the evolution of shorter (few intermediate transient amplifying stages) differentiation cascades over longer ones. The delay-induced extinction mechanism described in this section also favours the evolutionary prevalence of shorter cascades. The effect of self-renewal in the intermediate differentiation stages has not been explored in this section and it is left as the subject for future investigation.

Related models has been proposed by Traulsen et al. [31, 78, 120, 125], where they use a Moran process to study the competition between two populations as a function of the duplication probability to find that the probability of invasion is an increasing function of the duplication probability of the invader population. We observe similar results, only for small values of the duplication rate p. For larger values of p the probability of invasion decreases, as the invader population gets extinct due the extinction mechanisms that we have characterised in this section. This difference is due to the fact that we are considering a model with regulated-SC compartment size. Similarly, the models presented in [70, 87, 39, 75, 88, 86, 127] also lack feed-back, and, therefore do no exhibit any of phenomenology described in this work.

We also observe significant differences between deterministic and stochastic models. Whereas the mean-field behaviour model presents a critical point, characterised in terms of the net growth rate of the stem cell compartment, beyond which the resident population stops being robust, the stochastic model exhibits non-monotonic behaviour in which probability: The invasion probability is virtually zero below the deterministic critical point, however beyond the critical point it reaches a maximum and starts decreasing (due to the extinction mechanism studied in the symmetric division model).

5.2 Stochastic dynamics and extinction of HIV-1 in patients under potent anti-retroviral therapy

We have presented and analysed a stochastic model of HIV-1 dynamics in the blood stream under anti-retroviral therapy. The analysis of the behaviour of this model has provided us with valuable insight on the ability of a therapy based on stimulating the activation of latently infected cells through an study of the extinction of the infection.

In order to investigate the effect of the activation rate of the latently infected cells, a_L, on the average extinction time of the latent reservoir we have used several methods. We have studied the mean-field behaviour of our system to determine the range of parameter values in which a positive equilibrium (i.e. a steady-state associated to a persistent infection) exists. We have further performed Gillespie simulations of our stochastic model to study the extinction average time of the system. This simulation results allow us to determine if increasing the activation rate induces a reduction of the average extinction time. We have showed that, in the range of values of a_L that we have analysed, the

extinction time is dramatically reduced from decades to 2-3 years. This result supports the viability of increasing the rate of activation of latently infected cells by a possible therapeutic approach for total eradication of HIV-1 infection.

This problem presents a very particular multi-scale nature, each variable has a different time scale. This property has been used to reduce the dimensionality of the problem. We have performed a time-scale analysis of the Hamilton Equations to produce two different QSS approximations. We further assume that the generalised coordinate corresponding to the healthy cells, q_1, and its momentum, p_1 are constant.

Separation of time-scales have also been used to justify the uses of a multi-scale stochastic algorithm [20], which is excellent for our problem. We have used the semi-classical approximation [10, 73, 35] together with QSS approximations in the Hamilton equations [2] to approximate the generating function $G(p,t)$ and we have observed excellent agreement between the results of the semi-classical approximation and the ones obtained via Gillespie simulations, except in a small region near a_L^*, the value of a_L where the metastable state ceases to exist. In that region Gillespie simulations must be performed to compute the extinction probability. A better understanding of the Stokes phenomenon and analytic expressions for all the terms in the semi-classical approximation are left for future work.

5.3 Effects of density fluctuations on the statistics of viral blips

The aim of Chapter 4 is to contribute to the discussion of whether viral blips in HIV-1 infected patients treated with HAART are symptomatic of ensuing drug failure or if, on the contrary, they are random occurrences uncorrelated to drug-efficiency status and therefore lacking clinical significance. To this end, we have presented an inhomogeneous stochastic HIV-1 infection dynamics model, based on previous mean-field and stochastic models [110, 28], which accounts for local density fluctuations and burst virion production. Previous models [110, 28] assume that the system is well-stirred and, therefore, homogeneous. Given the small number of individuals involved in our model, in particular, regarding the number of virus copies during the latent infection phase, we have hypothesised that spatial inhomogeneities may play a role.

We have proposed an stochastic infection model which extends the model proposed in [28] by accounting for density inhomogeneities and bursty virion production. We have avoided the consideration of factors such as random activation of latently infected cells or upregulated virion production rate which have been introduced in previous models [110, 28]. We have further designed an *in silico* blood sample model, in order to reproduce as faithfully as possible the experimental protocol of Nettles et al. [95]. By doing so, we have been able to show that our model closely reproduces the blip statistics obtained in [95], in particular when burst virion production is considered (see Figs. 4.2, 4.3 and 4.4), thus supporting the hypothesis that viral blips in HAART-treated patients are random events unrelated to drug failure [76, 94].

Previous modelling approaches have made different claims regarding the origin of blips. Rong & Perelson [110] have postulated that random activation of latently infected cells by exposure to the corresponding antigens account for the presence of blips in HAART-treated patients. Conway & Coombs [28] have formulated a model in which a heightened rate of virion production is necessary for their model to reproduce realistic values of blip frequency, which could be interpreted as blips being the consequence of an evolutionary

process where new variants of the virus have emerged with an increased virion production rate. Whilst our model does not disprove any of these mechanisms as well as others proposed in the literature [37, 52, 41, 40, 43, 61, 62, 80], our model points out that viral blips may be purely random occurrences uncorrelated with factors of clinical significance.

Furthermore, our approach allows us to (partially) address the issue of whether laboratory and sample manipulation artifacts affect the observation of blips [76, 94]. We have investigated the effect that the post-extraction handling time, i.e. the time elapsed between sample extraction and the actual analysis, has on the statistics of the number of blips. According to our model, this factor contaminates the statistics of the number and duration of blips (see Fig. 4.5), which supports the position regarding the effects laboratory artifacts on viral blip observation [76].

5.4 Future work

The models and results presented in this thesis open a number of interesting avenues for future research.

In Chapter 2 we have shown how the tissues are protected against mutations that lead to symmetric division. However, according to our model, the optimal strategy is asymmetric division, since the number of stem cells remains constant and, therefore, the extinction probability is equal to zero, but this does not reflect the reality. The next step is to formulate a new model including more reactions such as mutations in the stem cell compartment (e.g. $SC \xrightarrow{\mu} SC_m$, with SC_m a mutant stem cell with another properties). This improvement would lead us to a more realistic situation in which the asymmetric division is not the best strategy.

In Chapter 3, using the semi-classical approximation we have obtained the mean extinction time $\tau = A\Omega^B e^{C\Omega}$. Although in simple problems such as the branching-annihilation [35] or branching-annihilation-decay [68] A and B can be determined. In more general situations the determination of A and B requires a careful analysis of the associated Stokes phenomenon [10]. Such analysis, together with the development of asymptotic methods to address this problem in more general settings is postponed for future work.

In Chapter 3 we have analysed the combination therapy of increasing the activation rate of the latently infected cells while continuously administering HAART, just by changing the value of a_L. A more realistic way to study this, is to formulate an accurate model of how the levels of histone deacetylases (HDAC) and other chromatin modifiers change the activation of the latently infected cells [121].

In this thesis we have used the semi-classic approximation in the Chapter 3 to compute the average extinction time of a population. But this methodology can be applied to compute the average extinction time in Chapter 2 or to count the number of blips in Chapter 4.

In Chapter 4, we have modelled the dynamics of the HIV-1 infection in the blood samples, assuming that there is no replenishment of new T cells and the clearance rate is reduced. However, post-extraction dynamics require a more careful study. It is not well known which changes in the dynamics are produced, if the samples are refrigerated, this can slow the viral replication. We left for future work a complete study of the dynamics in the blood samples.

Appendix A

Stochastic modelling and the Gillespie algorithm

This appendix is devoted to give a brief introduction to stochastic processes, stochastic modelling and a computational tool, called the Gillespie Stochastic Simulation Algorithm.

A.1 Basic definitions

Definition A.1. Let Ω be a set, let A be a collection of subsets of Ω. Then A is called a σ-algebra and the ordered pair (Ω, A) is called a measurable space if A satisfies:

1. $\Omega \in A$
2. If $B \in A$, then, $B^c := \{b : b \in \Omega, b \notin B\} \in A$.
3. If $\{A_n, n \in \mathbb{N}\} \subset A$, the union $\cup_{n=1}^{\infty} A_n \in A$.

Definition A.2. Let (Ω, A) be a measurable space. Let P be a real valued set function defined on the σ-algebra A. The function $P : A \to [0, 1]$ is called a probability measure if it satisfies:

1. $P(\Omega) = 1$.
2. (σ-additivity) If $\{A_n, n \geq 1\} \subset A$ and $A_i \cap A_j = \emptyset$ for $i \neq j$, then

$$P(\cup_{n=1}^{\infty} A_n) = \sum_{n=1}^{\infty} P(A_n).$$

The ordered triple (Ω, A, P) define a probability space.

Definition A.3. Let (Ω, A, P) a probability space. Let $A_1, A_2 \in A$. The conditional probability of A_1 given A_2 is

$$P(A_1|A_2) = \frac{P(A_1 \cap A_2)}{P(A_2)}.$$

Theorem A.1.

$$P(A|B) = \frac{P(A \cap B)}{P(B)} = \frac{P(B|A)P(A)}{P(B)}$$

Definition A.4. Let (Ω, A, P) be a probability space. Two $A_1, A_2 \in A$ are said to be independent if

$$P(A_1 \cap A_2) = P(A_1)P(A_2).$$

The σ-algebra generated by the open sets of $\mathbb{R}$ is denoted as $\mathbb{B}$ and it is called Borel's σ-algebra.

Definition A.5. A Random variable is an application $X : \Omega \to \mathbb{R}$ such that

$$\forall B \in \mathbb{B}, X^{-1}(B) \in A.$$

Definition A.6. Let X be a random variable taking values in $\mathbb{R}$. The probability that $X \in (x, x + dx)$ is given by $p(x)dx$ where $p(x)$ is the Probability Distribution Function (PDF) of X.

Some properties of the PDF are:

- $\int_{-\infty}^{\infty} p(x)dx = 1$
- $P(x_1 < X < x_2) = \int_{x_1}^{x_2} p(x)dx$

Definition A.7. Let (Ω, A, P) be a probability space. A stochastic process is a collection of random variables $\{X_t(s) : t \in T, s \in \Omega\}$ where T is some index.

Such systems are described in in terms of an infinite set of joint probability densities: $P(x_n, t_n, ...x_1, t_1)$ or, equivalently, by a set of joint conditional probability densities: $P(x_n, t_n, ...x_{k+1}, t_{k+1}|x_k, t_k, ...x_1, t_1)$. Obviously, such a system is not possible to deal with in practice, therefore additional conditions must be imposed in order to make the system tractable.

The Markov property is an additional condition whereby we assume that the system loses memory of all its past history except for the most recent event.

Definition A.8. An stochastic process is Markovian, or has the Markov Property, if it is satisfied the following property:

$$P(x_n, t_n|x_{n-1}, t_{n-1}, ...x_1, t_1) = P(x_n, t_n|x_{n-1}, t_{n-1}).$$

Remark: This statement is equivalent to claiming that the waiting time between two successive events is exponentially distributed [47].

This property allows us to write any joint PDF in the infinite hierarchy in terms of just one: the one-step PDF $P(x_n, t_n|x_{n-1}t_{n-1})$:

$$P(x_n t_n, x_{n-1}, t_{n-1}, ...x_2, t_2|x_1, t_1) = \prod_{i=2}^{n} P(x_i, t_i|x_{i-1}, t_{i-1})$$

A.1.1 The Chapman-Kolmogorov Equation

The Chapman-Kolmogorov equation (CKE) is a direct consequence of the Markov property and provides a first step towards writing an equation for the time evolution of the probability density. Consider the identity

$$P(x_3,t_3|x_1,t_1) = \int P(x_3,t_3,x_2,t_2|x_1,t_1)dx_2 \tag{A.1}$$

Now

$$\begin{aligned} P(x_3,t_3,x_2,t_2|x_1,t_1) &= \frac{P(x_3,t_3,x_2,t_2,x_1,t_1)}{P(x_1,t_1)} \\ &= \frac{P(x_3,t_3,x_2,t_2,x_1,t_1)}{P(x_2,t_2|x_1,t_1)}\frac{P(x_2,t_2,x_1,t_1)}{P(x_1,t_1)} \\ &= P(x_3,t_3|x_2,t_2,x_1,t_1)P(x_2,t_2|x_1,t_1). \end{aligned}$$

Applying the Markov property we get

$$P(x_3,t_3,x_2,t_2|x_1,t_1) = P(x_3,t_3|x_2,t_2)P(x_2,t_2|x_1,t_1).$$

This lead us to the Chapman-Kolmogorov Equation (CKE)

$$P(x_3t_3|x_1t_1) = \int P(x_3,t_3|x_2,t_2)P(x_2,t_2|x_1,t_1)dx_2 \tag{A.2}$$

A.1.2 The Master equation

The Master equation is a reformulation of the CKE that is easier to handle and more directly related to physical models. Consider $P(x_3,t_3|x_2t_2)$ and let $dt = t_3 - t_2$. Then

$$P(x_3,t_3|x_2,t_2) = (1 - a_0(x_2)dt)(x_3 - x_2) + W(x_3|x_2)dt. \tag{A.3}$$

$W(x_3|x_2)$ is the probability per unit time (transition rate) of the transition $x_2 \to x_3$, and $1 - a_0dt$ is the probability of no transition occurring. Therefore

$$a_0(x_2) = \int W(x_3|x_2)dx_3. \tag{A.4}$$

According to the Chapman Kolmogorov Equation

$$\frac{P(x_3,t_2+dt|x_1t_1) - P(x_2,t_2|x_1,t_1}{dt} = \int W(x_3|x_2)P(x_2,t_2|x_1,t_1)dx_2 - a_0(x_3)P(x_3t_2|x_1,t_1) \tag{A.5}$$

Using the definition of $a_0(x_3)$ and taking the limit $dt \to 0$, we obtain

$$\frac{dP(x_3,t|x_1,t_1)}{dt} = \int (W(x_3|x_2)P(x_2,t|x_1,t_1)dx_2 - W(x_2|x_3)P(x_3t|x_1,t_1))dx_2. \tag{A.6}$$

If only a discrete set of transitions $W_i(X)$, is possible, and, upon occurrence of reaction i, $X \to X + r_i$, then, the corresponding Master equation reads:

$$\frac{dP(X,t)}{dt} = \sum_i (W_i(X - r_i)P(X - r_i) - W_i(X)P(X,t)). \tag{A.7}$$

A.2 classic examples

A.2.1 The Moran process

The Moran process, named after the australian statistician Pat Moran, is a widely-used variant of the Wright-Fisher model and is commonly used in population genetics.

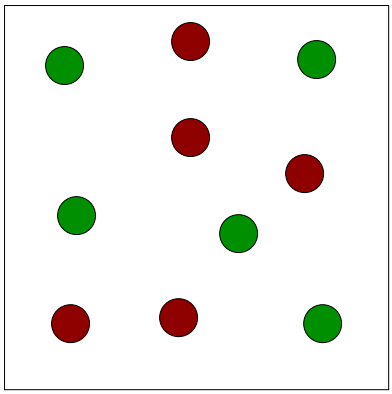

- N individuals of two types. N is keep fixed.
- n: number of normal individuals. m: number of mutant individuals. N=m+n.
- At each time step:
  - $n \to n+1$ and $m \to m-1$ with probability rate $W_+(n) = \frac{n}{N}\left(1-\frac{n}{N}\right)$.
  - $n \to n-1$ and $m \to m+1$ with probability rate $W_-(n) = \frac{n}{N}\left(1-\frac{n}{N}\right)$.

Note that $W(n+1) = W(n-1)$, i.e. $\mathbb{E}[\Delta n] = \mathbb{E}[n(t+\Delta t) - n(t)] = 0$. This implies that with $m = \mathbb{E}[n]$:

$$\frac{dm}{dt} = 0 \tag{A.8}$$

The system has two absorbing states: $W_+(n=0) = W_-(n=0) = 0$ and $W_+(n=N) = W_-(n=N) = 0$. This means that

$$\lim_{t\to\infty} P(n(t) = 0 \quad \cup \quad n(t) = N) = 1 \tag{A.9}$$

However, this behaviour is not at all captured by the deterministic equation, which predicts that the population will stay constant, as can be seen in Fig. A.1

A.2.2 The stochastic Logistic Equation

As a second example we choose the logistic equation A.10,

$$\frac{dm}{dt} = m\left(1-\frac{m}{K}\right), \tag{A.10}$$

has two steady states: $m = 0$ **unstable** and $m = K$ **stable**, i.e. regardless of the value of K and for any initial condition such that $m(t=0) > 0$, $m(t)$ will asymptotically approach K.

Consider now a continuous-time Markov process n_t whose dynamics are given by the following transition rate:

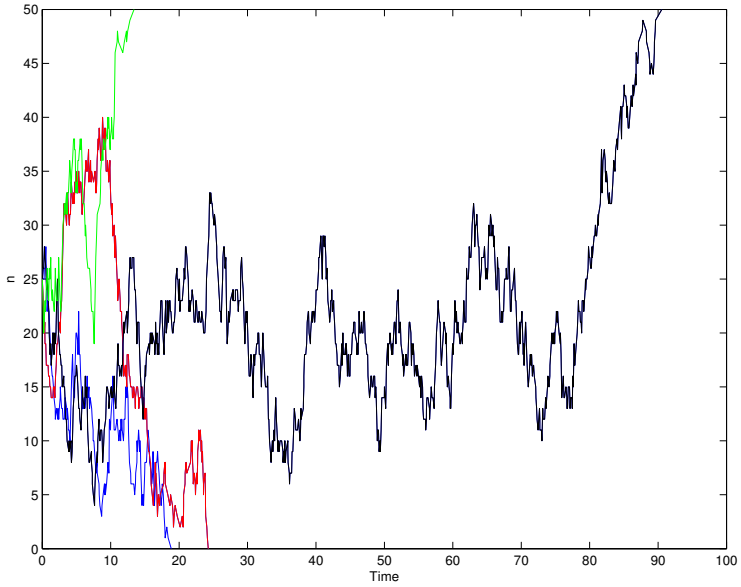

Figure A.1: Moran realizations

- $n \to n+1$ with probability rate n.
- $n \to n-2$ with probability rate $\frac{n(n-1)}{2}\frac{1}{K}$.

This stochastic process has a unique absorbing state: $n = 0$. This, together with the population can not grow to infinity (a linear term increasing population against quadratic term decreasing the population) leads to

$$\lim_{t\to\infty} P(n = 0, t) = 1. \tag{A.11}$$

We see in Fig A.2 that the stochastic dynamics show strong discrepancies with Equation A.10 when randomness is dominant. We observe that for small K fluctuations dominate the behaviour of the system. Extinctions are common for small K , in contradiction to the behaviour predicted by the logistic equation Eq A.10, and become rarer as K is allowed to increase.

A.2.3 Equilibrium and absorbing States

There are several definitions of equilibrium states in stochastic systems, we will explain our with an easy example. Consider again the stochastic logistic growth, i.e. a process n_t such that:

- $n \to n+1$ with probability rate $W_+(n) = n$
- $n \to n-2$ with probability rate $W_-(n) = \frac{n(n-1)}{2}\frac{1}{K}$

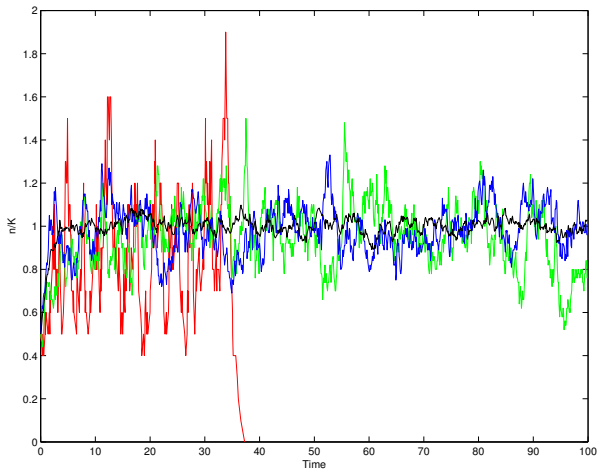

Figure A.2: Red line K = 10, green K = 50, blue K = 100, black K = 1000

Consider a state of system, n_s, is, roughly speaking, a state of the process such that $W_+(n_s) = W_-(n_s)$. $W_+(n_s)$ is the number of births within a population of n_s individuals, likewise, $W_-(n_s)$ = the number of deaths within a population n_s individuals. So an steady state of our population dynamics is reached when $n_t = n_s$, since death rate is balanced by birth rate and therefore the population stays roughly constant. It is easy to derive that $n_s = K$, which coincides with the deterministic stable fixed point. The idea is to note that $W_+(n) - W_-(n) > 0$ if $n < n_s$ and $W_+(n) - W_-(n) < 0$ if $n > n_s$.

Another important concept is the **absorbing state**. An absorbing state, n_0, is characterised by $W_i(n_0) = 0$ i.e. once the system has reached the absorbing state, it cannot leave anymore.

Consider again, the stochastic logistic growth rate, we have:

- Steady states are in general not absorbing states.
- $W_+(n_s) \neq 0$ and $W_+(n_s) \neq 0$.
- If $n = 0$ then $W_+(0) = W_-(0) = 0$ therefore $n = 0$ is an absorbing state.

n_s belongs to the set of accessible states of $n = 0$, that means there is at least one consecutive set of transition that connects n_s and n_0. For Example:

$$K \to K - 1 \to K - 2 \to \cdots \to 1 \to 0.$$

However, if $K \gg 1$ the probability of such a chain of events is vanishingly small.

n_s is an steady state in the sense that births and deaths are balanced. Moreover, $W_+(n) - W_-(n) > 0$ if $n < n_s$ and $W_+(n) - W_-(n) < 0$ if $n > n_s$. This is essentially equivalent to what happens in the deterministic logistic growth model. However, n_s is not an absorbing state of the stochastic dynamics. The only absorbing state is $n = 0$. Stochastic extinctions are relatively rare provided K is big, if this is the case, then, the deterministic system provides a reasonable approximation to the behaviour of the

model. If, on the contrary, K is small stochastic extinctions are relatively common and the deterministic description is not an accurate one. In general, we should expect non-trivial random effects for small populations or dynamics with absorbing states.

A.3 Monte Carlo Methods

There is no consensus on how Monte Carlo method should be defined, we use the following definition:

Definition A.9. a Monte Carlo Method is an algorithm which uses for any reason a pseudorandom number.

Example A.1. Approximate the value of π

Consider a random point P in the unit square, which is the probability that P is in the unit circle?

Clearly, the probability has to be the quotient of the areas, that is $\frac{\pi}{4}$. Using this we will use the following algorithm to compute the value of π:

1. Set $A = 0$.
2. Generate two random numbers $x, y \in [-1, 1]$ if $x^2 + y^2 < 1$, then $A = A + 1$.
3. Repeat (2) N times. When $N \to \infty$, then $\frac{A}{N} \to \frac{\pi}{4}$, this lead us to $\pi \approx 4\frac{A}{N}$.

A.4 Gillespie Stochastic Simulation Algorithm

Consider a Chemical reacting system, that is, molecules of N chemical species $S_1, ..., S_N$, inside some volume Ω, at some temperature T. Interacting through M elemental reaction channels $W_1, ..., W_M$, where W_j is assumed to describe a single instantaneous physical event which changes the population of at least one species.

Each reaction channel W_j can then be characterized by two entities [47]:

- Its **propensity function** $a_j(x)$: If the system is currently in state x,

$$a_j(x) \cdot dt := \text{probability that one } W_j \text{ event will occur in the next } dt.$$

- Its **state change vector** $v_j \equiv (v_{1j}, ..., v_{Nj})$:

$$v_{i,j} = \text{the change in } X_i \text{ caused by one } W_j \text{ event.}$$

W_j induces the state change $x \to x + v_j$.

Example A.2. Combustion of methane

Consider 4 different chemical species: Methane (CH_4), oxygen (O_2), carbon dioxide (CO_2) and water (H_2O). And the reaction

$$CH_4 + 2O_2 \to CO_2 + 2H_2O$$

The state change vector of this reaction is $v_1 = (-1, -2, +1, +2)$, and its propensity function $a_1(CH_4, O_2, CO_2, H_2O) = r_1 CH_4 \frac{O_2(O_2-1)}{2}$.

The Master equation describing this process has the form:

$$\begin{aligned} P(n_1, n_2, n_3, n_4, t) &= r_1(n_1+1)\frac{(n_2+2)(n_2-1)}{2}P(n_1-1, n_2+2, n_3-1, n_4-2) \\ &\quad -r_1 n_1 \frac{n_2(n_2-1)}{2}P(n_1, n_2, n_3, n_4) \end{aligned}$$

Note that, both, v_j do not determine the reaction, as con be seen in the following example

Example A.3. $S_1 \to S_2$: $v_j = (-1, 1, 0, ..., 0)$; $a_j(x)dt = (c_j dt)x_1 \implies a_j(x) = c_j x_1$
$S_1 + S_2 \to 2S_2$: same v_j; $a_j(x)dt = (c_j dt)x_1 x_2 \implies a_j(x) = c_j x_1 x_2$

The main idea of the Gillespie Stochastic Simulation Algorithm is to produce sample paths or realizations of $X(t)$. To do this, the method generates properly distributed random numbers for the time τ to the next reaction, and the index j of that reaction.

Let $p(\tau, j|x, t) \cdot d\tau \equiv$ be the probability that, given $X(t) = x$, the next reaction will occur in $[t+\tau, t+\tau+d\tau)$, and will be W_j.
Let

$$a_0(x) \equiv \sum_{k=1}^{M} a_k(x).$$

Then

$$p(\tau, j|x, t)d\tau = \left(1 - a_0(x)\frac{\tau}{n}\right)^n a_j(x)d\tau \to e^{-a_0(x)\tau}a_j(x)d\tau$$

Therefore,

$$p(\tau, j|x, t)d\tau = e^{-a_0(x)\tau}a_j(x)d\tau = a_0(x)e^{-a_0(x)\tau} \cdot \frac{a_j(x)}{a_0(x)}d\tau.$$

Note that τ is the exponential r.v. with mean $\frac{1}{a_0(x)}$, j is the integer r.v. with probability mass $\frac{a_j(x)}{a_0(x)}$ and j and τ are statistically independent.

The following scheme is a Method of implementing the SSA:

1. In state x at time t, evaluate $a_1(x), ..., a_M(x)$ and $a_0(x) = \sum_{k=1}^{M} a_k(x)$.
2. generate r_1 and r_2 random numbers in $[0, 1]$, and compute τ and j according to

   $$\tau = \frac{1}{a_0(x)} ln\left(\frac{1}{1-r_1}\right),$$

   $$j = \text{the smallest integer satisfying } \sum_{k=1}^{j} a_k(x) > r_2 a_0(x).$$

3. $t = t + \tau$ and $x = x + v_j$
4. Record (x, t). Go to 1 or end the simulation.

Appendix B

Semi-Classical Approach

This appendix is devoted to explain the semi-classical approximation used in Chapter 3 to approximate the solution of a Master equation.

The basic idea of the semi-classical approximation, is to transform a stochastic process described by a Master Equation.

Consider a stochastic process described by the following Master equation

$$\frac{\partial P(n,t)}{\partial t} = \sum_j \left(W_j(n-r_j,t)P(n-r_j,t)) - W_j(n,t)P(X,t)\right). \tag{B.1}$$

Let us define the generating function as Equation

$$G(p,t) = \sum_{n=0}^{\infty} p^n P(n,t) \tag{B.2}$$

Clearly, if G is known, the probability distribution function P_n, can be recovered [60]

$$P(n,t) = \frac{1}{n!}\left.\frac{\partial^n G}{\partial p^n}\right|_{p=0}. \tag{B.3}$$

G satisfies linear partial differential equation

$$\frac{\partial G}{\partial p}(p,t) = H\left(p, \frac{\partial}{\partial p}\right) G \tag{B.4}$$

satisfying $G(1,t) = 1$. This equality means the sum of the probabilities is equal to 1. The order of this partial linear differential equation is n if and only if, at most, reactions with n species reacting in the left hand side of the reaction appears, that is $A_1+...+A_n \to$ anything [35]. If the order is bigger than one, in general we can not solve this PDE. However, we can consider this as a Schrödinger Equation,

$$\frac{\partial}{\partial t}G = -\hat{H}G. \tag{B.5}$$

Equation (B.5) tell us that there exists an S such that $G = \exp(-S)$. When the system size, Ω, is big, one may employ the WKB approximation [73] and consider the re-scaled action $\bar{S}$ with $S = \Omega\bar{S}$, expanding up to order $O(\Omega^{-1})$ (neglecting $O(\Omega^{-2})$ terms), one obtains the classical Hamilton-Jacobi equations [6]

$$\frac{\partial \bar{S}}{\partial t} = H\left(p, \frac{\partial \bar{S}}{\partial p}\right). \tag{B.6}$$

Example B.1. Consider a stochastic process the binary annihilation reaction $A+A \xrightarrow{k} \emptyset$. This process is described by the Master equation

$$\frac{\partial}{\partial t}P(n,t) = \frac{(n+2)(n+1)}{2}kP(n+2,t) - \frac{(n)(n-1)}{2}kP(n,t), \tag{B.7}$$

consider the generating function

$$G(p,t) = \sum_{n\geq 0} p^n P(n,t), \tag{B.8}$$

then, Eq (B.7) can be written as

$$\begin{aligned}
\frac{\partial G}{\partial t} &= \sum_{n\geq 0} p^n \frac{(n+2)(n+1)}{2}kP(n+2,t) - \sum_{n\geq 0} p^n \frac{n(n-1)}{2}kP(n,t) \\
&= \sum_{n\geq 2} p^{n-2}\frac{n(n-1)}{2}kP(n,t) - p^2\sum_{n\geq 0} p^{n-2}\frac{n(n-1)}{2}kP(n,t) \\
&= \sum_{n\geq 0} p^{n-2}\frac{n(n-1)}{2}kP(n,t) - p^2\sum_{n\geq 0} p^{n-2}\frac{n(n-1)}{2}kP(n,t) \\
&= \frac{k}{2}(1-p^2)\frac{\partial^2 G}{\partial p^2}.
\end{aligned} \tag{B.9}$$

We consider this equation as a Schrödinger equation,

$$\frac{\partial}{\partial t}G = -\hat{H}G, \tag{B.10}$$

with

$$\hat{H}(\hat{p},\hat{q}) = \frac{k}{2}(\hat{p}^2-1)\hat{q}^2, \tag{B.11}$$

where $\hat{q} = -\dfrac{\partial}{\partial p}$.

Using the Ansatz $G(p,t) = \exp\left(-\Omega S(p,t)\right)$, Eq. (B.10) reads

$$\begin{aligned}
-\Omega\frac{\partial S}{\partial t}\exp\left(-\Omega S(p,t)\right) &= -\frac{k}{2}(p^2-1)\frac{\partial^2}{\partial p^2}\exp\left(-\Omega S(p,t)\right) \\
&= -\frac{k}{2}(p^2-1)\left(-\Omega\frac{\partial}{\partial p}\frac{\partial S}{\partial p}\exp\left(-\Omega S(p,t)\right) + \Omega^2\left(\frac{\partial S}{\partial p}\right)^2\exp\left(-\Omega S(p,t)\right)\right),
\end{aligned}$$

expanding up to order Ω^{-1}, we obtain the Hamilton-Jacobi equation

$$\frac{\partial S}{\partial t} = H\left(p,\frac{\partial S}{\partial p}\right) = \frac{\tilde{k}}{2}(p^2-1)\left(\frac{\partial S}{\partial p}\right)^2, \tag{B.12}$$

with $\tilde{k} = \Omega^{-1}k$.

Instead of dealing directly with the Hamilton-Jacobi equations, which, in general, we do not know how to solve, we exploit the analogy with the Schrödinger equation to use a Feynman path-integral representation further to obtain the solution of Eq. (B.5)

$$G(p,t) = \int_0^t \left(\exp\left(-S(p,q)\right) Dq(s) Dp(s)\right) ds + p^{x_0}, \tag{B.13}$$

with

$$S(p,q,t) = \int_0^t \left(-H(p,q) + \sum_{i=1}^{n} q_i(s)\dot{p}_i(s) \right) ds. \tag{B.14}$$

Too see this note that, in the Fourier representation [22],

$$\delta(p-p_0) = \int_{-\infty}^{\infty} d\pi e^{-i(p-p_0)\pi} d\pi. \tag{B.15}$$

The probability of pass from a p'' to a p' can be seen as

$$\begin{aligned}
(p'|\exp\left(-\Omega\Delta t H(x', \Omega^{-1}\frac{\partial}{\partial p'}, t)\right)|p'') &= \\
&= \int_{-\infty}^{\infty} dk \exp\left(-(\Omega\Delta t)H(p', i\epsilon k, t) + ik(p'-p'') + O(\Delta t^2)\right) \\
&= \int_{-\infty}^{\infty} d\pi \Omega \exp\left(-(\Omega\Delta t)H(p', i\pi, t) - i\pi\frac{p'-p''}{\Delta t}\right) + O(\Delta t^2).
\end{aligned} \tag{B.16}$$

for a short time Δt. Defining $exp_{\leftarrow}$ as an ordered exponential, the solution of Eq. (B.5) can be written as

$$\begin{aligned}
G(p_n, t_n|p_0, t_0) &= \exp_{\leftarrow}\left[-\Omega\int_{t_0}^{t} ds H\left(p, \Omega^{-1}\frac{\partial}{\partial p}, s\right)\right]\delta(p-p_0) \\
&= \lim_{\Delta t\to 0}\prod_{j=1}^{n} exp\left(-\Omega\Delta t H(p, \Omega^{-1}\frac{\partial}{\partial p_j}, t)\right)\delta(p_j - p_{j-1})dp_{j-1}.
\end{aligned} \tag{B.17}$$

Writing Eq. (B.17) in the representation of Eq. (B.16) we obtain

$$\begin{aligned}
G(p,t|p_0,t_0) &= \lim_{n\to\infty}\int\cdots\int dp_1 d\pi_1 \cdots p_n d\pi_n \Omega^n \\
&= \exp\left(\Omega\sum_{j=1}^{n}\Delta t\left[H(p_j, i\pi_j, t_j) - i\pi\frac{p_j - p_{j-1}}{\Delta t}\right]\right).
\end{aligned} \tag{B.18}$$

In the limit $\Delta t \to 0$ we recover Eq. (B.13). Note that, in fact, the integral of the Equation (B.13) represents all possible trajectories, we just have composed the solution at each infinitesimal time step.

The semiclassic approximation consists on taking just the most probable path, that is, to approximate the path integral (B.13) by

$$G(p,t) \approx \exp\left(-S(p,t)\right), \tag{B.19}$$

where p_i are the solution of the Hamilton equations of the (classic) Hamiltonian H, since these equations are the ones that maximizes $\exp\left(-S(p,q)\right)$.

The approximation of this integral B.13 is performed via a Laplace method or a steepest descent method, which is valid if Ω is large enough. The Laplace method consists in the following, if we have an integral of the form

$$\int_a^b \exp\left(\Omega f(x)\right) dx,$$

with Ω big enough and $f(x)$ has a unique maximum at $x_0 \in [a, b]$, then we can approximate

$$\int_a^b \exp\left(\Omega f(x)\right) dx \approx e^{\Omega f(x_0)} \int_a^b e^{-\Omega |f''(x)|(x-x_0)^2}. \tag{B.20}$$

For the values of x far from x_0 this decays exponentially fast.

And in Equation (B.13) the maximum is reached when S is the solution of the Hamilton-Jacobi equations. The path that maximizes the action integral, I_S:

$$I_S = \int S(p, q, s) ds, \tag{B.21}$$

is determined by the Euler Equation

$$\frac{d}{ds}\frac{\partial S}{\partial q} - \frac{\partial S}{\partial p} = 0, \tag{B.22}$$

or by the canonical equations of motion

$$\begin{aligned} \dot{p}(s) &= -\frac{\partial H}{\partial q}, \\ \dot{q}(s) &= \frac{\partial H}{\partial p}, \end{aligned}$$

with boundary conditions

$$\begin{aligned} q_i(0) &= x_i(0), \\ p_i(t) &= p_i. \end{aligned}$$

Remark: We have used the Generating function formulation for convenience, all this derivation can be done using directly the master equation, see for instance [73]

B.1 Metastablility

Equation (B.5) can, in general, be solved, only in few cases (e.g. if $\hat{H}$ is of order 1. In that case, one can use the characteristic method to solve that partial differential equation). In general we cannot solve the Hamilton-Jacobi PDE. However, taking advantage of the fact that H is linear to expand G in their eigenvalues λ_k and eigenmodes ϕ_k, we obtain

$$G(p, t) = G_{st}(p) - \sum_{k \geq 1} \phi(p) e^{-\lambda_k t} \tag{B.23}$$

where $G_{st}(p)$ is the stationary solution (corresponding to $\lambda_k = 0$), λ_k are the eigenvalues of $-\hat{H}$, $\phi_k(p)$ the eigenmodes.

Assume the system has a metastable state, which is an attractor of the mean-field dynamics. In the semi-classical approach we can think it as a positive fixed point on $p_i = 1$, or as an hyperbolic point of the Hamiltonian with stable manifold $p_i = 1$. We can expect the dynamics evolve according the mean-field behaviour until they reach the metastable state. However, we have to note that, although the metastable state is an stable fixed point of the mean-field behaviour, it is not thermodynamically stable. If it were, we would have reactions, that require energy, at infinite time, in an isolated system, and this contradicts the second-law of thermodynamics [38]. Thus, after a long time near the metastable the system will escape to the stochastic extinction or to a different metastable state in the case of multi-stable systems. If the system size is large enough, we can expect that the dynamics will follow a trajectory close to the heteroclinic connection as this trajectory is the optimal one. The probability of observing a different trajectory is exponentially small [35].

In this case, as we are interested in large values of t, we can to approximate the extinction probability by truncating Eq. B.23 at $k = 1$, since the exponential terms with negative eigenvalues ($-\lambda_k < -\lambda_1 < 0$) decay very fast and we obtain

$$G(0,t) \approx 1 - \exp\left(-\lambda_1 t\right). \tag{B.24}$$

with

$$\tau = \frac{1}{\lambda_1} \tag{B.25}$$

as the mean extinction time.

In Chapter 3 this mean extinction time is of the form $\tau = A\Omega^B \exp(C\Omega)$, where C is the integral of the re-scale action, $\bar{S}$, along the heteroclinic connection. In the particular case of the Lower bound 3.31, this can be solved analytically [10, 68], and this example is very illustrative.

Example B.2. Consider the stochastic process described by 3.31, that is:

$A \xrightarrow{r} A + A$.

$A \xrightarrow{a_L + d_L} \emptyset$.

$A + A \xrightarrow{\frac{r}{L_{max}}} \emptyset$.

The Master equation reads

$$\begin{aligned}\frac{dP(n,t)}{dt} &= r(n-1)P(n-1,t) - rnP(n,t) + (a_L + d_L)(n+1)P(n+1,t) - (a_L + d_L)nP(n,t) \\ &\quad + \frac{r}{L_{max}\Omega}\frac{(n+2)(n+1)}{2}P(n+2,t) - \frac{r}{L_{max}\Omega}\frac{(n)(n-1)}{2}P(n,t),\end{aligned} \tag{B.26}$$

and can be rewritten as

$$\frac{\partial G}{\partial t} = r(p - p^2)\frac{\partial G}{\partial p} + (a_L + d_L)(p-1)\frac{\partial G}{\partial p} + \frac{r}{2L_{max}\Omega}(p^2 - 1)\frac{\partial^2 G}{\partial p^2}. \tag{B.27}$$

As we have explained, we consider this as Schrödinger equation,

$$\frac{\partial G}{\partial t} = -\hat{H}G, \tag{B.28}$$

where

$$H(\hat{p},\hat{q}) = r(\hat{p}^2 - \hat{p})\hat{q} + (a_L + d_L)(1 - \hat{p})\hat{q} + \frac{r}{2L_{max}\Omega}(1 - \hat{p}^2)\hat{q}^2. \tag{B.29}$$

Making an eigenmode expansion of G one gets

$$G(p,t) = G_{st}(p) - \sum_{k\geq 1} \phi(p) e^{-\lambda_k t} \tag{B.30}$$

and, for large values of t, $G(p,t)$ can be approximated by

$$G(p,t) \approx 1 - \phi(p) e^{-\lambda_1 t}. \tag{B.31}$$

Note that if $G(p,t) = 1 - \phi(p)e^{-\lambda_1 t}$, then

$$\begin{aligned} \frac{\partial G}{\partial p} &= -\phi'(p)e^{-\lambda_1 t}, \\ \frac{\partial^2 G}{\partial p^2} &= -\phi''(p)e^{-\lambda_1 t}, \\ \frac{\partial G}{\partial t} &= \phi(p)e^{-\lambda_1 t}\lambda_1. \end{aligned}$$

This allows us to reduce our PDE to into an Sturm-Liouville problem of the form

$$-\hat{H}\phi + \lambda_1 \phi = 0 \tag{B.32}$$

To solve this problem we proceed as in [10] and we look for a solution in the momentum space. However, it was previously solved via a WKB approximation by Kessler and Shnerb [68]. Eq. (B.32) is

$$\frac{r}{2L_{max}\Omega}(1-p^2)\phi'' + (p-1)(rp - (a_L + d_L))\phi' + \lambda_1 \phi = 0, \tag{B.33}$$

We proceed as follows, we divide the problem in three regions: the first region is $A := \{p \mid p \approx 0\}$, $B := \{p \mid p \approx 0\}$ and $C := [0,1] - A - B$. We look for a solution near $p \approx 0$, where from Eq. (B.31) we have $\phi(p) \approx 1$, then a solution $p \approx 1$, where, from Eq. (B.31) we have $\phi(p) \approx 0$, and finally we match both solutions in the three regions.

We use a WKB Ansatz $\phi(p) = a(p)exp(-\Omega s(p))$, then

$$\begin{aligned} \phi(p) &= a(p)e^{-\Omega S(p)} \\ \phi'(p) &= a'(p)e^{-\Omega S(p)} + ae^{-\Omega S(p)}(-\Omega S') \\ \phi''(p) &= a''(p)e^{-\Omega S(p)} + 2a'(p)e^{-\Omega S(p)} + a(p)e^{-\Omega S(p)}(-\Omega S')^2. \end{aligned}$$

so, our Sturm-Liouvulle problem reads,

$$\begin{aligned} \frac{r}{2L_{max}\Omega}\left(a''(p)e^{-\Omega S(p)} + 2a'(p)e^{-\Omega S(p)} + a(p)e^{-\Omega S(p)}(-\Omega S')^2\right) & \\ +(p-1)(rp - (a_L + d_L)\left(a'(p)e^{-\Omega S(p)} + ae^{-\Omega S(p)}(-\Omega S')\right) &= 0. \end{aligned} \tag{B.34}$$

The terms in Ω, gives us a differential equation for $S(p)$

$$S'(p) = 2L_{max}\frac{rp - (a_L + d_L)}{r(p-1)} \tag{B.35}$$

note that, the right-hand term is exactly the heteroclinic connection between the metastable state and the stochastic extinction.

The terms without Ω gives as a differential equation for $a(p)$

$$a'(p) = L_{max}\frac{(p-1)[rp-(a_L+d_L)]}{r(1-p^2)S(p))} \tag{B.36}$$

To study the non-quasi-stationary region we add the term $\lambda_1\phi$ to the equation perturbatively, $\phi(p) = 1 + \delta\phi(p)$ with $\delta\phi(p) \ll 1$, and we get

$$\frac{r}{2L_{max}\Omega}(1-p^2)\phi'' + (p-1)(rp-(a_L+d_L))\phi' = -\lambda_1, \tag{B.37}$$

which gives us a differential equation for $\phi'(p)$

$$\phi''(p) = \frac{2L_{max}}{r(1-p^2)}\Omega - \lambda_1 - (p-1)(rp-(a_L+d_L)\phi', \tag{B.38}$$

in this case, the solution has been derived in [10] and is of the form

$$\phi'(p) = -2\Omega\lambda_1 e^{2\Omega\left(p-\left(1+\frac{a_L+d_L}{r}\right)log(1+p)\right)}\int_{-1}^{p}\frac{\exp\left(2\Omega\left(s-\left(1+\frac{a_L+d_L}{r}\right)log(1+s)\right)\right)}{1-s^2}ds \tag{B.39}$$

Eq. (B.39) can be evaluated by the saddle point approximation with a saddle point at $\dfrac{a_L+d_L}{r}$

$$\phi'(p) \approx -\frac{2\lambda_1\sqrt{L_{max}\pi\Omega}\left(\frac{r}{a_L+d_L}\right)^{3/2}}{\sqrt{\frac{r}{a_L+d_L}+1}\left(\frac{r}{a_L+d_L}-1\right)}e^{-2\Omega L_{max}I(p)}, \tag{B.40}$$

with

$$I(p) = \frac{a_L+d_L}{r} - \left(1+\frac{a_L+d_L}{r}\right)\log\left(1+\frac{a_L+d_L}{r}\right) - \left(p-\left(1+\frac{a_L+d_L}{r}\right)\log(1+p)\right). \tag{B.41}$$

The quasi-stationary solution is valid as long as $p\dfrac{r}{a_L+d_L} - 1 \gg \dfrac{1}{\sqrt{\Omega}}$, and the perturbative solution holds when $1-p \gg \dfrac{1}{\sqrt{\Omega}}$ [9, 8], so both solutions are valid when

$$\frac{1}{\sqrt{\Omega}} \ll p\frac{r}{a_L+d_L} - 1 \ll 1.$$

Finally, we find the eigenvalue λ_1 matching both solutions.

$$\lambda_1 = \sqrt{\frac{L_{max}}{4\pi}\left(\frac{r}{a_L+d_L}+1\right)}\frac{(\frac{r}{a_L+d_L}-1)^2}{(\frac{r}{a_L+d_L})^{5/2}}\sqrt{\Omega}e^{-\Omega S_0}, \tag{B.42}$$

with

$$S_0 = L_{max}\frac{r\frac{a_L+d_L}{r} - log\left(\frac{a_L+d_L}{r}+1\right)(r+a_L+d_L)}{r} - L_{max}\frac{r-log(2)(r+a_L+d_L)}{r}. \tag{B.43}$$

Appendix C

Computation of Heteroclinic Connections for Hamiltonian System

This chapter is devoted to give a brief introduction to the methods used in Chapter 3 for the computation of the invariant manifolds

C.1 The Taylor Method

Consider the initial value problem

$$\begin{aligned} \dot{x}(t) &= f(x,t), \\ x(t_0) &= x(0) \end{aligned} \tag{C.1}$$

One step of the taylor method of order m, to compute the solution $x(t)$ of the differential equation (C.1) from time t to $t+h$, of order m with step size h is

$$x_N = x_{N-1} + x'(t_{N-1})h + \cdots + \frac{x^{(p)}(t_{N-1})}{m!}h^m,$$

starting with $x_0 = x(0)$.

This high order method allow us to obtain high accuracy and large step-sizes h along the integration (in the implementation m is choosen large and h is choosen to keep the local error of the method beyond the precision required, for example $m = 24$ is a common value if double precision is required). Although this method is very simple, computing m derivatives of a vectorial field can be very hard. This problem is solve by using the so-called Automatic Differentiation Formulas.

C.2 Automatic Differentiation Formulas

Automatic Differentiation is a recursive algorithm to evaluate the derivatives of a closed expression on a given point [64, 51].

Definition C.1. Let f be a smooth function. The normalized $j-$th derivative of f at t is

$$f^{[j]}(t) = \frac{1}{j!} f^{(j)}(t).$$

Some of the differentiation formulas are as follows:

1. If $f(t) = g(t) \pm h(t)$, then $f^{[n]}(t) = g^{[n]}(t) \pm h^{[n]}(t)$.
2. If $f(t) = g(t)h(t)$, then $f^{[n]}(t) = \sum_{i=0}^{n} g^{[n-i]}(t)h^{[i]}(t)$.
3. If $f(t) = \dfrac{g(t)}{h(t)}$, then $f^{[n]}(t) = \dfrac{1}{h^{[0]}(t)} \left(g^{[n]}(t) - \sum_{i=1}^{n} h^{[i]}(t) f^{[n-i]}(t)\right)$.

There are automatic differentiation formulas for exponentials, logarithms, trigonometric functions, and so on.

Example C.1. In Chapter 3, the Weak QSS approximation produces a reduced system of 4 ordinary differential equations

$$\begin{aligned}
\frac{dp_2}{dt} &= \frac{1}{\epsilon_1}\left(-\kappa_3(p_2^2 - p_2) - \kappa_3\frac{L_0}{L_{max}}(1 - p_2^2)q_2 - \kappa_4(1 - p_2) - \kappa_5(p_3 - p_2)\right), \\
\frac{dq_2}{dt} &= \frac{1}{\epsilon_1}\left(\eta(1-\epsilon)q_1q_4 + \kappa_3 q_2(2p_2^2 - 1) - \kappa_3\frac{L_0}{L_{max}}p_2q_2^2 - \kappa_4 q_2 - \kappa_5 q_2\right), \\
\frac{dp_3}{dt} &= \frac{1}{\epsilon_2}\left(-\kappa_6(p_3p_4 - p_3) - \kappa_7(1 - p_3)\right), \\
\frac{dq_3}{dt} &= \frac{1}{\epsilon_2}\left((1-\eta)(1-\epsilon)q_1q_4 + \kappa_5 q_2 + \kappa_6(p_4 - 1)q_3 - \kappa_7 q_3\right),
\end{aligned} \tag{C.2}$$

where

$$\begin{aligned}
p_1 &= 1, \\
q_1 &= 1, \\
p_4 &= \frac{-(1-\eta)(1-\epsilon)q_1p_3 - \eta(1-\epsilon)p_2q_1 - \kappa_8 - \epsilon p_1q_1}{-(1-\eta)(1-\epsilon)q_1p_1 - \eta(1-\epsilon)p_1q_1 - \kappa_8 - \epsilon p_1q_1} \\
q_4 &= \frac{\kappa_6}{p_1q_1 + \kappa_8}p_3q_3,
\end{aligned}$$

for simplicity $p_4 = Ap_3 + Bp_2 + C$ and $q_4 = Dp_3q_3$.

In this problem, computation of the derivatives lead to very complicated expressions. For that reason, we define the following auxiliar variables

$e_1 = Dp_3q_3$,
$e_2 = Ap_3 + Bp_2 + C$,
$e_3 = p_2p_2$,
$e_4 = e_3 - p_2$,
$e_5 = 1 - e_3$,
$e_6 = e_5q_2$,
$e_7 = 1 - p_2$,
$e_8 = p_3 - p_2$,
$e_9 = \dfrac{1}{\epsilon_1}\left(-\kappa_3 e_4 - \kappa_3\dfrac{L_0}{L_{max}}e_5 - \kappa_4 e_7 - \kappa_5 e_8\right)$,
$e_{10} = (e_3 - 1)$,

$$
\begin{aligned}
e_{11} &= e_{10}q_3,\\
e_{12} &= \frac{1}{\epsilon_1}\left((1-\eta)(1-\epsilon)q_1e_1 + \kappa_5 q_2 + \kappa_6 e_{11} - \kappa_7 q_3\right),\\
e_{13} &= p_3 e_2,\\
e_{14} &= e_{13} - p_3,\\
e_{15} &= 1 - p_3,\\
e_{16} &= \frac{1}{\epsilon_2}\left(-\kappa_6 e_{14} - \kappa_7 e_{15}\right),\\
e_{17} &= e_2 - 1,\\
e_{18} &= e_{17}q_3,\\
e_{19} &= \frac{1}{\epsilon_2}\left((1-\eta)(1-\epsilon)q_1e_1 + \kappa_5 e_2 + \kappa_6 e_{18} - \kappa_7 q_3\right).
\end{aligned}
$$

Using the Automatic Differentiation formulas, for $e_i^{[n]}$, we obtain

$$
\begin{aligned}
p_2^{[n+1]} &= \frac{1}{n+1}e_9^{[n]},\\
q_2^{[n+1]} &= \frac{1}{n+1}e_{12}^{[n]},\\
p_3^{[n+1]} &= \frac{1}{n+1}e_{16}^{[n]},\\
q_3^{[n+1]} &= \frac{1}{n+1}e_{19}^{[n]}.
\end{aligned}
$$

In this particular case we only need the formulas for the sum and the product of two variables.

C.3 Heteroclinic connections

In Chapter 3, in Fig. 3.4 we compared two different approximations of the exponential growth of the mean relaxation time (3.30) for the semi-classical approximation. The estimates of ΩC are obtained after performing either a one-step (weak) or a two-step (strong) quasi-stationary approximation of the classical equations of motion and computing the integral of the classical (Lagrangian) action S along the only non-trivial path connecting the metastable state and the stochastic extinction of the system. Looking at the phase space of the mean field system, one realizes that this non-trivial path is given by the heteroclinic trajectory $\gamma(t)$ from the hyperbolic fixed point $\mathbf{p_1}$ (with $p_i = 1$ and $x_i > 0$) and the fixed point $\mathbf{x_0}$ located on $x_i = 0$ with $0 < p_i < 1$ (here $i = 2$ for the strong QSS approximation and $i = 1, 2$ for the weak QSS case).

It is a simple exercise to obtain an expression of the heteroclinic connection in the Strong QSS approximation, since, under this approximation, the system is reduced to one degree of freedom, and, therefore, the heteroclinic trajectory is simply determined by conservation of energy. However, the computation of $\gamma(t)$ requires numerical techniques for the Weak QSSA case since one has to deal with a 2 degrees of freedom (2-dof) Hamiltonian system. Moreover, the Weak QSSA reduction exhibits an slow-fast structure, hence one has to deal with two quite different time-scalings when performing the numerics. We should note that all the computations have been performed using multiprecision arithmetics (around 100 digits where enough for most of the a_L values considered) and the codes have been implemented in PARI/GP [11].

Let us consider, from now on, the 2-dof Hamiltonian case whose related equations of motion, given by (3.28), are expressed in the coordinates x_2, x_3, p_2, p_3. The hyperbolic-hyperbolic fixed point $\mathbf{p_1}$ has a 2-dimensional stable and a 2-dimensional unstable invariant

manifolds, to be denoted $W^s(\mathbf{p_1})$ and $W^u(\mathbf{p_1})$ respectively. Similarly, $W^{s/u}(\mathbf{x_0})$ will denote the 2-dimensional stable/unstable manifold associated to the fixed hyperbolic-hyperbolic point $\mathbf{x_0}$. The heteroclinic connection $\gamma(t)$ corresponds to the intersection $W^u(\mathbf{p_1}) \cap W^s(\mathbf{x_0})$.

To compute $W^u(\mathbf{p_1})$ (and also $W^s(\mathbf{x_0})$) we use the so-called parametrization method [17, 18]. Basically the idea is the following. We represent the local invariant manifold around $\mathbf{p_1}$ as a vector series $G(s_1, s_2)$, being $G : \mathbb{R}^2 \to \mathbb{R}^4$. That is, a point $X = (x_2, x_3, p_2, p_3) \in \mathbb{R}^4$ will be considered to be on $W^u(\mathbf{p_1})$ if $X = G(s_1, s_2) = \sum_{i,j\geq 0} a_{i,j} s_1^i s_2^j$. The coefficients $a_{i,j} \in \mathbb{R}$ can be order by order computed by imposing the so-called invariance condition. This condition requires that the dynamics within the invariant manifold, expressed in the s_1, s_2 coordinates, must be conjugated to the linear dynamics around the hyperbolic-hyperbolic point. Denote by $\lambda_1, \lambda_2 > 0$ (resp. < 0) the real eigenvalues associated to $\mathbf{p_1}$ (resp. to x_0, below we denote by G^{p_1} and G^{x_0} the corresponding parametrizations). Then, the linear dynamics is $\dot{s_1} = \lambda_1 s_1,\ \dot{s_2} = \lambda_2 s_2$. If $\dot{X} = f(X)$ refers to the equations 3.28, then the invariance condition requires

$$\frac{\partial G}{\partial s_\nu}(s_1, s_2)\lambda_\nu s_\nu = f(G(s_1, s_2)), \qquad \nu = 1, \ldots, 2.$$

By imposing this equality order by order, being $k = i + j \geq 1$ the total order, one gets a sequence of linear systems for the coefficients $a_{i,j}$, $k > 1$ (for $k = 0$ one gets the fixed point condition, and for $k = 1$ the eigenvectors system). See [115] for further details on this procedure.

In practice, we truncate the series representation to suitable order N and we require that the invariance condition holds up to a tolerance `tol`. Then, the invariance condition will hold for X in a domain of radius $r_{\mathbf{p_1}}$ around the fixed point $\mathbf{p_1}$ (similarly, for $\mathbf{x_0}$ we obtain $r_{\mathbf{x_0}}$). Typical values used in the computations are $N = 150$ and $\texttt{tol} = 10^{-40}$. The local domain size depends on the parameter a_L in the system. As an example, for $a_L = 0.15$ one obtains $r_{\mathbf{p_1}} = 265$ and $r_{\mathbf{x_0}} = 1470$.

Once the local representations G^{p_1} and G^{x_0}, of $W^u(\mathbf{p_1})$ and $W^s(\mathbf{x_0})$ respectively, are obtained we extend the $W^u(\mathbf{p_1})$ up to $\Sigma = \{p_2 = G_3^{x_0}(r_{x_0}, 0)\}$, where $G_3^{x_0}$ denotes the 3rd component of G^{x_0} (the one corresponding to the p_2-variable). This is done by integrating the equations (3.28) using a Taylor method, which turns out to be an appropiate time-stepper for the high precision computations required. Assume that $G^{p_1}(z_1, z_2) \in \mathbb{R}^4$ is a point such that the transported one $\hat{G}^{p_1}(z_1, z_2) \in \Sigma$ is close to a zero of $F(s_1, s_2, z_1, z_2) = G^{x_0}(s_1, s_2) - \hat{G}^{p_1}(z_1, z_2)$, $F : \mathbb{R}^4 \to \mathbb{R}^4$. Then we refine this initial condition, using a Newton method and we obtain a point of the heteroclinic orbit as a zero of F. Note that this requires to integrate the first variational equations. See [115] for further details.

Similar computations for a 2-dof system as well as for a 4D map were carried out in [45], where further technical details on the parametrization method and the computation of homo/heteroclinic trajectories can be found. For a recent overview of the parametrization method for computation of invariant manifolds in different contexts see [53].

Appendix D

Multi-scale Stochastic Simulations

The Gillespie Stochastic Simulation Algorithm (SSA) is exact. Its procedurally simple, even when the CME is intractable. There exist several implementations of the SSA, such as, the direct method [47], the first reaction method [47], the next reaction method [46],the first-family method [49], the modified direct method [21], the sorting direct method [84], the modified next reaction method [5], the composition-rejection SSA method [116] and the partial propensity direct method [103] among others. However, the stochastic simulation algorithm remains too slow for most practical problems: simulating every reaction event one at a time usually takes too much time if any reactants are present in very large numbers. For example, in the problem presented in Chapter 4 and Chapter 3, the healthy cells are given in a extremely big number, $O(10^9)$ cells, if we consider them in our stochastic model, the Gillespie algorithm takes very small time steps. In this appendix we describe a different method to avoid this problem.

D.1 Cao-Gillespie-Petzold Method

Cao et al. [20] presented a multi-scale stochastic simulation algorithm, based on a stochastic partial equilibrium assumption, which is much more efficient than the Gillespie stochastic simulation algorithm, particularly in the presence of very small populations or fast reactions.

D.1.1 Definitions

Assume we have N different species $S_1, ..., S_N$, $X_i(t)$ denotes the number of S_i particles at time t. Assume there are M different reactions $W_1, ..., W_M$. Each reaction channel, W_i, changes state vector of the system by r_i. The process is described by the following master equation:

$$\frac{dP(X,t)}{dt} = \sum_i (W_i(X - r_i)P(X - r_i) - W_i(X)P(X,t)). \tag{D.1}$$

Let $W_j^f = (W_j^1, ..., W_j^{m_f})$ be the set of fast reactions and $W_j^s = (W_j^1, ..., W_j^{m_s})$, the set of slow reactions.

Similarly, we define $X^s = (x_1^s, ..., x_{n_s}^s)$ as the set of the slow species and $X^f = (x_1^f, ..., x_{n_f}^f)$, the set of the fast species. A species is considered to be fast if it is altered by, at least, one of the fast reactions of the system. Otherwise it is a slow species.

We define two different propensity functions: The slow propensity functions

$$a_i^s(x) = a_i^s(x^f, x^s), \qquad i = 1, ..., m_s$$

and the fast propensity functions,

$$a_i^f(x) = a_i^f(x^f, x^s) \qquad i = 1, ...m_f.$$

We also define the fast and slow vector change as,

$$v_i^f = \left((v_1^{ff}, ..., v_{n_f}^{ff}, 0, ..., 0)\right),$$
$$v_i^s = \left(v_1^{fs}, ..., v_{n_f}^{fs}, v_1^{ss}, ..., v_{n_s}^{ss})\right),$$

where the superindex ff denotes the fast reaction affecting a fast species, fs the slow reaction affecting a fast species, and ss the slow reactions affecting a slow species.

In Appendix A, we have defined an equilibrium state in stochastic systems, as a state in which, roughly speaking, the births and deaths are balanced. Consider now just the reduced stochastic system described by the fast species with the fast variables. If the reduced stochastic system has an equilibrium state, $\bar{X}^f$, we say that the full stochastic process has a partial equilibrium, which is $(X^s, \bar{X}^f)$.

We can assume the existence of partial stochastic equilibria if two conditions are satisfied: the existence of an equilibrium state for the fast systems, and the relaxation time of the fast system being small in comparison with the time scale of the slow reactions.

Moreover we define the following new propensity density functions, in which the fast variables are in the equilibrium.

$$\bar{a}_j^s(X) = \mathbb{E}(a_i^s(\bar{X}^f)). \tag{D.2}$$

D.1.2 Computation of Partial equilibrium

How to decide which are the fast and the slow reactions, in general, is an open question, and usually the best way to determine them is to run few simulations of the SSA simulation algorithm and decide. Another option is to try to obtain some information of the propensity functions a_j and the different time scales of the system.

Compute $\bar{a}_j^s(X^s)$ is the most difficult part. There are 5 different cases [20]:

1. If $a_j^s(X)$ is independent of X^f, then $\bar{a}_j^s(X^s) = a_j^s(X)$.

2. If $a_j^s(X) = c_j^s X_i^f$, then $\bar{a}_j^s(X^s) = c_j^s(\bar{X}_i^f)$.

3. If $a_j^s(X) = c_j^s X_i^f x_k^s$, then $\bar{a}_j^s(X^s) = c_j^s X_k^s \mathbb{E}(\bar{X}_i^f)$.

4. If $a_j^s(X) = c_j^s X_i^f (X_i^f - 1)$, then $\bar{a}_j^s(X^s) = \dfrac{c_j^s}{2}\mathbb{E}(\bar{X}_i^f(\bar{X}_i^f - 1)) \approx \dfrac{c_j^s}{2}(\mathbb{E}(\bar{X}_i^f))^2$.

5. If $a_j^s(X) = c_j^s X_i^f X_k^f$, then $\bar{a}_j^s(X) = c_j^s \mathbb{E}(\bar{X}_i^f \bar{X}_k^f) \approx c_j^s \mathbb{E}(\bar{X}_i^f)\mathbb{E}(\bar{X}_k^f)$.

The computation of the partial equilibrium requires write and solve equations for the balance of the propensity functions. Consider that the fast system has the form,

$$\begin{aligned} A_1 + A_2 &\xrightarrow{c_1} A_1, \\ A_2 &\xrightarrow{c_2} A_2 + A_2. \end{aligned}$$

In this case $\bar{a}_1(X) = c_1 X_1 X_2$ and $\bar{a}_2(X) = c_2 X_2$, and the conservation law is

$$c_1 X_1 X_2 = c_2 X_2. \tag{D.3}$$

Remark: In general we do not obtain a linear system, however, if the partial equilibrium exists, we can solve the equations of the partial equilibrium via the Newton method [96].

However, there problematic cases. Consider the system described by

$$\begin{aligned} A_1 + A_1 &\xrightarrow{c_1} A_2 \\ A_2 &\xrightarrow{c_2} A_1 + A_1. \end{aligned}$$

In this case The equilibrium law given by the deterministic equations is

$$\frac{c_1}{2} X_1^2 = c_2 X_2 \tag{D.4}$$

however, the MSSA requires

$$\frac{c_1}{2} X_1 (X_1 - 1) = c_2 X_2. \tag{D.5}$$

For a large X_1 this is not problematic, however, when X_1 is small this is no longer valid.

Example D.1. To illustrate this methodology, we use as example the stochastic process described in Chapter 3. That is, the stochastic process described by the Eq. 3.1. As in Chapter 3 we assume that the variable T (the number of healthy cells) follows an ordinary differential equation.

From our time-scale analysis we already know that the variable V, corresponding to the number of virions, is the fast variable. But we can obtain the same running the SSA and counting the time that each variable occurs. From a few realizations, we observe that either the reaction corresponding to the virion clearance or the reaction corresponding to the virus production are chosen around 99.9% of times. Therefore we choose as fast reactions:

$$\begin{aligned} T^* &\xrightarrow{p_v} T^* + V \\ V &\xrightarrow{c} \emptyset \end{aligned}$$

The fast variables are the variables altered by the fast reactions, in this case the only variable which is altered by these two reactions is V, which account the number of the virus. The equation for the partial equilibrium come from the balance of this two ratios:

$$p_v T^* = c\mathbb{E}[V]. \tag{D.6}$$

Thus, partial equilibrium is $V = \dfrac{p_v T^*}{c}$.

D.1.3 Algorithm

The main idea of the algorithm is to produce an stochastic simulation for the slow species X^s, assuming that the fast species, X^f, evolves faster and have reached the partial stochastic equilibrium.

The Multi-scale Stochastic Simulation Algorithm steps are

1. Compute the equilibrium state for the fast system and update X^f according to the current state.
2. Compute $\bar{a}_j^s$, $\bar{a}_0^s = \sum \bar{a}_j^s$.
3. generate r_1 and r_2 random numbers in $[0, 1]$, and compute τ and j according to
   - $\tau = \frac{1}{\bar{a}_0^s(x)} ln\left(\frac{1}{1-r_1}\right)$,
   - $j =$ the smallest integer satisfying $\sum_{k=1}^{j} \bar{a}_k^s(x) > r_2 \bar{a}_0^s(x)$.
4. $t = t + \tau$ and $X^s = X^s + v_j^s$
5. go to 1 or stop.

Bibliography

[1] M. Adimy and F. Crauste. Mathematical model of hematopoiesis dynamics with growth factor-dependent apoptosis and proliferation regulations. *Mathematical and Computer Modelling*, 49(11–12):2128 – 2137, 2009.

[2] T. Alarcon. Stochastic quasi-steady state approximations for asymptotic solutions of the chemical master equation. *J. Chem. Phys.*, 140:184109, 2014.

[3] T. Alarcón and H. J. Jensen. Quiescence: a mechanism for escaping the effects of drug on cell populations. *Journal of The Royal Society Interface*, 8(54):99–106, 2011.

[4] B. Alberts, A. Johnson, J. Lewis, M. Raff, K. Roberts, and P. Walter. *Molecular Biology of the Cell*. Garland Publishing, New York, 5th edition, 2008.

[5] D. F. Anderson. A modified next reaction method for simulating chemical systems with time dependent propensities and delays. *The Journal of chemical physics*, 127(21):214107, 2007.

[6] V. I. Arnol'd. *Mathematical methods of classical mechanics*, volume 60. Springer, 1989.

[7] J. Ashbourn, J. Miller, V. Reumers, V. Baekelandt, and L. Geris. A mathematical model of adult subventricular neurogenesis. *Journal of The Royal Society Interface*, 9(75):2414–2423, 2012.

[8] M. Assaf and B. Meerson. Spectral theory of metastability and extinction in birth-death systems. *Physical review letters*, 97(20):200602, 2006.

[9] M. Assaf and B. Meerson. Spectral theory of metastability and extinction in a branching-annihilation reaction. *Physical Review E*, 75(3):031122, 2007.

[10] M. Assaf and B. Meerson. Extinction of metastable stochastic populations. *Phys. Rev. E*, 81:021116, 2010.

[11] C. Batut, K. Belabas, D. Bernardi, H. Cohen, and M. Olivier. *Users' guide to PARI/GP*. http://pari.math.u-bordeaux.fr/.

[12] H. C. Berg. *Random walks in biology*. Princeton University Press, Princeton, NJ, USA, 1993.

[13] D. Bernstein. Simulating mesoscopic reaction-diffusion systems using the Gillespie algorithm. *Phys. Rev. E*, 71:041103, 2005.

[14] R. P. Boland, T. Galla, and A. J. McKane. Limit cycles, complex floquet multipliers, and intrinsic noise. *Physical Review E*, 79(5):051131, 2009.

[15] D. Bray. *Cell movements: From molecules to motility.* Garland Publishing, New York, NY, USA, 2001.

[16] S. Buczacki, R. Davies, and D. Winton. Stem cells, quiescence and rectal carcinoma: an unexplored relationship and potential therapeutic target. *British journal of cancer*, 105(9):1253–1259, 2011.

[17] X. Cabré, E. Fontich, and R. de la Llave. The parameterization method for invariant manifolds. I. Manifolds associated to non-resonant subspaces. *Indiana Univ. Math. J.*, 52(2):283–328, 2003.

[18] X. Cabré, E. Fontich, and R. de la Llave. The parameterization method for invariant manifolds. II. Regularity with respect to parameters. *Indiana Univ. Math. J.*, 52(2):329–360, 2003.

[19] D. S. Callaway and A. S. Perelson. HIV-1 infection and low steady state viral loads. *Bulletin of Mathematical Biology*, 64(1):29–64, 2002.

[20] Y. Cao, D. Gillespie, and L. Petzold. Multiscale stochastic simulation algorithm with stochastic partial equilibrium assumption for chemically reacting systems. *Journal of Computational Physics*, 206(2):395–411, 2005.

[21] Y. Cao, H. Li, and L. Petzold. Efficient formulation of the stochastic simulation algorithm for chemically reacting systems. *The journal of chemical physics*, 121(9):4059–4067, 2004.

[22] J. Cerda. *Linear functional analysis*, volume 116. American Mathematical Soc., 2010.

[23] N. Chomont, M. El-Far, P. Ancuta, L. Trautmann, F. A. Procopio, B. Yassine-Diab, G. Boucher, M.-R. Boulassel, J. M. Brenchley, T. W. Schacker, B. J. Hill, D. C. D. G. Ghattas, J.-P. Routy, E. K. Haddad, and R.-P. Sekaly. HIV reservoir size and persistence are driven by T cell survival and homeostatic proliferation. *Nature Med.*, 15:893–901, 2009.

[24] T.-W. Chun, L. Carruth, D. Finzi, X. Shen, J. A. DiGiuseppe, H. Taylor, M. Hermankova, K. Chadwick, J. Margolick, T. C. Quinn, Y.-H. Kuo, R. Brookmeyer, M. A. Zeiger, P. Barditch-Crovo, and R. F. Siliciano. Quantification of latent tissue reservoirs and total body viral load in HIV-1 infection. *Nature*, 387:183–188, 1997.

[25] T. W. Chun, D. Finzi, J. Margolick, K. Chadwick, D. Schwartz, and R. F. Siliciano. In vivo fate of HIV-1-infected T cells: Quantitative analysis of the transition to stable latency. *Nat. Med.*, 1:1284–1290, 1995.

[26] C. Colijn and M. C. Mackey. A mathematical model of hematopoiesis–I. Periodic chronic myelogenous leukemia. *Journal of Theoretical Biology*, 237(2):117–132, 2005.

[27] C. Colijn and M. C. Mackey. A mathematical model of hematopoiesis–II. Cyclical neutropenia. *Journal of theoretical biology*, 237(2):133–146, 2005.

[28] J. M. Conway and D. Coombs. A Stochastic Model of Latently Infected Cell Reactivation and Viral Blip Generation in Treated HIV Patients. *PLoS Comput Biol*, 7:e1002033, 04 2011.

[29] F. Crauste. Delay model of hematopoietic stem cell dynamics: asymptotic stability and stability switch. *Mathematical Modelling of Natural Phenomena*, 4(02):28–47, 2009.

[30] M. DiMascio, M. Markowitz, M. Louie, C. Hogan, A. Hurley, C. Chung, D. D. Ho, and A. S. Perelson. Viral Blip Dynamics during Highly Active Antiretroviral Therapy. *J Virol*, 77(22):12165–12172, 2003.

[31] D. Dingli, A. Traulsen, and F. Michor. (a) symmetric stem cell replication and cancer. *PLoS computational biology*, 3(3):e53, 2007.

[32] D. Dingli, A. Traulsen, and J. M. Pacheco. Compartmental architecture and dynamics of hematopoiesis. *PLoS One*, 2(4):e345, 2007.

[33] G. Dornadula, H. Zhang, B. VanUitert, and et al. Residual HIV-1 RNA in blood plasma of patients taking suppressive highly active antiretroviral therapy. *JAMA*, 282(17):1627–1632, 1999.

[34] J. Elf and M. Ehrenberg. Spontaneous separation of bi-stable biochemical systems into spatial domains of opposite phases. *Syst. Biol.*, 1:230–235, 2004.

[35] V. Elgart and A. Kamenev. Rare event statistics in reaction-diffusion systems. *Phys. Rev. E*, 70:041106, 2004.

[36] R. Erban, J. Chapman, and P. Maini. A practical guide to stochastic simulations of reaction-diffusion processes. *arXiv preprint arXiv:0704.1908*, 2007.

[37] N. M. Ferguson, F. deWolf, A. C. Ghani, C. Fraser, C. A. Donnelly, P. Reissi, J. M. A. Langei, S. A. Danneri, G. P. Garnett, J. Goudsmit, , and R. M. Anderson. Antigen-driven CD41 T cell and HIV-1 dynamics: Residual viral replication under highly active antiretroviral therapy. *Proc. Natl. Acad. Sci.*, 96:15167–15172, 1999.

[38] E. Fermi. Thermodynamics, 1936. *Thermodynamics, 1936*, 1956.

[39] J. Foo, M. W. Drummond, B. Clarkson, T. Holyoake, and F. Michor. Eradication of chronic myeloid leukemia stem cells: a novel mathematical model predicts no therapeutic benefit of adding G-CSF to imatinib. *PLoS computational biology*, 5(9):e1000503, 2009.

[40] C. Fraser, N. M. Ferguson, and R. M. Anderson. Quantification of intrinsic residual viral replication in treated HIV infected patients. *Proc. Natl. Acad. Sci.*, 98:15167–15172, 2001.

[41] C. Frazer, N. M. Ferguson, F. de Wolf, and R. M. Anderson. The role of antigenic stimulation and cytotoxic T cel activity in regulating the long-term immunopathogenesis of HIV: Mechanisms and clinical implications. *Proc. R. Soc. London B.*, 268:2085–2095, 2001.

[42] M. I. Freidlin and A. D. Wentzell. Random perturbations of dynamical systems, volume 260 of grundlehren der mathematischen wissenschaften [fundamental principles of mathematical sciences], 1998.

[43] L. M. Frenkel, Y. Wang, G. H. Learn, J. L. McKernan, G. M. Ellis, K. M. Mohan, S. E. Holte, S. M. D. Vange, D. M. Pawluk, A. J. Melvin, P. F. Lewis, L. M. Heath, I. A. Beck, M. Mahalanabis, W. E. Naugler, N. H. Tobin, and J. I. Mullinhs. Multiple viral genetic analyses detect low-level human immunodeficency virus type I replication during effective highly active antiretroviral therapy. *J. Virol.*, 77:5721–5730, 2003.

[44] C. W. Gardiner. *Stochatic methods*. Springer-Verlag, Berlin, Germany, 2009.

[45] V. Gelfreich, C. Simó, and A. Vieiro. Dynamics of 4D symplectic maps near a double resonance. *Physica D*, 243(1):92–110, 2013.

[46] M. A. Gibson and J. Bruck. Efficient exact stochastic simulation of chemical systems with many species and many channels. *J. Phys. Chem. A*, 104:1876–1889, 2000.

[47] D. T. Gillespie. A general method for numerically simulating the stochastic time evolution of coupled chemical reactions. *Journal of computational physics*, 22(4):403–434, 1976.

[48] D. T. Gillespie. Exact stochastic simulation of coupled chemical reactions. *The journal of physical chemistry*, 81(25):2340–2361, 1977.

[49] D. T. Gillespie. Stochastic simulation of chemical kinetics. *Annu. Rev. Phys. Chem.*, 58:35–55, 2007.

[50] M. Götz and W. B. Huttner. The cell biology of neurogenesis. *Nature reviews Molecular cell biology*, 6(10):777–788, 2005.

[51] A. Griewank. Evaluating Derivatives: Principles and Techniques of Algorithmic Differentiation. Number 19 in Frontiers in Appl. Math. SIAM, Philadelphia, PA, 2000. Technical report, ISBN 08-987-1451-6.

[52] H. F. Gunthard, J. Wong, C. A. Spina, C. Ignacio, S. Kwok, C. Christopherson, J. Hwang, R. Haubrich, D. Havlir, and D. D. Richman. Effect of influenza vaccination on viral replication and immune response in persons infected with human immunodeficency virus receiving potent antiretroviral therapy. *J. Infect. Dis.*, 181:522–531, 2000.

[53] A. Haro, M. Canadell, J. Figueras, A. Luque, and J. Mondelo. The parameterization method for invariant manifolds: from rigorous results to effective comptutations. http://www.maia.ub.es/ alex/review/review.pdf/.

[54] D. V. Havlir, R. Bassett, D. Levitan, P. Gilbert, P. Tebas, A. C. Collier, M. S. Hirsch, C. Ignacio, J. Condra, H. F. Günthard, D. D. Richman, and J. K. Wong. Prevalence and Predictive Value of Intermittent Viremia With Combination HIV Therapy. *JAMA*, 286:171–179, 2001.

[55] A. V. M. Herz, S. Bonhoefer, R. M. Anderson, R. M. May, and M. A. Nowak. Viral dynamics in vivo: limitations on estimates of intracellular delay and virus decay. *Proc. Natl. Acad. Sci.*, 93:7247–7251, 1996.

[56] B. Hille. *Ionic channels of excitable membranes.* Sinauer Associates, Sunderland, MA, USA, 1992.

[57] D. D. Ho, A. U. Neumann, A. S. Perelson, W. Chen, J. M. Leonard, and M. Markowitz. Rapid turnover of plasma virions and CD4 lymphocytes in HIV-1 infection. *Nature*, 373:123–126, 1995.

[58] D. D. Ho, T. R. Rota, and M. S. Hirsch. Infection of monocyte/macrophages by human T lymphotropic virus type III. *J. CLin. Invest.*, 77:1712–1715, 1986.

[59] R. D. Hockett, J. M. Kilby, C. A. Derdeyn, M. S. Saag, M. Sillers, K. Squires, S. Chiz, M. A. Nowak, G. M. Shaw, and R. P. Bucy. Constant mean viral copy number per infected cell in tissues regardless of high, low, or undetectable plasma HIV RNA. *The Journal of experimental medicine*, 189(10):1545–1554, 1999.

[60] M. S. i Solé. Edicions universitat de barcelona, 1999.

[61] L. E. Jones and A. S. Perelson. Modelling the effects of vaccination on chronically infected HIV-positive patients. *J. Acquir. Immune Defic. Syndr.*, 31:369–377, 2002.

[62] L. E. Jones and A. S. Perelson. Opportunistic infections as a cause of transient viremia in chronically infected HIV patients under treatment with HAART. *Math. Biosci.*, 67:1227–1251, 2005.

[63] L. E. Jones and A. S. Perelson. Transient viremia, plasma viral load and reservoir replenishment in HIV-infected patients on antiretroviral therapy. *J. Acquir. Immune Defic. Syndr.*, 45:483–493, 2007.

[64] À. Jorba and M. Zou. A software package for the numerical integration of ODEs by means of high-order Taylor methods. 14(1):99–117, 2005.

[65] C. Katlama, S. G. Deeks, B. Autran, J. Martinez-Picado, J. van Luzen, C. Rouzioux, M. Miller, S. Vella, J. E. Schmitz, J. Ahlers, D. D. Richman, and R. P. Sekaly. Barriers to a cure for HIV: new ways to target and eradicate HIV-1 reservoirs. *Lancet*, 381:2109–2117, 2013.

[66] S. J. Kent, J. C. Reece, J. Petravic, A. Martyushev, M. Kramski, R. D. Rose, D. A. Cooper, A. D. Kelleher, S. Emery, P. U. Cameron, S. R. Lewin, and M. P. Davenport. The search for an HIV cure: tackling latent infection. *Lancet Infect. Dis.*, 13:614–621, 2013.

[67] T. B. Kepler and A. S. Perelson. Drug concentration heterogeneityof drug resistance facilitates the evolution of drug resistance. *Proc. Natl. Acad. Sci.*, 95:11514–11519, 1998.

[68] D. A. Kessler and N. M. Schnerb. Extinction rates for fluctuation-induced metastabilities: A real-space WKB approach. *J. Stat. Phys.*, 127:861–886, 2007.

[69] H. Kim and A. S. Perelson. Viral and latent reservoir persistence in HIV-1-infected patients on therapy. *PLoS Comp. Biol.*, 2:e135, 2006.

[70] A. Klinakis, C. Lobry, O. Abdel-Wahab, P. Oh, H. Haeno, S. Buonamici, I. van De Walle, S. Cathelin, T. Trimarchi, E. Araldi, et al. A novel tumour-suppressor function for the notch pathway in myeloid leukaemia. *Nature*, 473(7346):230–233, 2011.

[71] J. A. Knoblich. Mechanisms of asymmetric stem cell division. *Cell*, 132(4):583–597, 2008.

[72] J. A. Knoblich. Asymmetric cell division: recent developments and their implications for tumour biology. *Nature reviews Molecular cell biology*, 11(12):849–860, 2010.

[73] R. Kubo, K. Matsou, and K. Kitahara. Fluctuations and relaxation of macrovariables. *J. Stat. Phys.*, 9:51–96, 1973.

[74] T. Lechler and E. Fuchs. Asymmetric cell divisions promote stratification and differentiation of mammalian skin. *Nature*, 437(7056):275–280, 2005.

[75] K. Leder, J. Foo, B. Skaggs, M. Gorre, C. L. Sawyers, and F. Michor. Fitness conferred by bcr-abl kinase domain mutations determines the risk of pre-existing resistance in chronic myeloid leukemia. *PloS one*, 6(11):e27682, 2011.

[76] P. K. Lee, T. L. Kieffer, R. F. Siciliano, and R. E. Nettles. HIV-1 viral load blips are of limited clinical significance. *J. Antimicrob. Chemother.*, 57:803–805, 2006.

[77] J. Lei and M. C. Mackey. Multistability in an age-structured model of hematopoiesis: Cyclical neutropenia. *Journal of theoretical biology*, 270(1):143–153, 2011.

[78] T. Lenaerts, J. M. Pacheco, A. Traulsen, and D. Dingli. Tyrosine kinase inhibitor therapy can cure chronic myeloid leukemia without hitting leukemic stem cells. *haematologica*, 95(6):900–907, 2010.

[79] C. Lugo and A. J. McKane. Quasicycles in a spatial predator-prey model. *Phys. Rev. E*, 78:051911, 2008.

[80] J. Macias, J. C. Palomares, J. A. Mira, M. J. Torres, J. A. Garcia-Garcia, J. M. Rodriguez, S. Vergera, and J. A. Pineda. Transient rebounds of HIV plasma viremia are associated with the emergence of drug resistance mutations in patients of highly active antiretroviral therapy-. *J. Infection*, 5:195–200, 2005.

[81] J. M. Mahaffy, J. Bélair, and M. C. Mackey. Hematopoietic model with moving boundary condition and state dependent delay: applications in erythropoiesis. *Journal of Theoretical Biology*, 190(2):135–146, 1998.

[82] A. Marciniak-Czochra, T. Stiehl, A. D. Ho, W. Jäger, and W. Wagner. Modeling of asymmetric cell division in hematopoietic stem cells-regulation of self-renewal is essential for efficient repopulation. *Stem cells and development*, 18(3):377–386, 2009.

[83] M. Markowitz, M. Louie, A. Hurley, E. Sun, M. D. Mascio, A. S. Perelson, and D. D. Ho. A Novel Antiviral Intervention Results in More Accurate Assessment of Human Immunodeficiency Virus Type 1 Replication Dynamics and T-Cell Decay In Vivo. *J. Virol.*, 77:5037–5038, 2003.

[84] J. M. McCollum, G. D. Peterson, C. D. Cox, M. L. Simpson, and N. F. Samatova. The sorting direct method for stochastic simulation of biochemical systems with varying reaction execution behavior. *Computational biology and chemistry*, 30(1):39–49, 2006.

[85] A. J. McKane and T. J. Newman. Predator-prey cycles from resonant amplification of demographic stochasticity. *Physical review letters*, 94(21):218102, 2005.

[86] F. Michor. Quantitative approaches to analyzing imatinib-treated chronic myeloid leukemia. *Trends in pharmacological sciences*, 28(5):197–199, 2007.

[87] F. Michor, T. P. Hughes, Y. Iwasa, S. Branford, N. P. Shah, C. L. Sawyers, and M. A. Nowak. Dynamics of chronic myeloid leukaemia. *Nature*, 435(7046):1267–1270, 2005.

[88] F. Michor, Y. Iwasa, and M. A. Nowak. The age incidence of chronic myeloid leukemia can be explained by a one-mutation model. *Proceedings of the National Academy of Sciences*, 103(40):14931–14934, 2006.

[89] J. A. Mira, J. Macias, C. Nogales, J. Fernandez-Rivera, J. A. Garcia-Garcia, A. Ramos, and J. A. Pineda. Transient rebounds of low-level viraemia among HIV-infected patients under HAART are not associated with virological or immunological failure. *Antivir. Ther.*, 7:251–256, 2002.

[90] H. Mohri, S. Bonhoeffer, S. Monard, A. S. Perelson, and D. D. Ho. Rapid turnover of T lymphocytes in SIV-infected rhesus macaques. *Science*, 279(5354):1223–1227, 1998.

[91] S. J. Morrison and J. Kimble. Asymmetric and symmetric stem-cell divisions in development and cancer. *Nature*, 441(7097):1068–1074, 2006.

[92] S. J. Morrison and A. C. Spradling. Stem cells and niches: mechanisms that promote stem cell maintenance throughout life. *Cell*, 132(4):598–611, 2008.

[93] A. G. Murray and G. A. Jackson. Viral dynamics: a model of the effects of size shape, motion and abundance of single-celled planktonic organisms and other particles. *Mar. Ecol. Prog. Ser.*, 89:103–116, 1992.

[94] R. E. Nettles and T. L. Kieffer. Update on HIV-1 viral load blips. *Current Opinion in HIV and AIDS*, 1:157–161, 2006.

[95] R. E. Nettles, T. L. Kieffer, P. K. andDaphne Monie, Y. Han, T. Parsons, J. Cofrancesco, J. E. Gallant, T. C. Quinn, B. Jackson, C. Flexner, K. Carson, S. Ray, D. Persaud, and R. F. Siliciano. Intermittent hiv-1 viremia (blips) and drug resistance in patients receiving haart. *JAMA*, 293:817–829, 2005.

[96] J. Nocedal and S. J. Wright. Numerical optimization 2nd. 2006.

[97] J. E. Pearson, P. Krapivsky, and A. S. Perelson. Stochastic theory of early viral infection: Continuous versus burst production of virions. *PLoS Comp. Biol.*, 7:e1001058, 2011.

[98] J. W. Pepper, K. Sprouffske, and C. C. Maley. Animal cell differentiation patterns suppress somatic evolution. *PLoS computational biology*, 3(12):e250, 2007.

[99] A. S. Perelson, P. Essunger, Y. Cao, M. Vesanen, A. Hurley, K. Saksela, M. Markowitz, and D. D. Ho. Decay characteristics of HIV-1-infected compartments during combination therapy. *Nature*, 387:188–191, 1997.

[100] A. S. Perelson, D. E. Kirschner, and R. De Boer. Dynamics of HIV infection of CD4+ T cells. *Mathematical biosciences*, 114(1):81–125, 1993.

[101] A. S. Perelson, A. U. Neumann, M. Markowitz, J. M. Leonard, and D. D. Ho. HIV-1 dynamics in vivo: Virion clearance rate, infected cell life-span, and viral generation time. *Science*, 271:1582–1586, 1996.

[102] T. Pierson, J. McArthur, and R. F. Siciliano. Reservoirs for HIV-1: Mechanisms for viral persistence in the presence of antiviral immune response and antiretroviral therapy. *Annu. Rev. Immunol.*, 18:665–708, 2000.

[103] R. Ramaswamy, N. González-Segredo, and I. F. Sbalzarini. A new class of highly efficient exact stochastic simulation algorithms for chemical reaction networks. *The Journal of chemical physics*, 130(24):244104, 2009.

[104] B. Ramratnam, S. Bonhoeffer, J. Binley, A. Hurley, L. Zhang, and et al. Rapid production and clearance of HIV-1 and hepatitis C virus assessed by large volume plasma apheresis. *Lancet*, 354:1782–1785, 1999.

[105] D. D. Richman, D. M. Margolis, M. Delaney, W. C. Greene, D. Hazuda, and R. J. Pomerantz. The challenge of finding a cure for HIV infection. *Science*, 323:1304–1307, 2009.

[106] I. A. Rodriguez-Brenes, D. Wodarz, and N. L. Komarova. Asymmetric cell division: Recent developments and their implications for tumour biology. *Front. Oncol.*, 3:82, 2013.

[107] I. A. Rodriguez-Brenes, D. Wodarz, and N. L. Komarova. Minimizing the risk of cancer: tissue architecture and cellular replication limits. *Journal of The Royal Society Interface*, 10(86):20130410, 2013.

[108] A. Roesch, M. Fukunaga-Kalabis, E. C. Schmidt, S. E. Zabierowski, P. A. Brafford, A. Vultur, D. Basu, P. Gimotty, T. Vogt, and M. Herlyn. A temporarily distinct subpopulation of slow-cycling melanoma cells is required for continuous tumour growth. *Cell*, 141:583–594, 2010.

[109] L. Rong and A. S. Perelson. Asymmetric cell division of activated latently infected cells may explain the decay kinetics of the HIV-1 latent reservoir and intermittent viral blips. *Math. Biosci.*, 217:77–87, 2009.

[110] L. Rong and A. S. Perelson. Modeling Latently Infected Cell Activation: Viral and Latent Reservoir Persistence, and Viral Blips in HIV-infected Patients on Potent Therapy. *PLoS Comput. Biol.*, 5:e1000533, 10 2009.

[111] L. Rong and A. S. Perelson. Modelling HIV persistence, the latent reservoir, and viral blips. *J. Theor. Biol.*, 260:308–331, 2009.

[112] N. J. Savill. Mathematical models of hierarchically structured cell populations under equilibrium with application to the epidermis. *Cell proliferation*, 36(1):1–26, 2003.

[113] L. Shan, K. Deng, N. S. Shroff, C. M. Durand, S. A. Rabi, H.-C. Yang, H. Zhang, J. B. Margolick, J. N. Blankson, and R. F. Siciliano. Stimulation of HIV-1-specific cytolityc T lymphocytes facilitates elimination of latent viral reservoir after virus reactivation. *Immunity*, 36:491–501, 2012.

[114] H. Shenghui, D. Nakada, and S. J. Morrison. Mechanisms of stem cell self-renewal. *Annual Review of Cell and Developmental*, 25:377–406, 2009.

[115] C. Simó. On the analytical and numerical approximation of invariant manifolds. In *Les Méthodes Modernes de la Mécanique Céleste. Modern Methods in Celestial Mechanics*, volume 1, pages 285–329, 1990.

[116] A. Slepoy, A. P. Thompson, and S. J. Plimpton. A constant-time kinetic monte carlo algorithm for simulation of large biochemical reaction networks. *The journal of chemical physics*, 128(20):205101, 2008.

[117] F. Spill, P. Guerrero, T. Alarcón, P. K. Maini, and H. M. Byrne. Mesoscopic and continuum modelling of angiognesis. *J. Math. Biol.*, page To appear., 2014.

[118] T. Stiehl and A. Marciniak-Czochra. Characterization of stem cells using mathematical models of multistage cell lineages. *Mathematical and Computer Modelling*, 53(7):1505–1517, 2011.

[119] Z. Sun and N. L. Komarova. Stochastic modeling of stem-cell dynamics with control. *Mathematical biosciences*, 240(2):231–240, 2012.

[120] A. Traulsen, T. Lenaerts, J. M. Pacheco, and D. Dingli. On the dynamics of neutral mutations in a mathematical model for a homogeneous stem cell population. *Journal of The Royal Society Interface*, 10(79):20120810, 2013.

[121] D. Trono, C. V. Lint, C. Rouziux, E. Verdin, F. Barre-Sinoussi, T.-W. Chun, and N. Chomont. HIV persistence and the prospect of long-term drug-free remissions for HIV-infected individuals. *Science*, 329:174–180, 2010.

[122] N. G. Van Kampen. *Stochastic processes in Physics and Chemistry*. Elsevier, The Netherlands, 2007.

[123] S. Wang and L. Rong. Stochastic population switch may explain the latent reservoir stability and intermittent viral blips in HIV patients on suppresive. *J. Theor. Biol.*, 360:137–148, 2014.

[124] X. Wei, S. K. Ghosh, M. E. Taylor, V. A. Johnson, E. A. Emini, P. Deutsch, J. D. Lifson, S. Bonhoeffer, M. A. Nowak, B. H. Hahn, M. S. Saag, and G. M. Shaw. Viral dynamics in human immunodeficiency virus type 1 infection. *Nature*, 373:117–122, 1995.

[125] B. Werner, D. Dingli, and A. Traulsen. A deterministic model for the occurrence and dynamics of multiple mutations in hierarchically organized tissues. *Journal of The Royal Society Interface*, 10(85):20130349, 2013.

[126] Z.-Q. Zhang, T. Schuler, M. Zupancic, S. Wietgrefe, K. A. Staskus, K. A. Reimann, T. A. Reinhart, M. Rogan, W. Cavert, C. J. Miller, R. S. Veazey, D. Notermans, S. Little, S. A. Danner, D. D. Richman, D. Havlir, J. Wong, H. L. Jordan, T. W. Schacker, P. Racz, K. Tenner-Racz, N. L. Letvin, S. Wolinsky, and A. T. Haase. Sexual Transmission and Propagation of SIV and HIV in Resting and Activated CD4+ T Cells . *Science*, 286:1712–1715, 1999.

[127] R. Zhao and F. Michor. Patterns of proliferative activity in the colonic crypt determine crypt stability and rates of somatic evolution. *PLoS computational biology*, 9(6):e1003082, 2013.